ISSN : 2456-3307

IJSRCSEIT

INTERNATIONAL JOURNAL OF SCIENTIFIC RESEARCH IN COMPUTER SCIENCE, ENGINEERING AND INFORMATION TECHNOLOGY

Volume 4, Issue 4, March-2019

Email: editor@ijsrcseit.com

National Conference on
"Recent Trends in Mathematical Modeling, Simulation Methods, Computations, and Physical Sciences"
(MMSCP-2019)
Monday, 11th March 2019

In Association with
International Journal of Scientific Research in Computer Science, Engineering and Information Technology
ISSN : 2456-3307
Volume 4, Issue 4, March-2019

Organized by

Department of Mathematics, Department of Computer Science &
Department of Physics and Electronics
HISLOP COLLEGE, NAGPUR
www.hislopcollege.ac.in

Published By
Technoscience Academy (The International Open Access Publisher)
[http://technoscienceacademy.com]

Aims and objectives

This conference intends to provide a common platform for scientists, academicians, industrialist and researchers about recent developments and advancements in the basic sciences. Our approach is to find out the possibilities of methods and tools applicable to characterize the real time problems to understand their properties and behavior, through the discussions which will be held in this conference based on mathematical modeling, simulations and computations and physical sciences. Indeed, there is a need to conduct groundbreaking research on a number of fundamental and applied scientific approaches using breakthroughs in physics, computer-science, and mathematics in novel ways.

As new methods of building of manufacturing products are developed, mathematical formulas and Physical models may be applied to test the structure, characterization and functional soundness of the design. Computer aided analysis and design is becoming increasingly important in this type of use. This conference will provide an opportunity in exchange ideas and identify the priority areas of future research in advancements of technology to uplift the society and industry.

About the Institution

Hislop College, Nagpur is not just an institution but a byword for excellence, a synonym for quality, and a signature of the best in higher education. The College is established by a Scottish missionary Rev. Stephen Hislop in 1883, is now backed by the liberal and proactive management Hislop Education Society under the aegis of the Church of North India Synod. It was the first institution to provide higher education in Vidarbha region and even predates the establishment of RTM Nagpur University. In 2016, the College was reaccredited with A-grade 3.31 CGPA by NAAC and also granted as Heritage status by UGC. Hislop College caters to all the three streams with 12 post graduate departments and 10 recognized centers of research. Department of Physics, Mathematics and Computer Science are the blend of quality faculties and vibrant students, providing the undergraduate program and striving hard to impart the quality education under the 136 years old proficient management.

Chief Patron
Dr. Sudipta Singh
Secretary
Hislop Education Society

Patron
Dr. (Ms.) D. R. Christian
Principal
Hislop College, Nagpur

Joint Patrons
Dr. R. J. Andrew (Vice Principal)
Dr. P. Shelke (Vice Principal)
Dr. P. Banerjee (Vice Principal)

Chief Guest and Keynote Speaker
Dr. Shekhar C. Mande
Director General, CSIR,
Secretary, DSIR, New Dehli

Guest of Honour
Dr. J. S. Pandey
Chief Scientist, CSIR- NEERI, Nagpur

Invited Talk
Dr. K. V. Kale
Professor , Department of Computer Science,
Former Director, BCUD,
Dr. Babasaheb Ambedkar Marathwada Univ. Aurangabad

Keynote Speaker (Session-II)
Dr. Vilas A. Tabhane
Emeritus-Professor, Department of Physics,
S. P. Pune University, Pune

Invited Talk
Dr. Phool Singh
Associate Professor,
Department of Mathematics,
Central University of Haryana,
Jant Pali Mahendergarh, Haryana

Convener
Dr. Rishi Agrawal (9822942110)
Head, Department of Mathematics

Organizing Secretary
Dr. Ajay Yoel (9421704630)
Asst. Prof., Department of Physics
Dr. Mamta Baheti (8308339391)
Head, Department of Computer Science

Treasurer
Mrs. J. N. Christy (9890045387)
Asso. Prof., Department of Physics

National Advisory Committee

Dr. R. Manza, Dr. B.A.M. University, Aurangabad
Dr. D. S. Dhote, Biyani College, Amravati
Dr. V. M. Thakare, Dept. of Computer Sc., SGB Amravati Univ., Amravati
Dr. K.S. Adhav, Maths Dept., IGNT Univ., Amarkantak
Dr. G. S. Khadekar, Dean, Science & Tech, RTM Nagpur Univ.
Dr. S.D. Katore, Maths Dept., SGB Amravati Univ.
Dr. Kalpana Pawar, Asst Prof. Lahoti College, Morshi
Dr. D. D. Pawar, Director, Sch. Math. Sc., SRTMU, Nanded
Dr. B. S. S. Daniel, Mat. Sc. & Metallurgy Engn, IIT Roorkee.
Dr. J. C. Prasana, Physics Dept., Madras Christian College, Chennai
Dr. A. Anuradha, Physics Dept., Queen Mary's College, Chennai
Dr. K. Y. Madhavi, Govt. F. G. College, Chennapatna, Karnataka
Dr. Kamal Singh, Former Vice Chancellor, SGB Amravati Univ. Amravati
Dr. K.C. James Raju, School Of Physics, University of Hyderabad
Dr. Shivanand Gornale Rani Channamma University Belgavi-Karnataka
Dr. Mukti Jadhav Principal, Marathwada Institute of Technology, Aurangabad
Dr. Prapti Deshmukh Principal,MGM Dr. G.Y. Pathrikar College of CS&IT, Aurangabad

Local Advisory Committee

Dr. S. Sharma, Dept. of Elect. & Comp. Sc., RTM Nagpur Univ.
Dr. M. P. Dhore, Dept. of Elect. & Comp. Sc., RTM Nagpur Univ.
Dr. S. R. Pande, Dept. of Comp. Sc., Shivaji Sc. College, Nagpur
Dr. R. N. Jugele Shivaji Sc. College, Nagpur
Dr. T. M. Karade, Former Vice Chancellor, Indian Univ. Raipur
Dr. G. D. Rathod, Former Jt. Director, Higher Education, Nagpur
Dr. U. Datta, Former Vice Principal, Hislop College, Nagpur
Dr. A.W. Wyvahare, Former Head, Math., M.M.Sc. Col. Nagpur
Dr. A. S. Muktibodh, Former Head, Math., M.M.Sc. Col. Nagpur
Dr. P. S. Muktibodh, Rtd. Prof. Math., Hislop College Nagpur
Dr. K. G. Rewatkar,Dept. of Physics, Dr. Ambedkar Col., Nagpur
Dr. S. J. Dhoble, Dept. of Physics, RTM Nagpur Univ.
Dr. S. B. Kondawar, Dept. of Physics, RTM Nagpur Univ.
Dr. O. P. Chimankar, Dept. of Physics, RTM Nagpur Univ.
Dr. N. M. Patil, Dept. of Physics, LIT, Nagpur

Organizing Committee Members

Dr. Thomas Philip
Mr. M. G. Raut
Dr. Ashish Jha
Dr. Parama Majumdar
Ms. Shubhangi Raut
Ms. Ankita Pal
Mr. Yajna Vipradas
Mr. Abhijit Kshirsagar
Dr. Sarita Narkhede
Mrs. Madhavi Melag
Mr. Ashish Shah
Ms. Aina Gupta
Ms. Dhanashree Gomase
Ms. Dhanashree Raut
Ms. Sonal Ghawade
Mr. Mohan Naidu
Mr. Amol Gurnule
Dr. Mrunal Yawalkar

CONTENTS

National Conference on "Recent Trends in Mathematical Modeling, Simulation Methods, Computations, and Physical Sciences"
(MMSCP-2019), Organised by Hislop College, Nagpur, Maharashtra, India
International Journal of Scientific Research in Computer Science, Engineering and Information Technology
© 2019 IJSRCSEIT | Volume 4 | Issue 4 | ISSN : 2456-3307

Adsorption Kinetics for Removal of Congo Red Dye from Textile Waste Water using Al-TiO_2/PANI Nanocomposites

Subhash B. Kondawar*, Nasim Fatima Iqbal Khan, Neha V. Nerkar,
Department of Physics, Rashtrasant Tukadoji Maharaj Nagpur University, Nagpur, Maharashtra, India

ABSTRACT
In this paper we report the fabrication of Al doped TiO_2 nanofibers by electrospinning and preparation of electrospun Al-TiO_2/polyaniline (PANI) nanocomposites by in-situ chemical oxidation polymerization and its application for the removal of Congo red dye from aqueous solution. The morphology of the prepared nanocomposites was studied by scanning electron microscopy. Adsorption kinetics of synthesised nanocomposites was studied by UV-visible spectroscopy. Percentage of removal of Congo red dye using Al-TiO_2/PANI was found to be 76%. In order to evaluate adsorption kinetics, the pseudo first order model, pseudo second order model, and intra particle diffusion model were studied. The pseudo second order model was found to me more linear than other models which indicate that the adsorption of dye is a surface phenomenon and it depend on both concentration of dye and concentration of material. Experimental data suggested that adsorption is one of the best methods to remove Congo red dye from waste water disposed by textile industries.
Keywords: Polyaniline, Nanocomposites, Titanium dioxide, Aluminium, UV-Vis spectroscopy, Congo red dye.

I. INTRODUCTION

In this modern era where population is expanding day by day and the essential need water scarcity can be removed by the help of nanotechnology. The nanotechnology can provide the solution of removal of dyes from textile [1]. Dye is the substance used to add colour or to change the colour. The use of these dyes led to water pollution. Most of them are azo dyes, more than half of the commercial dyes belong to this class. These azo dyes can cause various health related issues. So, we require a method for the removal of these dyes [2]. There are various technologies for removing dyes from textile industry like reverse osmosis, ion exchange, precipitation biodegradation, coagulation and adsorption. Among which adsorption is fine, fruitful and manageable technique [3]. Congo red dye is an azo (anionic), water soluble, yielding a red colloidal solution and a pH indicator dye [4]. TiO_2 is accepted as photocatalyst due to its stability, non-toxicity highly photoactive and cost effective [5]. Photocatalytic activity can be enhanced by using conducting polymer such as polyaniline (PANI), polypyrole (PPY) etc. PANI has many properties such as low cost, good environmental stability, good electrical conductivity also it provides better binding site for the adsorption of the dye molecule. There are many methods to go to Nano-range like sol gel, phase separation, self-assembly, electrospinning. However, electrospinning process is deemed technically sound, environment friendly cost-effective and viable method for synthesising Al doped TiO_2 nanofibers [6].

II. EXPERIMENTAL

2.1 Fabrication of Al -TiO_2 nanofibers
Solution A was prepared by dissolving 1g of titanium isopropoxide (TiP) in acetic acid and ethanol of 2 ml each, 3 wt% aluminium nitrate nonahydrate which

was followed by magnetic stirring for 10 min. The solution A was mixed with the solution B which was made up of 0.2 g polyvinyl pyrrolidone (PVP) in 3 ml of ethanol and 0.5 ml N-N dimethyl formamide (DMF). The resultant solution was magnetically stirred for 24 hours. The prepared solution was filled into 10 ml syringe then it has been subjected to electrospin. The flow rate was adjusted to 0.6 mlh^{-1}. Voltage was kept at 18 KV and distance between needle tip and collector plate was kept at 15 cm then these nanofibers have been collected. These samples were calcinated at 600 ^{o}C for 3 hours to remove PVP and other moieties.

2.2 Preparation of PANI-Al-TiO_2 nanocomposites

In-situ polymerization method was carried out for preparation of PANI-Al-TiO_2 nanocomposites. Solution A was prepared by dispersing Al doped TiO_2 nanofibers for 30 min by ultrasonication in 25 ml de-ionised water, 1 M HCl and 0.25 M aniline and then magnetically stirred for 15 min. Solution B was made in 25 ml distilled water, 1 M HCl and 0.25 M ammonium peroxydisulfate (APS) and then magnetic stirred for 15 min. Solution B was added drop wise with continuous stirring for 6 hours into solution A. The nanocomposite of PANI with Al-TiO_2 nanofibers was obtained as precipitate. This precipitate was isolated by filtration, washed with distilled water several times and dried at 80 ^{o}C overnight.

III. RESULTS AND DISCUSSION

3.1 Scanning electron microscopy (SEM)

Morphology of as-fabricated Al-TiO_2 nanofibers and PANI/Al-TiO_2 nanocomposite was studied by SEM. Fig.1 shows SEM images of (a) Al-TiO_2 nanofibers and (b) PANI/Al-TiO_2 nancomposite. Fig.1(a) clearly showed that Al-TiO_2 nanofibers have been successfully fabricated by electrospinng and Fig. 1(b) showed that polyaniline have been encapsulated over Al-TiO_2 nanofibers and confirmed the formation of nanocomposites due to which adsorption will be more and Congo red dye will be reduced easily.

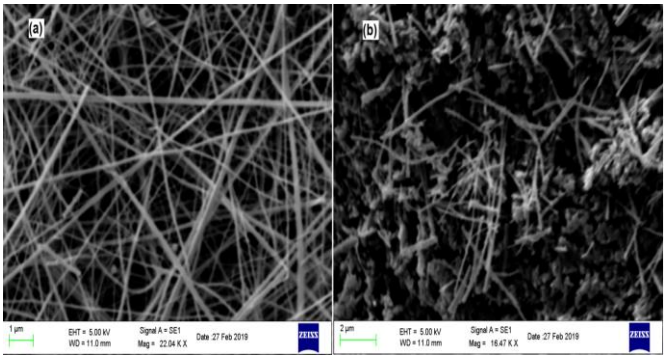

Figure 1. SEM images of (a) Al-TiO_2 nanofibers and (b) PANI/Al-TiO_2 nanocomposite

3.2 UV-Visible Spectroscopy

Photodegradation experiment was carried out by using UV-Visible absorption spectroscopy. Dye concentration was taken as 50 mg/L in de-ionized water and the mixture was magnetically stirred and reading were taken after every 15 min interval and the experiment was carried up to equilibrium. So, when a beam of ultraviolet rays falls on PANI/Al-TiO_2 nanocomposite electron and hole pairs are generated. This electron will combine with oxygen to form $O_2^{\cdot-}$ (super oxide anion) and hole will react with H_2O to form $OH^{\cdot}$ (hydroxy radical). Now this $OH^{\cdot}$ and $O_2^{\cdot-}$ will directly react with Congo red dye and give decolourisation product [7]. Kinetic studies have been done by pseudo first order, pseudo second order and intra particle-diffusion model. Fig. 2(a) shows the absorbance of dye by PANI/Al-TiO_2 in different time interval.

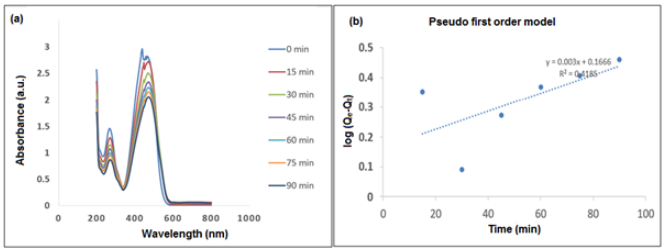

Figure 2(a). Absorbance of dye by PANI/Al-TiO_2 and **(b)** Pseudo first order model of PANI/Al-TiO_2

The percentage of removal of dye was calculated by the equation (1)

$$\% \text{ dye removal} = \frac{(C - C_e)100}{C} \quad \ldots\ldots\ldots (1)$$

Where, C= initial concentration and C_e= final concentration. The percentage of removal of dye by using PANI/Al-TiO_2 was found to be 76%. Fig. 2(b) shows Pseudo first order model, Fig. 3(a) shows the pseudo second order and Fig. 3(b) shows intra particle diffusion model of PANI/Al-TiO_2 for the study of removal of Congo red dye. These models have been studied by using equation (2), (3) and (4) respectively.

$$\log(Q_e - Q_t) = \log Q_e - \frac{Kt}{2.303} \quad \ldots\ldots\ldots (2)$$

$$\frac{t}{Q_t} = \frac{Q^2_e}{k} + \frac{t}{Q_e} \quad \ldots\ldots\ldots (3)$$

$$Q_t = kt^{0.5} + C \quad \ldots\ldots\ldots (4)$$

Where, Q_e = initial concentration, Q_t = concentration at time t, and k = rate constant

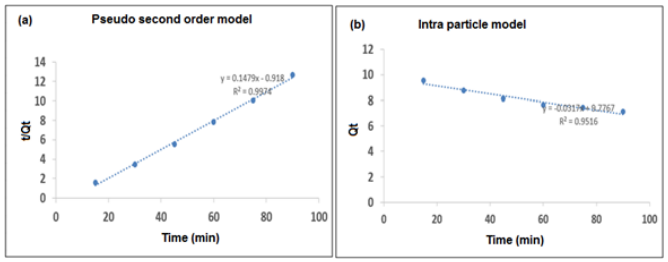

Figure 3(a). Pseudo second order and **(b)** Intra particle diffusion model of PANI/Al-TiO_2

The rate constant k was found to be 2.74 $mole^{-1}min^{-1}$obtained from pseudo second order model. From these models we can infer that the second order model reaction shows more linearity. This gives the validity of pseudo second order reaction [8].

IV. CONCLUSIONS

Al-TiO_2 nanofibers and PANI/Al-TiO_2 nanocomposite have been successfully synthesised by electrospinning and in-situ chemical oxidation polymerization. Photocatalytic degradation of Congo red dye by using PANI/Al-TiO_2 nanocomposite was achieved under UV-visible light irradiation. Percentage removal of dye for PANI/Al-TiO_2 was found to be 76%. Thus PANI/Al-TiO_2 can be used for photocatalytic decolorization of various pollutants and are expected to play an important role in solving environmental pollution challenges due to their relatively high oxidative power, photostability and non-toxicity.

V. REFERENCES

[1]. B. Pant, H.R. Pant, N. A.M. Barakat, M. Park, K. Jeon, Y. Choi, H. K. Kim "Carbon nanofibers decorated with binary semiconductor (〖TiO〗_2/ZnO) nanocomposites for the effective removal of organic pollutants and the enhancement of antibacterial activities" Ceramics International 39 (2013) 7029.

[2]. R. Saravanan, S. Karthikeyan, V.K. Gupta, G. Sekaran, V. Narayanan, A. Stephen: " enhanced photocatalytic activity of ZnO/CuO nanocomposite for the degradation of textile dye on visible light illumination" material science and engineering C 33 (2013) 91-98

[3]. N.V. Nerkar, S.B. Kondawar "Polyaniline/ZnO nanaocomposites for the removal of methyl orange dye from waste water" International Journal of Modern Physics B, 32, (2018) 19.

[4]. M.S. Alam, R.K. Rahman "Removal of Congo Red Dye from industrial wastewater by untreated sawdust" American Journal of Environmental Protection, 4 (2015) 207-213.

[5]. E. Alzahrani "photodegradation of Binary Azo Dyes using core-shell Fe3O4/SiO2/TiO2 Nanospheres" American Journal of Analytical Chemistry, 8 (2017) 95-115.

[6]. Q. Liu, J.Z. Zhang, Y. Qiu "Recent advances in energy materials by electrospinning" Reneavable and Sustainable Energy Reviews, 81 (2018) 1825-1858.

[7]. R. Giovanneti, E. Rommozzi, M. Zannotti, C.D Amato "Recent advances in Graphene based TiO2 Nanocomposites (GTiO2) for Photocatalytic Degradation of Synthetic Dyes" Catalysts, 7 (2017) 305.

[8]. M.M Ayad, A.A. El-Nasr, "Anionic dye (acid green 25) adsorption from water by using polyaniline nanotubes salt/silica composite" Journal of Nanostructure in Chemistry, 3 (2012) 3.

National Conference on "Recent Trends in Mathematical Modeling, Simulation Methods, Computations, and Physical Sciences"
(MMSCP-2019), Organised by Hislop College, Nagpur, Maharashtra, India
International Journal of Scientific Research in Computer Science, Engineering and Information Technology
© 2019 IJSRCSEIT | Volume 4 | Issue 4 | ISSN : 2456-3307

Common Fixed Point Result for a Pair of Multi Valued Maps in a Partially Ordered Metric Space

Kavita B. Bajpai[1], Manjusha P. Gandhi[2]
[1]K. D. K. College of Engineering, Nagpur, Maharashtra, India
[2]Yeshwantrao Chavan College of Engineering, Wanadongri, Nagpur, Maharashtra, India

ABSTRACT

In this paper we prove a unique common fixed point theorem for a pair of multi-valued mappings satisfying a generalized (ξ,η) weak contractive condition in complete partially ordered metric space. Present paper is the improved version of result proved earlier in the literature.

Keywords: Fixed point , Partially ordered metric space , Multi valued mappings , Mappings ξ and η.

I. INTRODUCTION

The Banach fixed point theorem is an important tool in the theory of metric spaces, it guarantees the existence and uniqueness of fixed points of certain self maps of metric spaces and provides a constructive method to find those fixed points.

In 1969, Nadler [19] established the multi-valued version of Banach contraction principle. Later on , many fixed point theorems have been proved by various authors as generalization of the Nadler's theorem where the nature of contractive mapping is weakened along with some additional requirements, one may refer S. Reich(1972), , E. Zeidler (1985) I. Beg and A. Azam(1992), P.Z. Daffer (1995), P.Z. Daffer, H. Kaneko and W. Li(1996), C.Y. Qing(1996), Y. Feng and S. Liu(2006), D. Klim and D.Wardowski(2007).

Ran and Reurings established the existence of unique fixed point for single valued mapping in partially ordered metric spaces. Their result was further extended by A. Petrusel and I.A. Rus (2005), J.J. Nieto and R. Rodriguez-Lopez (2005), T.G. Bhaskar and V. Lakshmikantham (2006), J.J. Nieto and R. Rodriguez-Lopez(2007), D. O'Regan and A. Petrusel (2008) I. Beg and A.R. Butt (2009), J. Harjani, K. Sadarangani (2009), I. Beg and A.R. Butt(2010). Further Bhaskar and Lakshmikantham studied the existence and uniqueness of a coupled fixed point in partially ordered metric space with assumption that the single valued mapping satisfies the weaker contraction condition.

The aim of this paper is to improve, extend and unify the above existing results and prove common fixed point theorem for a pair of multi valued mappings satisfying a generalized (ξ,η) weak contractive condition in complete partially ordered metric space.

Definition 1.1: Let (X,d) be a metric space and let $B(X)$ be the class of all nonempty bounded subsets of X. We define the functions $\delta: B(X)\times B(X)\to R^+$ and $D: B(X)\times B(X)\to R^+$ as follows:

$$\delta(A,B)=\sup\{d(a,b): a\in A, b\in B\}$$
$$D(A,B)=\inf\{d(a,b): a\in A, b\in B\}$$

where R^+ denotes the set of all positive real numbers. For $\delta(\{a\},B)$ and $\delta(\{a\},\{b\})$, we write $\delta(a,B)$ and $d(a,b)$ respectively. Clearly , $\delta(A,B)=\delta(B,A)$. We appeal to the fact that $\delta(A,B)=0$ if and only if $A=B=\{x\}$, for $A,B\in B(X)$ and $0\le\delta(A,B)\le\delta(A,C)+\delta(C,B)$, for all $A,B,C\in B(X)$.

A point $x\in X$ is called a fixed point of T if $x\in Tx$. If there exists a point $x\in X$ such that $Tx=\{x\}$, then x is called the end point of the mapping T.

Definition1.2: A partial order relation is a binary relation $\le$ on X which satisfies the following conditions:

i) $x\le x$ (reflexivity),

ii) if $x\le y$ and $y\le x$ then $x=y$ (anti symmetry),

iii) if $x\le y$ and $y\le z$ then $x\le z$ (transitivity), for all $x,y,z\in X$

A set with a partial order relation $\le$ is called a partially ordered set.

Definition1.3: Let $(X,\le)$ be a partially ordered set and $x,y\in X$. Elements x and y are said to be comparable elements of X if either $x\le y$ or $y\le x$.

Definition1.4: Let $(X,\le)$ be a partially ordered set and 'd' be a metric defined on X then (X,d) is called a partially ordered metric space.

Definition1.5: A function $\xi:[0,\infty)\to[0,\infty)$ is called an altering distance function if it is

Continuous , Monotonically non-decreasing and $\xi(t)=0$ if and only if $t=0$.

Theorem 2.1: Let $(X,\le)$ be a partially ordered set and suppose that there exists a metric 'd' in X such that (X,d) is a complete metric space. Let $F,G:X\to B(X)$ be two multi valued mappings such that the following conditions are satisfied :

i) There exists $x_0\in X$ such that $x_1=Fx_0\le GFx_0=Gx_1=x_2=Gx_1\le FGx_1=Fx_2=x_3$

ii) If $x_n\to x$ is a non-decreasing sequence in X , then $x_n\le x$, for all n.

iii) $\xi(\delta(Fx,Gy))\le\xi\left\{\max.\left[d(x,y),D(x,Fx),D(y,Gy),\frac{D(x,Gy)+}{2}\right.\right.$

$-\eta\{\max.[d(x,y),\delta(x,Fx),\delta(y,Gy)]\}$

for all comparable $x,y\in X$, where ξ is an altering distance function and $\eta:[0,\infty)\to[0,\infty)$ is any continuous function with $\eta(t)=0$ if and only if $t=0$.

Then F and G will have a common fixed point in X.

Proof: Let x_0 be an arbitrary point of X. We can define a sequence $\{x_n\}$ in X as follows:

$x_{2n+1}=Fx_{2n}$ and $x_{2n+2}=Gx_{2n+1}$, for $n\in\{0,1,2,----\}$, where the successive terms of $\{x_n\}$ are all different.

Since we have ,

$x_1=Fx_0\le GFx_0=Gx_1=x_2=Gx_1\le FGx_1=Fx_2=x_3$

Continuing this process , we have ,

$x_1\le x_2\le x_3\le---\le x_n\le x_{n+1}\le---$

Using the monotone property of ξ and condition (iii) , we have for all $n\ge0$

$\xi(d(x_{n+1},x_{n+2}))\le\xi(\delta(Fx_n,Gx_{n+1}))$

$\le\xi\left\{\max.\left[d(x_n,x_{n+1}),D(x_n,Fx_n),D(x_{n+1},Gx_{n+1}),\frac{D(x_n,Gx_{n+1})+D(x_{n+1},Fx_n)}{2}\right.\right.$

$-\eta\{\max.[d(x_n,x_{n+1}),\delta(x_n,Fx_n),\delta(x_{n+1},Gx_{n+1})]\}$

$\le\xi\left\{\max.\left[d(x_n,x_{n+1}),d(x_n,x_{n+1}),d(x_{n+1},x_{n+2}),\frac{d(x_n,x_{n+2})+d(x_{n+1},x_{n+1})}{2}\right]\right\}$

$-\eta\{\max.[d(x_n,x_{n+1}),d(x_n,x_{n+1}),d(x_{n+1},x_{n+2})]\}$

--------- (2.1.1)

Since $\frac{d(x_n, x_{n+2})}{2} \leq \max.[d(x_n, x_{n+1}) + d(x_{n+1}, x_{n+2})]$

Therefore from (2.1.1) , we can write ,

$\xi(d(x_{n+1}, x_{n+2})) \leq \xi\{\max.[d(x_n, x_{n+1}), d(x_{n+1}, x_{n+2})]\} - \eta\{\max.[d(x_n, x_{n+1}), d(x_{n+1}, x_{n+2})]\}$

----- (2.1.2)

If $d(x_n, x_{n+1}) \leq d(x_{n+1}, x_{n+2})$, for some positive integer 'n' .

Then from (2.1.2) , we have ,

$\xi(d(x_{n+1}, x_{n+2})) \leq \xi(d(x_{n+1}, x_{n+2})) - \eta(d(x_{n+1}, x_{n+2}))$

i.e. $\eta(d(x_{n+1}, x_{n+2})) \leq 0$, which implies that $d(x_{n+1}, x_{n+2}) = 0$ or $x_{n+1} = x_{n+2}$, which contradicts to our assumption that $x_n \neq x_{n+1}$, for each n.

$\therefore$ $d(x_{n+1}, x_{n+2}) < d(x_n, x_{n+1})$, for all $n \geq 0$ and $\{d(x_n, x_{n+1})\}$ is a monotone decreasing sequence of non- negative real numbers. Hence there exists $r \geq 0$ such that $\lim_{n\to\infty} d(x_n, x_{n+1}) = r$

--- (2.1.3)

$\therefore$ From (2.1.2) we will have for all $n \geq 0$,

$\xi(d(x_{n+1}, x_{n+2})) \leq \xi(d(x_n, x_{n+1})) - \eta(d(x_n, x_{n+1}))$

Taking limit as $n \to \infty$, using (2.1.3) and the continuities of functions ξ and η, we get

$\xi(r) \leq \xi(r) - \eta(r)$, which is a contradiction unless $r = 0$.

Hence,

$\lim_{n\to\infty} d(x_n, x_{n+1}) = 0$ --(2.1.4)

Now , we show that $\{x_n\}$ is a Cauchy sequence .

We prove this by method of contradiction i.e. we assume that $\{x_n\}$ is not a Cauchy sequence.

$\therefore$ There exists an $\in > 0$ for which we can find two sequences of positive integers $\{m(k)\}$ and $\{n(k)\}$ such that for all positive integers k , $n(k) > m(k) > k$ and $d(x_{m(k)}, x_{n(k)}) \geq \in$

Assuming that $n(k)$ is the smallest such positive integer , we get $n(k) > m(k) > k$,

$d(x_{m(k)}, x_{n(k)}) \geq \in$ and $d(x_{m(k)}, x_{n(k)}) < \in$

Now , $\in \leq d(x_{m(k)}, x_{n(k)}) \leq d(x_{m(k)}, x_{n(k-1)}) + d(x_{n(k-1)}, x_{n(k)})$

i.e. $\in \leq d(x_{m(k)}, x_{n(k)}) < \in + d(x_{n(k-1)}, x_{n(k)})$

Taking limit as $k \to \infty$ in the above inequality and using (2.1.4) ,

we have , $\lim_{k\to\infty} d(x_{m(k)}, x_{n(k)}) = \in$

----------(2.1.5)

Again ,

$d(x_{m(k)}, x_{n(k)}) \leq d(x_{m(k)}, x_{m(k+1)}) + d(x_{m(k+1)}, x_{n(k+1)}) + d(x_{n(k+1)}, x_{n(k)})$

and

$d(x_{m(k+1)}, x_{n(k+1)}) \leq d(x_{m(k+1)}, x_{m(k)}) + d(x_{m(k)}, x_{n(k)}) + d(x_{n(k)}, x_{n(k+1)})$

Taking limit as $k \to \infty$ in the above inequalities , using (2.1.4) and (2.1.5) , we have ,

$\lim_{k\to\infty} d(x_{m(k+1)}, x_{n(k+1)}) = \in$

--------- (2.1.6)

Also , $d(x_{m(k)}, x_{n(k)}) \leq d(x_{m(k)}, x_{n(k+1)}) + d(x_{n(k+1)}, x_{n(k)})$

and $d(x_{m(k)}, x_{n(k+1)}) \leq d(x_{m(k}, x_{n(k)}) + d(x_{n(k)}, x_{n(k+1)})$

Taking limit as $k \to \infty$ in the above inequalities and using (2.1.4) , (2.1.5) , we get ,

$\lim_{k\to\infty} d(x_{m(k)}, x_{n(k+1)}) = \in$

-------- (2.1.7)

Similarly , we will have ,

$\lim_{k\to\infty} d(x_{n(k)}, x_{m(k+1)}) = \in$ -------(2.1.8)

For each positive integer 'k' , $x_{m(k)}$ and $x_{n(k)}$ are comparable. Then using the monotone property of ξ and the condition (iii) , we have ,

$$\xi(d(x_{m(k+1)}, x_{n(k+1)})) \leq \xi(\delta(Fx_{m(k)}, Gx_{n(k)}))$$

$$\leq \xi\left\{\max.\left[d(x_{m(k)}, x_{n(k)}), D(x_{m(k)}, Fx_{m(k)}), D(x_{n(k)}, Gx_{n(k)}), \frac{D(x_{m(k)}, Gx_{n(k)}) + D(x_{n(k)}, Fx_{m(k)})}{2}\right]\right\}$$

$$- \eta\{\max.[d(x_{m(k)}, x_{n(k)}), \delta(x_{m(k)}, Fx_{m(k)}), \delta(x_{n(k)}, Gx_{n(k)})]\}$$

$$\leq \xi\left\{\max.\left[d\left(x_{m(k)},x_{n(k)}\right),d\left(x_{m(k)},x_{m(k+1)}\right),d\left(x_{n(k)},x_{n(k+1)}\right),\frac{d\left(x_{m(k)},x_{n(k+1)}\right)+d\left(x_{n(k)},x_{m(k+1)}\right)}{2}\right]\right\}$$
$$-\eta\{\max.[d\left(x_{m(k)},x_{n(k)}\right),d\left(x_{m(k)},x_{m(k+1)}\right),d\left(x_{n(k)},x_{n(k+1)}\right)]\}$$

Taking $k\to\infty$, using (2.1.5) , (2.1.6) , (2.1.7) , (2.1.8) and using the continuities of ξ and η,

We have , $\xi(\in)\leq\xi(\in)-\eta(\in)$, which is a contradiction by virtue of a property of η.

Hence $\{x_n\}$ is a Cauchy sequence , and since X is a complete metric space , there exists a point $u\in X$ such that $x_n\to u$ as $n\to\infty$.

i.e. $\lim_{n\to\infty} d\left(x_n,u\right)=d\left(u,u\right)=0$,

$\lim_{n,m\to\infty} d\left(x_n,x_m\right)=0$

By the assumption (ii) $x_n\leq u$, for all *n*.

$\therefore$ By monotone property of ξ and by substituting $x=x_{2n+1}$, $y=Gu$ in (iii) , we have ,

$$\xi\left(d\left(x_{2n+1},Gu\right)\right)\leq\xi\left(\delta\left(Fx_{2n},Gu\right)\right)$$
$$\leq\xi\left\{\max.\left[d\left(x_{2n},u\right),D\left(x_{2n},Fx_{2n}\right),D\left(u,Gu\right),\frac{D\left(x_{2n},Gu\right)+D\left(u,Fx_{2n}\right)}{2}\right]\right\}$$
$$-\eta\{\max.[d\left(x_{2n},u\right),\delta\left(x_{2n},Fx_{2n}\right),\delta\left(u,Gu\right)]\}$$
$$\leq\xi\left\{\max.\left[d\left(x_{2n},u\right),D\left(x_{2n},x_{2n+1}\right),D\left(u,Gu\right),\frac{D\left(x_{2n},Gu\right)+D\left(u,x_{2n+1}\right)}{2}\right]\right\}$$
$$-\eta\{\max.[d\left(x_{2n},u\right),\delta\left(x_{2n},x_{2n+1}\right),\delta\left(u,Gu\right)]\}$$

Taking limit as $n\to\infty$, we get ,

$$\xi(\delta(u,Gu))\leq\xi\left[D(u,Gu),\frac{D(u,Gu)}{2}\right]-\eta[\delta(u,Gu)]$$

i.e. $\xi(\delta(u,Gu))\leq\xi(\delta(u,Gu))-\eta(\delta(u,Gu))$, which is a contradiction unless $\delta(u,Gu)=0$,

i.e. $\{u\}=Gu$, i.e. 'u' is a fixed point of *G*.

Now , we show that 'u' is also a fixed point of *F*.

$\therefore$ Substitute $x=x_{2n+2}$, $y=Fu$ in (iii) , we have ,

$$\xi\left(d\left(x_{2n+2},Fu\right)\right)\leq\xi\left(\delta\left(x_{2n+2},Fu\right)\right)\leq\xi\left(\delta\left(Gx_{2n+1},Fu\right)\right)$$
$$\leq\xi\left\{\max.\left[d\left(u,x_{2n+1}\right),D\left(u,Fu\right),D\left(x_{2n+1},Gx_{2n+1}\right),\frac{D\left(u,Gx_{2n+1}\right)+D\left(x_{2n+1},Fu\right)}{2}\right]\right\}$$
$$-\eta\{\max.[d\left(u,x_{2n+1}\right),\delta\left(u,Fu\right),\delta\left(x_{2n+1},Gx_{2n+1}\right)]\}$$

On taking limit as $n\to\infty$, we get

$$\xi(\delta(u,Fu))\leq\xi\left[D(u,Fu),\frac{D(u,Fu)}{2}\right]-\eta[\delta(u,Fu)]$$

i.e. $\xi(\delta(u,Fu))\leq\xi(\delta(u,Fu))-\eta(\delta(u,Fu))$, which is again a contradiction unless $\delta(u,Fu)=0$,

which implies that $\{u\}=Fu$, i.e. 'u' is a fixed point of *F*.

Hence 'u' is a common fixed point of *F* and *G*.

Corollary 2.2: Let $(X,\leq)$ be a partially ordered set and suppose that there exists a metric 'd' in X such that (X,d) is a complete metric space. Let $F:X\to B(X)$ be a multi valued mapping such that the following conditions are satisfied :

i) There exists $x_0\in X$ such that $x_1=Fx_0$

ii) If $x_n\to x$ is a non-decreasing sequence in X , then $x_n\leq x$, for all *n*.

iii) $$\xi(\delta(Fx,Fy))\leq\xi\left\{\max.\left[d(x,y),D(x,Fx),D(y,Fy),\frac{D(x,Fy)+D(y,Fx)}{2}\right]\right\}$$
$$-\eta\{\max.[d(x,y),\delta(x,Fx),\delta(y,Fy)]\}$$

for all comparable $x, y \in X$, where ξ is an altering distance function and $\eta : [0,\infty) \to [0,\infty)$ is any continuous function with $\eta(t) = 0$ if and only if $t = 0$.

Then F has a fixed point in X.

Proof: If we substitute $F = G$ in Theorem 2.1 then we get the proof of Corollary 2.2 which is same as the result proved in [3].

II. ACKNOWLEDGMENT

The authors are thankful to the reviewers for giving their valuable suggestions. Also the college authorities for providing all kind of support for carrying out the research activity.

III. REFERENCES

[1]. A.C.M. Ran and M.C.B. Reurings, A fixed point theorm in partially ordered sets and some applications to matrix equations, Proc. Amer. Math. Soc., 132 (2004), 1435-1443.

[2]. A. Petrusel and I.A. Rus, Fixed point theorems in ordered L-spaces, Proc. Amer. Math.Soc., 134 (2005), 411-418.

[3]. B. S. Choudhury , N. Metiya , Multivalued and singlevalued fixed point results in partially ordered metric spaces, Arab Journal of Mathematical Sciences (2011) 17, 135–151.

[4]. C.Y. Qing, On a Fixed point problem of Reich, Proc. Amer. Math. Soc., 124 (1996), 3085-3088.

[5]. D. Klim and D.Wardowski, Fixed point theorems for set-valued contractions in complete metric spaces, J. Math. Anal.Appl., 334 (2007), 132-139.

[6]. D. O'Regan and A. Petrusel, Fixed point theorems for generalized contractions in ordered metric spaces, J. Math. Anal. Appl., 341 (2008), 1241-1252.

[7]. E. Zeidler, Nonlinear Functional Analysis and its Applications I: Fixed point Theorems, Springer Verlag, New York 1985.

[8]. I. Beg and A. Azam, Fixed points of asymptotically regular multivalued mappings, J. Austral. Math. Soc. (Series-A) 53(3) (1992), 313-326.

[9]. I. Beg and A.R. Butt, Fixed point for set valued mappings satisfying an implicit relation in partially ordered metric spaces, Nonlinear Anal. 71 (2009), 3699-3704.

[10]. I. Beg and A. R. Butt, Fixed points for weakly compatible mappings satisfying an implicit relation in partially ordered metric spaces, Carpathian J. Math. 25 (2009), 1-12.

[11]. I. Beg and A.R. Butt, Common fixed point for generalized set valued contractions satisfying an implicit relation in partially ordered metric spaces, Mathematical Communications, 15 (2010), 65-76.

[12]. J. Harjani, K. Sadarangani, Fixed point theorems for weakly contractive mappings in ordered sets, Nonlinear Anal. 71 (2009), 3403-3410.

[13]. J. Harjani, K. Sadarangani, Generalized contractions in partially ordered metric spaces and applications to ordinary differential equations, Nonlinear Anal. (2009), doi:10.1016/j.na.2009.08.003 (in press).

[14]. J.J. Nieto, R.L. Pouso and R. Rodriguez-Lopez, Fixed point theorems in ordered abstract spaces, Proc. Amer. Math. Soc., 135 (2007), 2505-2517.

[15]. J.J. Nieto and R. Rodriguez-Lopez, Contractive mapping theorms in partially ordered sets and applications to ordinary differential equations, Order, 22 (2005), 223-239.

[16]. J.J. Nieto and R. Rodriguez-Lopez, Existence and uniqueness of fixed point in partially ordered sets and applications to ordinary differential equations, Acta. Math. Sinica, (English Ser.) 23 (2007), 2205-2212.

[17]. P.Z. Daffer, Fixed points of generalized contractive multivalued mappings, J. Math. Anal. Appl., 192 (1995), 655-666.

[18]. P.Z. Daffer, H. Kaneko and W. Li, On a conjecture of S. Reich, Proc. Amer. Math. Soc., 124 (1996), 3159-3162.

[19]. S.B. Nadler, Jr., Multi-valued contraction mapping. Pacific J. Math., vol. 30, 1969, 475–488.

[20]. S. Reich, Fixed points of contractive functions, Boll. Unione. Mat. Ital., (4) (1972), 26-42.

[21]. T.G. Bhaskar and V. Lakshmikantham, Fixed point theorems in partially ordered metric spaces and applications, Nonlinear Anal., 65 (2006), 1379-1393.

[22]. Y. Feng and S. Liu, Fixed point theorems for multivalued contractive mappings and multivalued Caristi type mappings, J. Math. Anal. Appl., 317 (2006), 103-112.

National Conference on "Recent Trends in Mathematical Modeling, Simulation Methods, Computations, and Physical Sciences"
(MMSCP-2019), Organised by Hislop College, Nagpur, Maharashtra, India
International Journal of Scientific Research in Computer Science, Engineering and Information Technology
© 2019 IJSRCSEIT | Volume 4 | Issue 4 | ISSN : 2456-3307

Approximate value of a irrational number using Duplex

Sanjay M. Deshpande[1], Rishikumar K. Agrawal [2]

[1]Department of Mathematics, Bhawabhuti Mahavidyalaya, Amgaon, Dist. Gondia, RTM NU, Nagpur, Maharashtra, India

[2]Department of Mathematics, Hislop College, RTM NU, Nagpur, Maharashtra, India

ABSTRACT

Swami Bharthi Krshnatrthji Maharaj is the author of book Vedic Mathematics. This book was first published in1965. This book contains many mathematical calculations in various fields of mathematics. In this book Swamiji explained by coating examples in each chapter. All the formulas in Vedic Mathematics have a logical mathematical application. Some important most useful chapters in Vedic Mathematics are Division by Paravartya method or Dwajank method, recurring decimals, Complex Mergers, Partial Fractions etc. In this paper we will discuss the method of straight squaring (to obtain square of a number) by creating duplex (Dwandwa Yoga). This method is very powerful to obtain the square of a number. In the same chapter Swamiji explained that the reverse process of finding a square of a number (By creating duplex) gives us square root of a number. Swamiji developed this concept of duplex (Dwandwa Yoga) from algebra. In the expansion of (ax + b)2, (ax2 + bx + c)2, (ax3 + bx2 + cx + d)2,..... the coefficients of descending powers are always a2, 2ab, (b2 + 2ac), (2ad +2bc),..... Swamiji called these coefficients as duplex. So duplex of single digit number is square of itself, square of two digit number is two times the product of two numbers, duplex of three digit number is sum of square of the middle number and two times the product of first and third number, and so on. Putting these duplex at proper place we obtain the square of a number. Similarly if we subtract the duplex from the given number we obtain the square root of a number. This method has a powerful application of finding the approximate value of irrational numbers (a number which have non recurring and non repeating decimal numbers). Irrational numbers are real numbers and we never obtain its exact value. So we obtain its approximate value always. Here we discuss how to find the approximate value of irrational number by creating duplex (Dwandwa Yoga).

I. INTRODUCTION

This method of finding the approximate value of irrational number is very simple. This method is applicable for the computer programming. This method of finding the square of a number is the application of algebra in arithmetic. Finding the square root is the reverse process of finding the square.

II. METHOD AND PROCEDURE

The Dwandwa Yoga or The Duplex combination process

How to generate the duplex ?

1) For single digit number 'a' duplex of 'a' =D(a) = a^2
2) For two digit number 'ab' duplex of 'ab' = D(a) = 2ab

3) For three digit number 'abc' duplex of 'abc' =D(abc) = $2ac+b^2$
4) For four digit number 'abcd' duplex of 'abcd' =D(abcd) =2ad+2bc

Square of two digit number ab that is ax+b x = 10

$(ab)^2 = (ax+b)^2 = a^2x^2 + 2abx + b^2 = a^2 / 2ab / b^2 =$ D(a) / D(ab) / D(b)

Find the square of following numbers by duplex method

(1) 23, (2) 78, (3) 28, (4) 31, (5) 54, (6) 83, (7) 7.4, (8) 44, (9) 91, (10) 39

Square of three digit number abc that is $ax^2 + bx + c$

$(abc)^2 = (ax^2 + bx + c)^2 = a^2x^4 + 2abx^3 + (2ac + b^2) x^2 + 2bcx + c^2$

$= a^2 / 2ab / (2ac + b^2) / 2bc / c^2$

= D(a) / D(ab) / D(abc) / D(bc) / D(c)

Find the square of following numbers by duplex method

(1) 103, (2) 624, (3) 567, (4) 9.38, (5) 220, (6) 396, (7) 481, (8) 808, (9) 514, (10) 286

Square of four digit number abcd

$(abcd)^2 = (ax^3 + bx^2 + cx + d)^2$

$= a^2 / 2ab / (2ac + b^2) / (2ad+2bc) / (2bc + c^2) / 2cd / d^2$

= D(a) / D(ab) / D(abc) / D(abcd) / D(bcd) / D(cd) / D(d)

Find the square of following numbers by duplex method

(1) 1111, (2) 2308, (3) 8568, (4) 36.68, (5) 2219, (6) 2694, (7) 4186, (8) 7059

Special cases

1) Yavadunam used when numbers are nearer to 10, 100, 1000,……

$(104)^2 = (104+4) / 4^2 = 10816$

Find the square of the numbers 80 to 99 and 101 to120.

2) Ekaadhikena Purvena means one more than the previous

Square of number ending with 5

$(35)^2 = 3*4/ 25 = 1225$

Find the square of following numbers

(1) 65, (2) 475, (3) 1235, (4) 105, (5) 55, (6) 26.5 (7) 355, (8) 6065, (9) 135, (10) 215

3) Squares of numbers near 50, 500 or 5000

Table 1

Base	Number N Near to	Deviation (a)	LP	RP	Digits in RP
100	50	a = N-50	25 + a	a^2	2
1000	500	a = N-500	250 + a	a^2	3
10000	5000	a = N-5000	2500 + a	a^2	4

LP = left part, RP = right part

$54^2 = 25 +4 / 4^2 = 29 / 16 = 2916$ $48^2 = 25 + \bar{2} / \bar{2}^2 = 23/04 = 2304$

Find the square of following numbers

(1) 510, (2) 497, (3) 5015, (4) 4992, (5) 58, (6) 49, (7) 502, (8) 482, (9) 491,

(10) 4995, (11) 5007, (12) 5011

Find the square of following numbers

(1) 39, (2) 199, (3) 604, (4) 2011, (5) 7992, (6) 788, (7) 685, (8) 3021

Find by duplex method

(1) $42^2 + 612^2$, (2) $72^2 - 37^2$, (3) $213^2 + 65^2 - 189^2$, (4) $3241^2 + 4035^2$, (5) $44^2 + 88^2$,

(6) $34.6^2 + 2.35^2$, (7) $49^2 + 14^2 - 49^2$, (8) $231^2 + 425^2$, (9) $45.6^2 + 38.9^2$,

III. SQUARE ROOT OF A NUMBER

There are two methods to find square root of number.

1) Vilokanam means by observation,

2) Dvandvayogah means by adding duplexes

Facts

1) The squares of first nine natural numbers are 1, 4, 9, 16, 25, 36, 49, 64, & 81. Observe that 1, 4, 5, 6, 9 are digits at unit place. Hence no perfect square no has 2, 3, 7 & 8 at its unit place.

2) Square of 1 and 9 has 1 at its unit place. Square of 2 and 8 has 4 at its unit place. Square of 3 and 7 has 9 at its unit place. Square of 4 and 6 has 6 at its unit place. Square of 5 has 5 at its unit place.

3) Conversely for any **perfect square number,** digit at its unit place and 'digit at units' place' of square root are related as follows.

Table 2

Unit place digit of Perfect square number	Unit place digit of Square root
1	1 or 9
4	2 or 8
5	5
6	4 or 6
9	3 or 7

4) Number with odd numbers of zeros as consecutive right most digits is not a perfect square number.

Square root by Vilokanam:- This method is most suitable for perfect square number which has atmost four digit. **Method:- 1)** Group the numbers in two parts. Right part (RP) will consists of unit and tens place and left part will have remaining one or two digits.

2) Select a number p (say) whose square is nearest less than last part.

3) Observe the unit place digit of RP and choose possible unit place digit of square root. Let d_1 and d_2 be the digits as in the table.

4) Then square root of given number is pd_1 or pd_2. Observe $pd_1 \leq p5^2 \leq pd_2$.

5) This comparison gives exact square root.

Find the square root of the following numbers by vilokanam.

(1) 784, (2) 2304, (3) 6561, (4) 5929, (5) 7056, (6) 2025, (7) 1369, (8) 2704, (9) 676 , (10) 4356

Square root by Dwandvayoga:- This method is applicable to evaluate square root of any number. This is the reverse process to find the square of number by dwandvayoga.

1) Group the digits by selecting two at a time from right to left. The left part (LP) may contain one or two digits.

2) Select number 'a' (say) whose square is nearest less than LP and write 'a' as first digit in answer.

3) Find $r = LP - a^2$ and add r*10 to next right place. Select 2a as divisior. Divide the number obtain after adding r*10 by 2a. The quotient is b which is second digit of answer. Remainder is r_1. Add r_1*10 to next right place. Obtain the number by adding r_1*10 . Form which subtract b^2. Divide the remaining number by 2a. The quotient is c which third digit of answer. Remainder is r_2. Add r_2*10 to next right place. Obtain the number by adding r_2*10 . Form which subtract 2bc. Divide the remaining number by 2a. The quotient is d which fourth digit of answer. And the process is continued till we obtain the answer.

Find the Square root of 20439441

	2	0	4	3	9	4	4	1
			40	40	20	10	0	0
				$\bar{2}\,\bar{5}$	$\bar{2}\,\bar{0}$	$\bar{1}\,\bar{4}$	$\bar{4}$	$\bar{1}$
2a = 8_			44	18	9	0	0	0
		4	**5**	**2**	**1**	**0**	**0**	**0**

Square root of 20439441 is $\pm$ 4521

Find the Square root of 1052 up to two decimal places.

1 0	5 2		
	10	30	40 60
		$\bar{4}$	$\bar{1}\bar{6}$ $\bar{2}\bar{8}$
2a = 6_		15	28 24 32
	3	**2. 4**	**3 0**

Square root of 1052 is $\pm$ 32.43

Find the Square root of the following number.

(1) 625, (2) 1521, (3) 61009, (4) 1849, (5) 46225, (6) 32761, (7) 6482116,

(8) 915849

Find the Square root of the following number up to two decimal places.

(1) 58, (2) 45, (3) 652,

IV. CONCLUSIONS

This method has a powerful application of finding the approximate value of irrational numbers (a number which have non recurring and non repeating decimal numbers). Irrational numbers are real numbers and we never obtain its exact value. So we obtain its approximate value always.

V. REFERENCES

[1]. Jagadguru Swami Bharati Krisna Tirthaji Maharaja, Vedic Mathematics, Motilal Banarasidass, Delhi

[2]. V.G.Unkalkar, Magical World of mathematics, Vandana Publishers, Banglore

[3]. Shriram Chauthaiwale and Dr. Ramesh Kollru, Enjoy Vedic Mathematics, Sri Sri Publication, Banglore

National Conference on "Recent Trends in Mathematical Modeling, Simulation Methods, Computations, and Physical Sciences"
(MMSCP-2019), Organised by Hislop College, Nagpur, Maharashtra, India
International Journal of Scientific Research in Computer Science, Engineering and Information Technology
© 2019 IJSRCSEIT | Volume 4 | Issue 4 | ISSN : 2456-3307

Non-Classical Thermoelasticity in a Half Space under the influence of a Heat Source

J. J. Tripathi
Department of Mathematics, Dr. Ambedkar College, Deekshabhoomi, Nagpur, Maharashtra, India

ABSTRACT

A two dimensional problem for an infinite half space is formulated, to study the thermoelastic response due to the presence of a heat source varying periodically with time. The Lord-Shulman theory of thermoelasticity with one relaxation time is considered. The bounding surface is traction free and subjected to a known temperature distribution. Integral transform technique is developed to find the analytic solution in the transform domain by using direct approach. Inversion of transforms is done by employing Gaver-Stehfast algorithm. Mathematical model is prepared for Copper material and numerical results for temperature, displacements and stresses thus obtained are illustrated graphically.

Keywords: Thermoelastic; half-space; Lord-Shulman; heat source.

I. INTRODUCTION

Thermoelastic problems are used to study the thermal stresses in an elastic body under high temperature gradients. The problems of thermoelasticity are broadly classified into two categories, namely static and dynamic problems. The problems dealing with dynamic thermal stresses are fundamentally important in engineering processes and have paved the way for technologies which operate in high temperatures such as nuclear reactors, aerodynamic structures, etc. The classical coupled thermoelasticity theory finds its first mention in Biot [1]. In non-classical theories of thermoelasticity, the Fourier heat conduction equation is generalized with the introduction of one relaxation time obtained by Lord and Shulman [2]. Various authors [3-8] contributed to the problems on generalized thermoelasticity. Recently, a lot of interest has developed in fractional order theory of thermoelasticity [9-15].

In this paper, a non-classical thermoelastic problem in a half space with a heat source is studied. The bounding surfaces are free of all loadings and subjected to a known temperature distribution. Gaver-Stehfast algorithm [7-9] is used to invert the Laplace transforms. All the integrals were evaluated using Romberg's integration technique [10] with variable step size.

II. FORMULATION OF THE PROBLEM

Consider a homogeneous isotropic thermoelastic solid occupying the region $z \geq 0$ and $0 < r < \infty$ .The z-axis is perpendicular to the bounding plane. The problem formulation is under the perview of Lord-Shulman theory of generalized thermoelasticity with one relaxation time. We shall assume that the initial state of the medium is quiescent at a temperature T_0. The surface of the medium is free from mechanical loads and a known temperature distribution is applied. A

heat source is applied on the domain. Cylindrical polar coordinates (r,φ,z) are used.

The problem is thus two-dimensional with all functions considered depending on the spatial variables r and z as well as on the time variable t.

The displacement vector, thus, has the form $\vec{u}=(u,0,w)$.

The equations of motion can be written as

$$\mu\nabla^2 u-\frac{\mu}{r^2}u+(\lambda+\mu)\frac{\partial e}{\partial r}-\gamma\frac{\partial T}{\partial r}=\rho\frac{\partial^2 u}{\partial t^2} \tag{1}$$

$$\mu\nabla^2 w+(\lambda+\mu)\frac{\partial e}{\partial z}-\gamma\frac{\partial T}{\partial z}=\rho\frac{\partial^2 w}{\partial t^2} \tag{2}$$

The generalized equation of heat conduction has the form

$$k\nabla^2 T=\left(\frac{\partial}{\partial t}+\tau_0\frac{\partial^2}{\partial t^2}\right)(\rho C_E T+\gamma T_0 e)-\rho\left(1+\tau_0\frac{\partial}{\partial t}\right)Q \tag{3}$$

where T is the absolute temperature, ρ is the density of the medium, τ_0 is the relaxation time, Q is the heat source and e is the cubical dilatation given by the relation

$$e=\frac{u}{r}+\frac{\partial u}{\partial r}+\frac{\partial w}{\partial z}=\frac{1}{r}\frac{\partial}{\partial r}(ru)+\frac{\partial w}{\partial z} \tag{4}$$

$$\nabla^2=\frac{\partial^2}{\partial r^2}+\frac{1}{r}\frac{\partial}{\partial r}+\frac{\partial^2}{\partial z^2} \tag{5}$$

The following constitutive relations supplement the above equations

$$\sigma_{rr}=2\mu\frac{\partial u}{\partial r}+\lambda e-\gamma(T-T_0) \tag{6}$$

$$\sigma_{zz}=2\mu\frac{\partial w}{\partial z}+\lambda e-\gamma(T-T_0) \tag{7}$$

$$\sigma_{rz}=\mu\left(\frac{\partial u}{\partial z}+\frac{\partial w}{\partial r}\right) \tag{8}$$

We shall use the following non-dimensional variables

$$r'=c_1\eta r,\ z'=c_1\eta z,\ u'=c_1\eta u,\ w'=c_1\eta w,\ t'=c_1^2\eta t,$$

$$\tau_0'=c_1^2\eta\tau_0,\ \sigma_{ij}'=\frac{\sigma_{ij}}{\mu},\ \theta=\frac{\gamma(T-T_0)}{(\lambda+2\mu)},\ Q'=\frac{\rho\gamma Q}{k c_1^2\eta^2(\lambda+2\mu)}$$

where $\eta=\frac{\rho c_E}{k}$, $c_1=\sqrt{\frac{\lambda+2\mu}{\rho}}$ is the speed of propagation of isothermal elastic waves.

Using the above non-dimensional variables, the governing equations take the form (dropping the primes for convenience)

$$\nabla^2 u-\frac{u}{r^2}+(\beta^2-1)e-\beta^2\frac{\partial\theta}{\partial r}=\beta^2\frac{\partial^2 u}{\partial t^2} \tag{9}$$

$$\nabla^2 w+(\beta^2-1)\frac{\partial e}{\partial z}-\beta^2\frac{\partial\theta}{\partial z}=\beta^2\frac{\partial^2 w}{\partial t^2} \tag{10}$$

$$\nabla^2\theta=\left(\frac{\partial}{\partial t}+\tau_0\frac{\partial^2}{\partial t^2}\right)(\theta+\varepsilon e)-\left(1+\tau_0\frac{\partial}{\partial t}\right)Q \tag{11}$$

while the constitutive relations (6)-(8), becomes

$$\sigma_{rr}=2\frac{\partial u}{\partial r}+(\beta^2-2)e-\beta^2\theta \tag{12}$$

$$\sigma_{zz}=2\frac{\partial w}{\partial z}+(\beta^2-2)e-\beta^2\theta \tag{13}$$

$$\sigma_{rz}=\left(\frac{\partial u}{\partial z}+\frac{\partial w}{\partial r}\right) \tag{14}$$

Here $\beta^2=\frac{(\lambda+2\mu)}{\mu}$

Combining equations (9) and (11), we obtain upon using equation (5),

$$\nabla^2 e-\nabla^2\theta=\frac{\partial^2 e}{\partial t^2} \tag{15}$$

We assume that the initial state is quiescent, that is, all the initial conditions of the problem are homogeneous.

The thermal and mechanical boundary conditions of the problem at $z=0$ are taken as

$$\theta(r,0,t)=f(r,t),\quad 0<r<\infty \tag{16}$$

$$\sigma_{zz}(r,0,t)=0,\quad 0<r<\infty \tag{17}$$

$$\sigma_{rz}(r,0,t)=0,\quad 0<r<\infty \tag{18}$$

where $f(r,t)$ are known function of r and t.

Eqns. (1)-(18) constitute the generalized thermoelastic formulation of the problem on axisymmetric half space.

III. SOLUTION OF THE PROBLEM

Applying the Laplace transform defined by the relation,

$$\bar{f}(r,z,s)=L\left[f(r,z,t)\right]=\int_0^\infty e^{-st}f(r,z,t)dt \qquad (19)$$

to all the non-dimensional equations (9)-(18), we get,

$$\nabla^2\bar{u}-\frac{\bar{u}}{r^2}+\left(\beta^2-1\right)\bar{e}-\beta^2\frac{\partial\bar{\theta}}{\partial r}=\beta^2 s^2\,\bar{u} \qquad (20)$$

$$\nabla^2\bar{w}+\left(\beta^2-1\right)\frac{\partial\bar{e}}{\partial z}-\beta^2\frac{\partial\bar{\theta}}{\partial z}=\beta^2 s^2\,\bar{w} \qquad (21)$$

$$\left(\nabla^2-s-\tau_0 s^2\right)\bar{\theta}=\left(1+\tau_0 s\right)\left(\varepsilon s\bar{e}-\bar{Q}\right) \qquad (22)$$

$$\left(\nabla^2-s^2\right)\bar{e}=\nabla^2\bar{\theta} \qquad (23)$$

$$\bar{\sigma}_{rr}=2\frac{\partial\bar{u}}{\partial r}+\left(\beta^2-2\right)\bar{e}-\beta^2\bar{\theta} \qquad (24)$$

$$\bar{\sigma}_{zz}=2\frac{\partial\bar{w}}{\partial z}+\left(\beta^2-2\right)\bar{e}-\beta^2\bar{\theta} \qquad (25)$$

$$\bar{\sigma}_{rz}=\left(\frac{\partial\bar{u}}{\partial z}+\frac{\partial\bar{w}}{\partial r}\right) \qquad (26)$$

$$\bar{\theta}=\bar{f}(r,s) \qquad (27)$$

$$\bar{\sigma}_{zz}=\bar{\sigma}_{rz}=0 \qquad (28)$$

Eliminating $\bar{e}$ between the equations (22) and (23), one obtains,

$$\left\{\nabla^4-\left(s^2+s(1+\tau_0 s)(1+\varepsilon)\right)\nabla^2+s^3(1+\tau_0 s)\right\}\bar{\theta}=-\left(1+\tau_0 s\right)\left(\nabla^2-s^2\right)\bar{Q} \qquad (29)$$

After factorization the above equation becomes,

$$\left(\nabla^2-k_1^{\,2}\right)\left(\nabla^2-k_2^{\,2}\right)\bar{\theta}=-\left(1+\tau_0 s\right)\left(\nabla^2-s^2\right)\bar{Q} \qquad (30)$$

where $k_1^{\,2}$ and $k_2^{\,2}$ are the roots with positive real parts of the characteristic equation

$$k^4-\left(s^2+s(1+\tau_0 s)(1+\varepsilon)\right)k^2+s^3(1+\tau_0 s)=0 \qquad (31)$$

The solution of Eq. (30) is written in the form,

$$\bar{\theta}=\bar{\theta}_1+\bar{\theta}_2+\bar{\theta}_p \qquad (32)$$

where $\bar{\theta}_i$ is a solution of the homogenous equation,

$$\left(\nabla^2-k_1^{\,2}\right)\bar{\theta}_i=0 \quad ,i=1,2. \qquad (33)$$

and $\bar{\theta}_p$ is a particular integral of equation (30).

In order to solve the problem, the Hankel transform of order zero with respect to r is used. The Hankel transform of a function $\bar{f}(r,z,s)$ is defined by the relation,

$$\bar{f}^*(\alpha,z,s)=H\left[\bar{f}(r,z,s)\right]=\int_0^\infty \bar{f}(r,z,s)\,r\,J_0(\alpha r)dr \qquad (34)$$

where J_0 is the Bessel function of the first kind of order zero and α is the Hankel transform parameter.

The inversion of Hankel transform is given by the relation

$$\bar{f}(r,z,s)=H^{-1}\left[\bar{f}^*(\alpha,z,s)\right]=\int_0^\infty \bar{f}^*(\alpha,z,s)\,\alpha\,J_0(\alpha r)d\alpha \qquad (35)$$

Applying the Hankel transform to equation (33), we get,

$$\left\{D^2-\left(k_1^{\,2}+\alpha^2\right)\right\}\bar{\theta}_i^*=0 \quad ,i=1,2., \text{ where } D=\partial/\partial z \qquad (36)$$

The solution of the above equation is written in the form

$$\bar{\theta}_i^*=A_i(\alpha,s)\left(k_i^{\,2}-s^2\right)e^{-q_i z} \qquad (37)$$

where $q_i=\sqrt{\alpha^2+k_i^{\,2}}$

Applying Hankel transform to the equation (30), we get,

$$\left(D^2-q_1^{\,2}\right)\left(D^2-q_2^{\,2}\right)\bar{\theta}_p^{\,*}=-(1+\tau_0 s)\left(D^2-q^2\right)\bar{Q}^* \qquad (38)$$

where $q=\sqrt{\alpha^2+s^2}$

The periodically varying heat source $Q(r,z,t)$ in cylindrical co-ordinates is taken in the following form

$$Q(r,z,t)=Q_0\frac{\delta(r)}{2\pi r}.\frac{\sin\pi t}{\tau},\ 0\le t\le\tau \qquad =0 \quad ,\ t>\tau \qquad (39)$$

where Q_0 is the strength of the heat source and $\delta(r)$ is the well known Dirac's delta function.

On applying Laplace transform and Hankel transform to equation (39), we get,

$$\bar{Q}^*=\frac{Q_0\pi\tau\left(1+e^{-s\tau}\right)}{(s^2\tau^2+\pi^2)} \qquad (40)$$

The solution of the equation (38) has the form,

$$\bar{\theta}_p^{\,*}=\frac{(1+\tau_0 s)q^2}{q_1^{\,2}q_2^{\,2}}\frac{Q_0\pi\tau\left(1+e^{-s\tau}\right)}{(s^2\tau^2+\pi^2)} \qquad (41)$$

Then the complete solution in the transformed domain is obtained as

$$\bar{\theta}^*(\alpha,z,s) = A_i(\alpha,s)\left(k_i{}^2 - s^2\right)e^{-q_i z} + \frac{(1+\tau_0 s)q^2}{q_1{}^2 q_2{}^2}\frac{Q_0\pi\tau\left(1+e^{-s\tau}\right)}{(s^2\tau^2+\pi^2)} \quad (42)$$

On applying the inverse Hankel transform to equation (42), we get,

$$\bar{\theta}(r,z,s) = \int_0^\infty \left\{ \sum_{i=1}^{n} A_i(\alpha,s)\left(k_i{}^2 - s^2\right)e^{-q_i z} + \frac{(1+\tau_0 s)q^2}{q_1{}^2 q_2{}^2}\frac{Q_0\pi\tau\left(1+e^{-s\tau}\right)}{(s^2\tau^2+\pi^2)} \right\} \alpha J_0(\alpha r)\, d\alpha \quad (43)$$

Similarly eliminating θ between equations (22) and (23), we get,

$$\left(\nabla^2 - k_1{}^2\right)\left(\nabla^2 - k_2{}^2\right)\bar{e} = -(1+\tau_0 s)\nabla^2\bar{Q} \quad (44)$$

On applying Hankel transform to equation (44), we get,

$$\left(D^2 - q_1{}^2\right)\left(D^2 - q_2{}^2\right)\bar{e}^* = -(1+\tau_0 s)\left(D^2 - \alpha^2\right)\bar{Q}^* \quad (45)$$

Complete solution of equation (45) is obtained as,

$$\bar{e}^*(\alpha,z,s) = \sum_{i=1}^{2} A_i(\alpha,s)\,k_i{}^2 e^{-q_i z} + \frac{(1+\tau_0 s)\alpha^2}{q_1{}^2 q_2{}^2}\frac{Q_0\pi\tau\left(1+e^{-s\tau}\right)}{(s^2\tau^2+\pi^2)} \quad (46)$$

Taking the inverse Hankel Transform to equation (46), one obtains,

$$\bar{e}(r,z,s) = \int_0^\infty \left\{ \sum_{i=1}^{2} A_i(\alpha,s)\,k_i{}^2 e^{-q_i z} + \frac{(1+\tau_0 s)\alpha^2}{q_1{}^2 q_2{}^2}\frac{Q_0\pi\tau\left(1+e^{-s\tau}\right)}{(s^2\tau^2+\pi^2)} \right\} \alpha J_0(\alpha r)\, d\alpha$$

Applying Hankel transform to equation (21) and then using equations (42) and (46), the axial displacement component is obtained as,

$$\bar{w}^*(\alpha,z,s) = B(\alpha,s)\, e^{-q_3 z} - \sum_{i=1}^{2} A_i(\alpha,s)\,q_i e^{-q_i z} \quad (48)$$

where $q_3 = \sqrt{\alpha^2 + \beta^2 s^2}$

On applying the inverse Hankel transform to equation (48), we get,

$$\bar{w}(r,z,s) = \int_0^\infty \left\{ B(\alpha,s)\, e^{-q_3 z} - \sum_{i=1}^{2} A_i(\alpha,s)\,q_i e^{-q_i z} \right\} \alpha J_0(\alpha r)\, d\alpha \quad (49)$$

Applying the Hankel transform to equation (20) and using equations (42), (46) and (48), we get,

$$H\left[\frac{1}{r}\frac{\partial}{\partial r}(r\bar{u})\right] = \begin{Bmatrix} B(\alpha,s)\,q_3\, e^{-q_3 z} \\ -\alpha^2\left[\sum_{i=1}^{2} A_i(\alpha,s)\, e^{-q_i z} - \frac{(1+\tau_0 s)}{q_1{}^2 q_2{}^2}\frac{Q_0\pi\tau\left(1+e^{-s\tau}\right)}{(s^2\tau^2+\pi^2)} \right] \end{Bmatrix} \quad (50)$$

On applying inverse Hankel transform to equation (50), one obtains,

$$\bar{u} = \int_0^\infty \left\{ \begin{matrix} B(\alpha,s)\,q_3\, e^{-q_3 z} \\ -\alpha^2\left[\sum_{i=1}^{2} A_i(\alpha,s)\, e^{-q_i z} - \frac{(1+\tau_0 s)}{q_1{}^2 q_2{}^2}\frac{Q_0\pi\tau\left(1+e^{-s\tau}\right)}{(s^2\tau^2+\pi^2)} \right] \end{matrix} \right\} J_1(\alpha r)\, d\alpha \quad (51)$$

On using equations (43), (47), (49) and (51) in equations (25) and (26), we obtain the stress components as,

$$\bar{\sigma}_{zz} = \int_0^\infty \left\{ \begin{matrix} -2B(\alpha,s)\,q_3\, e^{-q_3 z} \\ +\left(\alpha^2 + q_3{}^2\right)\left[\sum_{i=1}^{2} A_i(\alpha,s)\, e^{-q_i z} - \frac{(1+\tau_0 s)}{q_1{}^2 q_2{}^2}\frac{Q_0\pi\tau\left(1+e^{-s\tau}\right)}{(s^2\tau^2+\pi^2)} \right] \end{matrix} \right\} \alpha J_0(\alpha r)\, d\alpha$$

$$\bar{\sigma}_{rz} = \int_0^\infty \left\{ \begin{matrix} -\left(1+q_3{}^2\right)B(\alpha,s)\, e^{-q_3 z} \\ +\left[\sum_{i=1}^{2} A_i(\alpha,s)\, q_i(1+\alpha^2) e^{-q_i z} \right] \end{matrix} \right\} J_1(\alpha r)\, d\alpha \quad (53)$$

After applying the Hankel transform to equations (27) and (28), the boundary conditions take the form,

$$\bar{\theta}^*(\alpha,0,s) = \bar{f}^*(\alpha,s) \quad (54)$$

$$\bar{\sigma}_{zz}^*(\alpha,0,s) = \bar{\sigma}_{rz}^*(\alpha,0,s) = 0 \quad (55)$$

On applying the boundary conditions (54) and (55) to equations (43), (52) and (53), the system of linear equations involving unknown parameters $A_1(\alpha,s), A_2(\alpha,s)$ and $B(\alpha,s)$ are obtained as follows,

$$\sum_{i=1}^{n} A_i(\alpha,s)\left(k_i{}^2 - s^2\right) + \frac{(1+\tau_0 s)q^2}{q_1{}^2 q_2{}^2}\frac{Q_0\pi\tau\left(1+e^{-s\tau}\right)}{(s^2\tau^2+\pi^2)} = \bar{f}^*(\alpha,s) \quad (56)$$

$$-2B(\alpha,s)\,q_3 + \left(\alpha^2 + {q_3}^2\right)\left[\begin{array}{l}\sum_{i=1}^{2} A_i(\alpha,s) \\ -\dfrac{(1+\tau_0 s)}{{q_1}^2 {q_2}^2}\dfrac{Q_0\pi\tau\left(1+e^{-s\tau}\right)}{(s^2\tau^2+\pi^2)}\end{array}\right] = 0 \qquad (57)$$

$$-\left(1+{q_3}^2\right)B(\alpha,s) + \left[\sum_{i=1}^{2} A_i(\alpha,s)\; q_i(1+\alpha^2)\right] = 0 \qquad (58)$$

On solving the system of linear equations (56) - (58) unknown parameters are determined and the complete solution of the problem is obtained in the Laplace transform domain.

IV. INVERSION OF DOUBLE TRANSFORMS

Due to the complexities involved in the inversion of the Laplace transforms, we employ a numerical scheme based on Gaver-Stehfast algorithm. Gaver [16] and Stehfast [17 ,18] derived the formula given below. By this method the inverse $f(t)$ of the Laplace transform $\bar{f}(s)$ is approximated by,

$$f(t) = \frac{\ln 2}{t}\sum_{j=1}^{K} D(j,K)\,F\left(j\frac{\ln 2}{t}\right) \qquad (59)$$

With

$$D(j,K) = (-1)^{j+M}\sum_{n=m}^{\min(j,M)} \frac{n^M (2n)!}{(M-n)!\,n!\,(n-1)!\,(j-n)!\,(2n-j)!} \qquad (60)$$

where K is an even integer, whose value depends on the word length of the computer used. $M = K/2$ and m is the integer part of the $(j+1)/2$. The optimal value of K was chosen as described in Gaver-Stehfast algorithm, for the fast convergence of results with the desired accuracy. The Romberg numerical integration technique [19] with variable step size was used to evaluate the integrals involved. All the programs were made in mathematical software Matlab.

V. NUMERICAL CALCULATIONS

$$f(r,t) = \theta_0 H(a-r)H(t) \qquad (61)$$

where θ_0 is a constant temperature, $H(.)$ is a Heaviside unit step function.

On applying Hankel and Laplace transform to equation (61), we get,

$$\bar{f}^*(\alpha,s) = \frac{a\theta_0 J_1(\alpha a)}{\alpha s} \qquad (62)$$

For the purpose of illustration, a mathematical model is prepared for a Copper material with the following material properties,

$k = 386\,J.K^{-1}.m^{-1}.s^{-1}$, $\alpha_t = 1.78\times10^{-5}K^{-1}$, $C_E = 383.1\,J.Kg^{-1}.K^{-1}$, $\mu = 3.86\times10^{10}\,N.m^{-2}$, $\lambda = 7.76\times10^{10}\,N.m^{-2}$, $\rho = 8954\ kg.m^{-3}$ $\tau_0 = 0.02s$, $T_0 = 293\ K$, $\varepsilon = 0.0168\,N.m.J^{-1}$, $c_1 = 4.158\times10^{3}\,m.s^{-1}$ $,\eta = 8886.73\,s.m^{-2}$, $\beta^2 = 4$, $a = 1$, $\theta_0 = 1$, $b = 1$.

The numerical values for temperature θ and the axial stress component σ_{zz} have been calculated for different time instants $t = 0.1, 0.4, 1$, along the radial direction and are displayed graphically for Lord-Shulman theory (L-S theory) and the particular case of Classical Coupled thermoelasticity (CT theory) as shown in figure 1-2 respectively .

Figure 1 depicts the non-dimensional temperature distribution along the radial direction at different time instants. The variation in values observed for the two theories (CT and LS) in the plots. Due to the application of the heat source, it is observed that the values of non-dimensional temperature θ drops gradually along the radial direction till $r = 5.2$ and then it increases till $r = 7$.

Figure 2 describes the axial stress σ_{zz} along the radial at different time instants. Different profiles of axial stress are seen at small times (i.e. at $t = 0.1, 0.4$) and large times (i.e. at $t = 1$). The difference in results for LS and CT is observed.

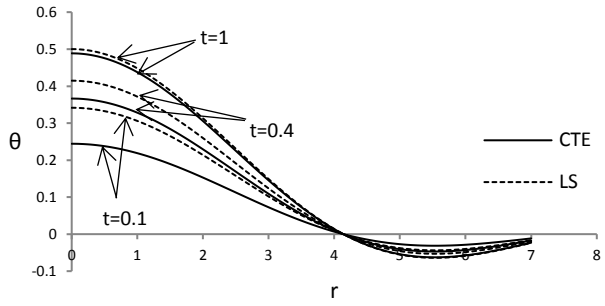

Figure 1. Distribution of dimensionless temperature along radial direction.

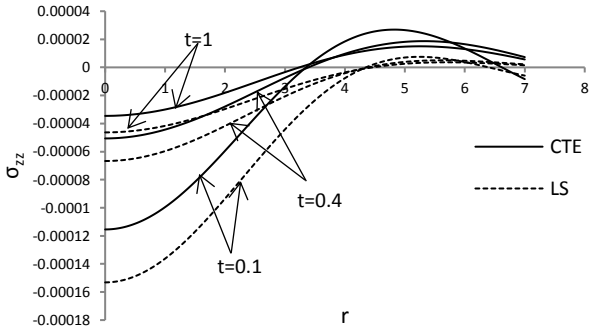

Figure 2. Distribution of dimensionless axial stress along radial direction.

VI. CONCLUSION

A problem in non-classical thermoelasticity (LS model) is formulated for half space with a heat source and the results are compared for the model with CT. It is observed that the non-dimensional temperature and axial stress component along the radial direction predicts changes for small and large times. This type of behaviour of the variables is observed due to the presence of the periodically varying heat source distributed over the radial direction. Due to the presence of relaxation parameter in the field equations, the heat wave assumes finite speed of propagation. Finally, it is concluded that the solutions in this problem will prove to be useful to determine the thermal behaviour in important engineering problems by using the more realistic non-classical model of thermoelasticity.

VII. REFERENCES

[1]. M. Biot, "Thermoelasticity and irreversible thermodynamics," J. Appl. Phys., 27, 240- 253, 1956.

[2]. H. Lord, Y. Shulman, "A generalized dynamical theory of thermo-elasticity," J. Mech. Phys. Solids, 15, 299–309, 1967.

[3]. J. J. Tripathi, G. D. Kedar, K. C. Deshmukh, "Theoretical study of disturbances due to mechanical source in a generalized thermoelastic diffusive half space," International Journal of Chemical Engineering, Vol. 2(1), pp. 73-77, 2015.

[4]. J. J. Tripathi, G. D. Kedar, K. C. Deshmukh , "Dynamic Problem of Generalized Thermoelasticity for a Semi-infinite Cylinder with Heat Sources," Journal of Thermoelasticity, 2(1), 01-08, 2014.

[5]. J. J. Tripathi, G. D. Kedar, K. C. Deshmukh, "Generalized thermoelastic diffusion problem in a thick circular plate with axisymmetric heat supply," Acta Mechanica, 226, 2121-2134, 2015. doi: 10.1007/s00707-015-1305-7.

[6]. J. J. Tripathi, G. D. Kedar, K. C. Deshmukh, "Two dimensional generalized thermoelastic diffusion in a half space under axisymmetric distributions," Acta Mechanica, 226(10), 3263-3274, 2015. doi: 10.1007/s00707-015-1383-6.

[7]. J. J. Tripathi, G. D. Kedar, K. C. Deshmukh, Generalized thermoelastic diffusion problem in a thick circular plate with axisymmetric heat supply due to heat source, Alexandria Engineering Journal, Elsevier, 2016. DOI: 10.1016/j.aej.2016.06.003.

[8]. J. J. Tripathi, G. D. Kedar, K. C. Deshmukh, "Generalized Thermoelastic Problem of a Thick Circular Plate Subjected to Axisymmetric Heat Supply," Journal of Solid Mechanics, Vol. 8, issue 3, pp. 578-589, 2016.

[9]. M. A. Ezzat, A. S. El-Karamany, Fractional order theory of a perfect conducting

thermoelastic medium, Can. J. Phys., 89, 311-318, 2011.

[10]. H. H. Sherief, A. El-Sayed, A. A. El-Latief, Fractional order theory of thermoelasticity, Int. J. Solids Struct., 47, 269–275, 2010.

[11]. J. J. Tripathi, G. D. Kedar, K. C. Deshmukh, "Dynamic problem of fractional order thermoelasticity for a thick circular plate with finite wave speeds," Journal of Thermal Stresses 39 (2), 220-230, 2016.

[12]. JJ Tripathi, SD Warbhe, KC Deshmukh, J Verma, Fractional Order Thermoelastic Deflection in a Thin Circular Plate, Applications and Applied Mathematics: An International Journal 12 (2), 898-909.

[13]. JJ Tripathi, SD Warbhe, KC Deshmukh, J Verma, Fractional Order Theory of Thermal Stresses to A 2 D Problem for a Thin Hollow Circular Disk, Global Journal of Pure and Applied Mathematics 13 (9), 6539-6552.

[14]. JJ Tripathi, SD Warbhe, KC Deshmukh, J Verma, Fractional Order Theory of Thermal Stresses to A 2 D Problem for a Thin Hollow Circular Disk, Global Journal of Pure and Applied Mathematics 13 (9), 6539-6552, 2017.

[15]. Jitesh Tripathi, Shrikant Warbhe, K.C. Deshmukh, Jyoti Verma, (2018) "Fractional order generalized thermoelastic response in a half space due to a periodically varying heat source", Multidiscipline Modeling in Materials and Structures, Vol. 14 Issue: 1, pp.2-15, https://doi.org/10.1108/MMMS-04-2017-0022

[16]. D. P. Gaver, "Observing Stochastic processes and approximate transform inversion," Operations Res., 14, 444-459, 1966.

[17]. H. Stehfast, "Algorithm 368: Numerical inversion of Laplace transforms," Comm. Ass'n. Comp. Mach., 1970, 13, 47-49, 1970.

[18]. H. Stehfast, "Remark on algorithm 368, Numerical inversion of Laplace transforms", Comm. Ass'n. Comp., 13, 624, 1970.

[19]. W. H. Press , B. P. Flannery, S. A. Teukolsky, W. T. Vetterling, Numerical Recipes, Cambridge University Press, Cambridge, the art of scientific computing ,1986.

Appendix:

Nomeclature:

r Radius

t Time

T Temperature

T_0 Reference temperature

θ Temperature change

$Q(r,z,t)$ Heat source

k Thermal conductivity of material

η Dimensionless characteristic length

c_1 Speed of propagation of the longitudinal wave

u Radial displacement component

w Axial displacement component

$\sigma_{rr}, \sigma_{zz}, \sigma_{rz}, \sigma_{\varphi\varphi}$ Components of stress function

E Young's modulus

ρ Density

C_E Specific heat at constant strain

μ, λ Lamé's constants

L Laplace transform

δ Dirac delta function

(r,ϕ,z) Cylindrical polar coordinates

τ_0 Relaxation times

e Cubical dilatation

$H(.)$ Heaviside unit step function

National Conference on "Recent Trends in Mathematical Modeling, Simulation Methods, Computations, and Physical Sciences"
(MMSCP-2019), Organised by Hislop College, Nagpur, Maharashtra, India
International Journal of Scientific Research in Computer Science, Engineering and Information Technology
© 2019 IJSRCSEIT | Volume 4 | Issue 4 | ISSN : 2456-3307

Hexagonal Ferrite with their Structural Studies

B. T. Borkar[1], S. R. Choubey[1], L. P. Damodare[1], A. B. Borkar[2], G. C. Vandile[1], Hitesha B. Bobade[1]

[1]Department of Physics, VMV Commerce JMT Arts & JJP Science College, Wardhaman Nagar, Nagpur, Maharashtra, India

[2]Institude of Chemical Technology, Mumbai Matunga, Maharashtra, India

ABSTRACT

The calcium ferrite nano-particle Ca Al1.5Fe10.5O19 were synthesized using a ceramic method to investigate its properties. Ferrite are large class of oxides with astonishing magnetic proparties. Which have been investigated and applied for the past 50 yaers. The application of ferrite are based on very basic properties of ferrites; such as significant saturation magnetisation high electrical resistivity, low electoral losses, and good chemical stability. ferrite can be obtained in different crystal systems by many methods. The prepared power was characterized by using X-ray diffraction (XRD), Scanning Electronic microscope (SEM). XRD shows hexagonal Magnetoplumbite (M) type structure having unit cell dimension 'a' and 'b' varies betweem and . The Sem imager of the sample prepare appear irregular in shape but nearly vertically and seemed to be hexagonal plate like structure.

Keyword : Hexagonal ferrite (Hexaferrite), X-ray Diffraction (XRD), Scanning Electrons Microscope (SEM), Magnetoplumbite (M-type), Calcium oxide and Iron Oxide

I. INTRODUCTION

Ferromagnetic material are usually Known as Ferrites. With the discovery of hexagonal ferrite[1] . there has been an extensive study of ferromagnetism of such compound because of their applications in the field of material science as a permanent magnetoplumbite with general formula M (Fe12O19) where M is usually barium, strontium, Calcium or Lead, are interesting and attracting researchers due to their specific magnetic behavior. The basic structure consists of 38 oxygen ions occupying the interstitial sites forming a close packed hexagonal structure. 24 ferric ions occupy five different locations in the unit cell [2].

To prepared Hexagonal ferrite nanoparticles, various synthesis methods such as chemical co-precipitation [3], Hydrothermal[4], Sol-gel [5],Solution combustion method [6], ceramic method etc. have been developed.In the present work, Calcium hexaferrites substituted with trivalent Al ions synthesized in ceramic method.Their structural properties are studied and reported.

Experiment:

Synthesis:- The preparation of compounds with chemical formula $CaAl_xFe_{12-x}O_{19}$ (with x=1.5) is perform by standard ceramic method. The molecular concentration x is substituted cation in the chemical formula. The oxides Cao,Al_2O_3, Fe_2O_3 of merck grade (with 99.90%) were used as starting materials for the synthesis of present series of compounds. The stoichmetric proportion of weight oxides were mixed thoroughly by grinding for 3days in agate morter with help of acetone ultra-fine homogeneous powder

of sample. the resulting powder pre-sintered at 200°c for half hours to moisture free homogeneous, calcination. The calcination powder were pressed into the pallet machine to form pallet at 7.5kg/cm^2 and then sintered at 1130°c in air atmosphere for about 74 hours and slowly cooled to room temperature at the rate of 200^{0}c/half hours using a microprocessor controlled furnace [10]. The synthesized pallet were broken with hydraulic pressure of pallet machine at 1.20 tone kg/cm^2. Then grinding in agate mortar to get ultra-fine powder of sample. The synthesized powder of sample. The synthesized powder of sample again heated at 300^{0}C for 30minute to remove impurity[11].

Characterization:

- X-ray Diffraction Pattern of $CaAl_{1.5}Fe_{10.5}O_{19}$ hexagonal ferrite under investigation were obtained using X-ray Diffractometer.
- Determination of grain size and Aspect Factor Form SEM data.

II. RESULT AND DISCUSSION:

Structural analysis: The XRD pattern of Ca $Al_{1.5}Fe_{10.5}O_{19}$ powder (fig 1) investigated ferrite sample synthesized by ceramic method correnspond to M-type calcium hexaferrite structure fig1 JCPDS pattern file no. 27-1029. The hexagonal M-type structure with space group (SG:$P6_3/mmc$) (NO.194), which confirms that phase belonges to magnetoplumbite, indicating that the crystal structure were single phase hexagonal magnetoplumbite after substitution with Al^{+3} ions respectively. The lattice constant a and c of hexagonal calcium ferrite were calculated using equation (1).

$$\frac{1}{d^2}=\frac{4(h^2+k^2+hk)}{3a^2}+\frac{l^2}{c^2} \text{----------(1)}$$

Where h, k, l are miller indices, d is interplanar distance. The lattice parameter a and c found to be 5.6463 A^0 and 22.7163 A^o respectively. The crystallite size measurements of were also carried out using the XRD data and using scherrer equation.

$$D=\frac{k\lambda}{\beta cos\theta} \text{----------(2)}$$

Where β is width of the observed diffraction peak at its half maximum intensity, K is the space factor which take value of about 0.9 & λ is the wavelength (Cuk radiation equation to 1.54 A^0) And the average particle size was found to be about nm.

Table 1

Sample	A (Å)	C (Å)	Particle size D)nm	Volume (A^3)
Ca $Al_{1.5}$ $Fe_{10.5}O_{19}$	5.6463	22.7162	48.87	627.614

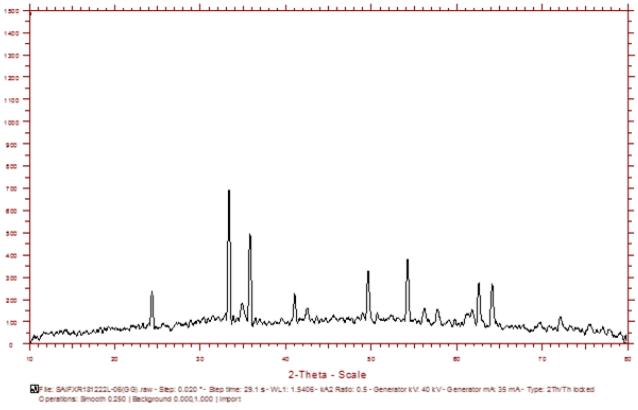

Figure 1. X- ray Diffraction of Ca $Al_{1.5}$ $Fe_{10.5}$ O_{19}

Table 2. Observation table for X-R-D result

Sr. No	2θ	D value (A)	Observe Intensity count	Intensity in %	(h,k,l)
1	24.276	3.6635	234	337	(1 1 2)
2	33.318	2.68705	694	100	(1 1 3)
3	35.771	2.50817	494	712	(2 2 2)

4	41.018	2.19874	102	146	(0 1 4)
5	49.606	1.83825	326	47	(2 2 4)
6	62.578	1.483319	274	39.5	(0 1 6)
7	64.153	1.45052	267	38.4	(1 1 6)

SEM Studies:

The Scanning Electronmicroscopy (SEM) Fig. shows the morphological information of the hexagonal ferrite containing irregular grain, but nearly vertically arranged shape flakes. The particles seemed to be hexagonal plate like mould which spreed out homogeneously were examined by [8-9] ceramic method.

Figure 2 shows the representative SEM micrographs of fractured surface of Al- Substituted sintered CaM the micrograph Shows that Al-substitution reduce the particle size. Al Substituted Calcium Hexaferrite. Aspect Factor calculated from following reaction.

Aspect Factor = $\frac{lenght}{diameter}$

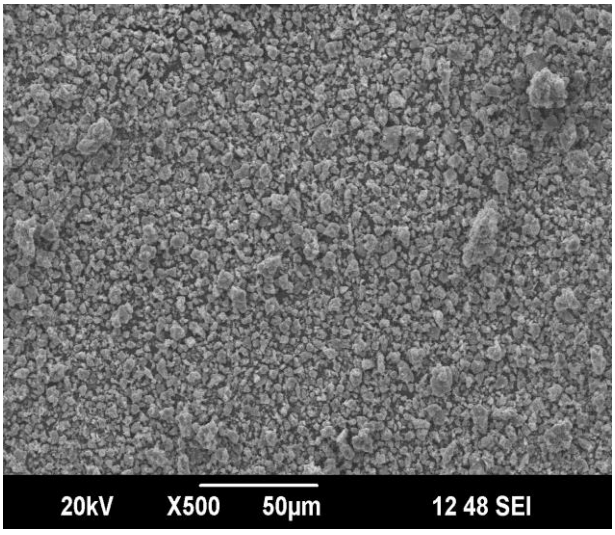

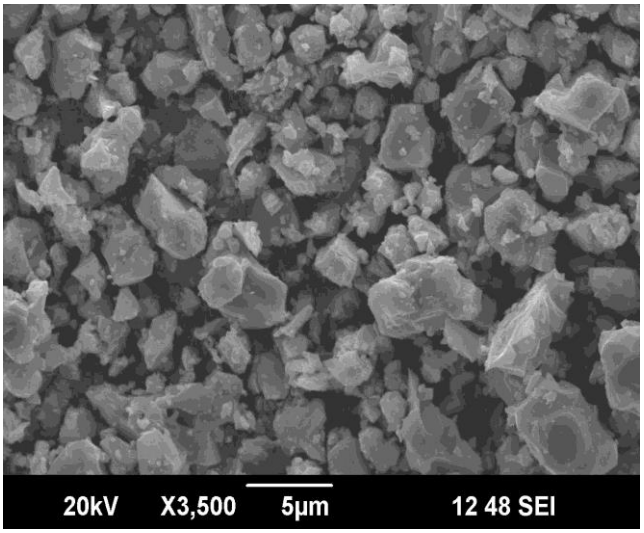

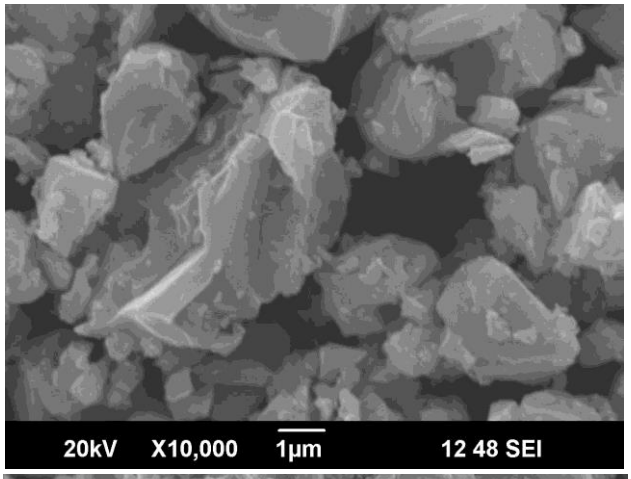

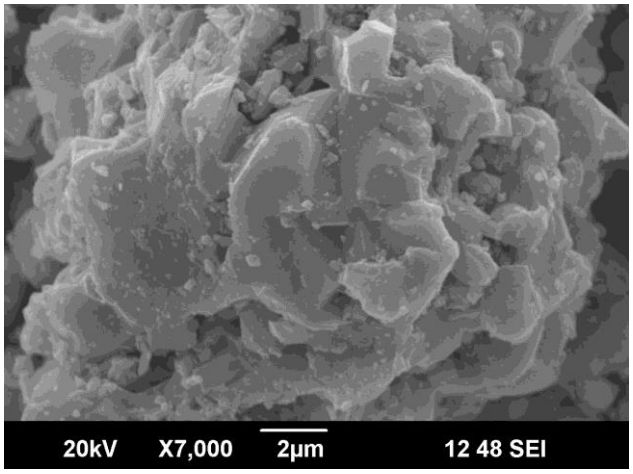

Figuer 2. SEM images of $CaAl_{1.5}Fe_{10.5}O_{19}$

Table 3

sample	particle size	Aspect Factor
$CaAl_{1.5}Fe_{10.5}O_{19}$	865.6	2.5312

III. CONCLUSION

Al Substituted $CaAl_xFe_{12-x}O_{19}$ (with x=1.5) Calcium hexaferrite have been prepared by standard ceramic method. The XRD confirms that Calcium hexaferrite have hexagonal Structure and single phase. the cystallite size is reduce due to less ionic radius of Aluminum. Lattice constant also found to decreases with substitution. Particle size is determined by shcerrer formula. Substitution of Aluminum increase with increasing particle size.

IV. ACKNOWLEDGEMENT

The authors thanks to Sphisticated test and instrumentation Centre, STIC, Cochin university Keral, India for giving us best results for X-ray diffraction (XRD) and Scaninng electron microscope (SEM) in needed hour. The authors are also thankful to the management, principle Prof. Dr.K.P.Kariya of VMV College also thanks for providing the basic facilities of synthesis of the sample.

V. REFERENCES

[1]. V. Adelskold, Arkiv Kemi Min. Geol 1938, 12/A/29, 1.

[2]. H. Kojima, K. Goto, in Proceeding of Inter Conference on Ferrites, Center for Academic publication, Japan, 198 p. 335.

[3]. Ataei A. and Heshmati- Manesh S.J. European Ceram. Soc., 21, 1951- 1955 (2001).

[4]. Wang J.F., Paton C.B., Ciossinger R., Harris I.R. J. Alloys. Compd., 369, 170-177 (2004).

[5]. Jotania R.B., Khomane R.B., Chauhan C.C., Menon S.K., Kulkari B.D. J. Magn. Magn. Mater. 310, 2477-2479 (2002).

[6]. Junliang L., Yanwei Z., Cuijing C., WeiZ., Xiaowei Y. J. European Ceram. Soc., 30, 993-997 (2010).

[7]. J. Huang, H. Zhuang, W. Li, J. Magn. Magn. Mater. 256 390 (2003).

[8]. Khalid Mehmood Ur .Rehman. Xionzong Lia. Shaongjiu Ferg. Mohanmmad Wasim Khau. Z. Wazir. Zhang Zogyang J. Supercond nov Magn. DOI 10.1007/S 10948-017-4272-5 Springer Sciences LLC 2017.

[9]. Chaocheng Liu, Xiansong Lia, Shuangiu Feng, Khalid Mehmood Ur Rehman, Mingling Li, Cong Zanug, Hoohao Li, Xiangyu Meng. Journal of Magnetism and magnetic Materials (2017), 2017.08.079.

[10]. Gleiter H. Nanocrystalline material Prog. Matter Sci. 1989,33,223-230

[11]. S. Sugimoto, K.Haga, T. Kagotani and K. Inonato, “Microwave absorption properties of Ba M-type ferrite prepared by a modified co-precipitation method”, Journal of magnetism and magnetic materials, Vol.290,PPP.1188-1191(2205).

National Conference on "Recent Trends in Mathematical Modeling, Simulation Methods, Computations, and Physical Sciences"
(MMSCP-2019), Organised by Hislop College, Nagpur, Maharashtra, India
International Journal of Scientific Research in Computer Science, Engineering and Information Technology
© 2019 IJSRCSEIT | Volume 4 | Issue 4 | ISSN : 2456-3307

X-ray Diffraction Studies of Synthesized M-type Compound

Deoshri A. Mahajan[1], S. R. Choubey[1], B. T. Borkar[1], L. P. Damodare[1], A.B. Borkar[2] , G. C. Vandile[1]
[1]Department of Physics, VMV Commerce JMT Arts & JJP Science College, Nagpur, Maharashtra, India
[2]Institute of Chemical Technology, Mumbai Matunga, Maharashtra, India

ABSTRACT

M-type calcium Hexaferrites with Substituted of Trivalent Aluminum ions (Al^{+3}) substituted $CaAl_6Fe_6O_{19}$ were synthesized by Standard ceramic method. The Characterization by using various instrument Techniques. The structural studied of the sample were studied by using X-ray Diffraction (XRD), and Scanning Electron Microscope (SEM). XRD shows hexagonal magnetoplumbite M-type structuring and having unit cell dimension 'a=b' & 'c' varies between 5.7639Å & 22.31Å. The SEM Morphology of the particle was studied & particle size was confirmed using SEM.

Keyword: Hexagonal ferrites (hexaferrite), X-ray Diffraction (XRD), Scanning Electron Microscope (SEM).

I. INTRODUCTION

Hexagonal ferrites (Also known as hexaferrites), were discovered in the 1938 at V. Adelskold [1]. Since then, the degree of interest in these ferrites has been increasing exponentially due to their cost effectiveness and suitability for a wide range of industrial and technological application [2-9]. Hexaferrite are industrially important material that have numerous technological application such as permanent magnets, microwave device, magnetic recording media and magneto-optical device. Magnetoplumbite (M) type is a hard ferromagnetic material possessing hexagonal structure which was first observed by the general Chemical formula by which M-type hexaferrite are represented is $MFe_{12}O_{19}$[10]. The basic structure of magnetoplumbites consists of 38 oxygen and 24 ferric ions.

All ferric ions occupy five different locations in the unit cell such as 2a, $4f_2$ and 12k, which are octahedral sites, $4f_1$-tetrahedral and 2b-bipyramidal sites [11-14].The magnetic properties of magnetoplumbites are determined by the substituted trivalent ions for ferric ions, which occupy different sites in the structure [15]. When doped with other trivalent metal ions, the magnetic properties of the calcium ferrite would get altered [16-17]. There are many methods for synthesis of Hexagonal ferrite nanoparticles [18].In the present work, Calcium hexaferrites doped with trivalent Al ions with general formula $CaAl_xFe_{12-x}O_{19}$(x=6) have been synthesized successfully by Standard ceramic method.

II. EXPERIMENTAL DETAILS

Synthesis:

The preparation of compounds with chemical formula $CaAl_xFe_{12-x}O_{19}$ (with x=6) by standard ceramic method. The molecular concentration x substituted cations in the chemical formula. The oxides CaO, Al_2O_3, Fe_2O_3 of Merck grade (with 99.90% purity) were used as starting material for the synthesis of present series of compounds. The stoichmetric proportion of weight oxides were mixed thoroughly by grinding for 6 hours in agate mortar

with help of acetone to get ultra-fine homogeneous powder of sample. The resulting powder pre-sintered at 200^0c for half hours to moisture free, homogeneous, calcinations. The calcination powder were pressed into the pellet machine to form pellet at 75 tons kg/cm^2 and then sintered at 1130^0c in air atmosphere for about 72 hours and slowly cooled to room temperature at the rate of 200^0c /half hours using a microprocessor controlled furnace. The synthesized pellet break with hydraulic pressure of pellet machine at 120 kg/cm^2 . Then grinding in agate mortar to get ultra-fine powder of sample. The synthesized powder of sample again heated at 300^0c for 30 minute to remove impurity.

Characterization:

- X-ray diffraction pattern of $CaAl_6Fe_6O_{19}$ hexagonal ferrite under investigation were obtained using X-ray Diffractometer.
- Determination of grain size and aspect factor from SEM data.

III. RESULT AND DISCUSSION:

Structural analysis: The XRD pattern of $CaAl_6Fe_6O_{19}$ powder (fig1) investigated ferrite sample synthesized by ceramic method correspond to M-type calcium hexaferrite structure fig (1). The hexagonal M-structure with space group (SG:P63/mmc) (No. 194), which confirms that phase belongs to magnetoplumbite, indicating that the crystal structure were single phase hexagonal magnetoplumbite after substitution with La^{3+} ions respectively. The lattice constant a and c of hexagonal calcium ferrite were calculated using equation (1)

$$\frac{1}{d2} = \frac{4(h^2+k^2+hk)}{3a^2}+\frac{l^2}{c^2} \text{ ----------(1)}$$

Where h, k, l are miller indices, d is interplaner distance. The lattice parameter a and c found to be 5.7639 and 22.31 respectively. The crystallite size measurements were also carried out using the XRD data and using scherrer equation

$$D = \frac{k\lambda}{\beta cos\theta} \text{ ---------- (2)}$$

Where β is width of the observed diffraction peak at its half maximum intensity, K is the space factor which take value of about 0.94 & is the wavelength (Cu). And the average particle size was found to be about 46.49nm.

Table 1

Sample	a (Å)	c (Å)	Particle size (D)nm	Volume (Å^3)	Maximum intensity	c/a ratio
$CaAl_6Fe_6O_{19}$	5.7639	22.31	46.49	641.89	735	3.8706

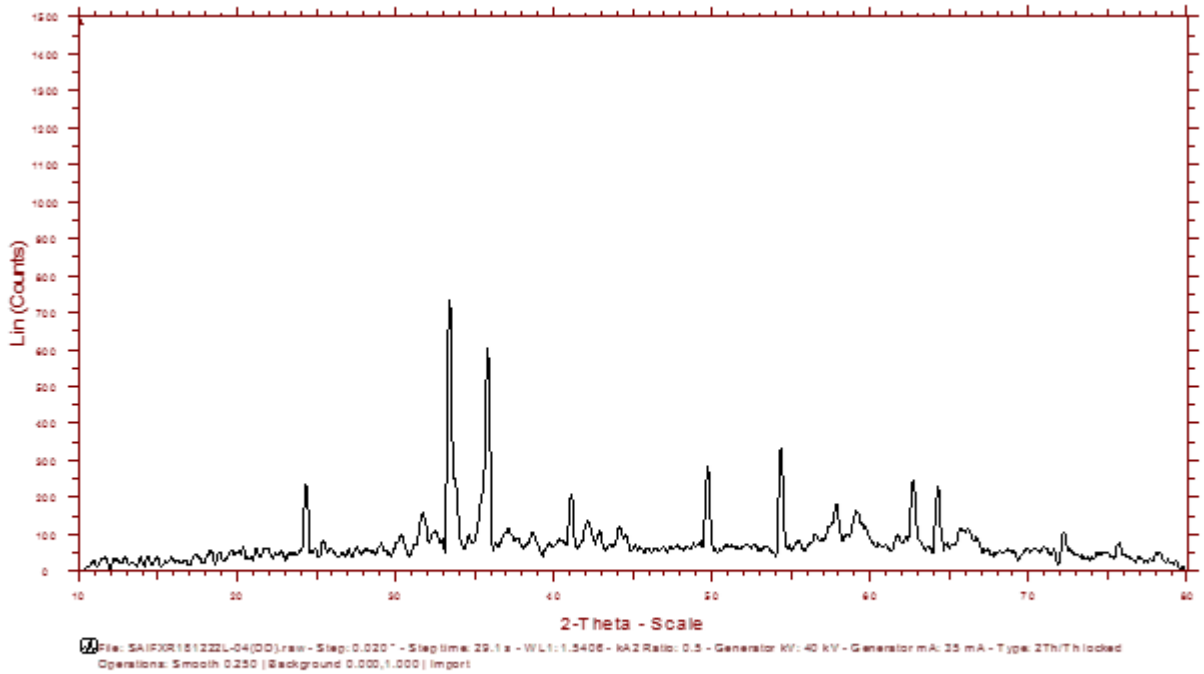

Fig(1) X-Ray Diffraction of $CAAl_6Fe_6O_{19}$

Table 2. Observation table of $CaAl_6Fe_6O_{19}$

Sr. No.	2Θ	d value (Å)	Observe intensity count (I)	Intensity in (I) %	h k l
1	24.297	3.66035	232	31.5	(1 1 2)
2	30.308	2.94663	96	13.1	(1 2 2)
3	31.687	2.82154	156	21.2	(0 1 3)
4	33.371	2.68290	735	100	(1 1 3)
5	35.792	2.50675	600	81.7	(0 2 3)
6	41.073	2.19580	206	28	(0 1 4)
7	42.223	2.13861	132	17.9	(1 1 4)
8	44.181	2.04830	116	15.8	(1 3 3)
9	49.717	1.8329	283	38.5	(2 2 4)
10	57.812	1.59358	171	23.3	(0 4 4)
11	62.719	1.48018	244	33.2	(0 1 6)
12	64.298	1.4476	228	31.4	(1 1 6)

SEM Studies:

The scanning electronmicroscopy (SEM) Fig(2) shows the morphological information of the hexagonal ferrite containing irregular grain, but nearly vertically arranged shaped flakes. The particle seemed to be hexagonal plate like mould which spreed out homogeneously were examined by ceramic method.

Figure 2 shows the representative SEM micrographs of fractured surface of Al-substituted sintered CaM The micrograph shows that Al substitution reduces the particle size. Al substituted calcium hexaferrite. Aspect factor calculated from following relation.

$$\text{Aspect Factor} = \frac{lenght}{diameter}$$

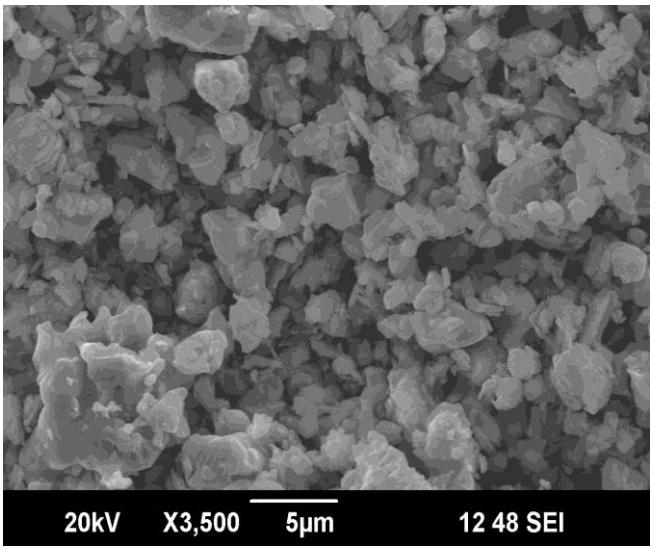

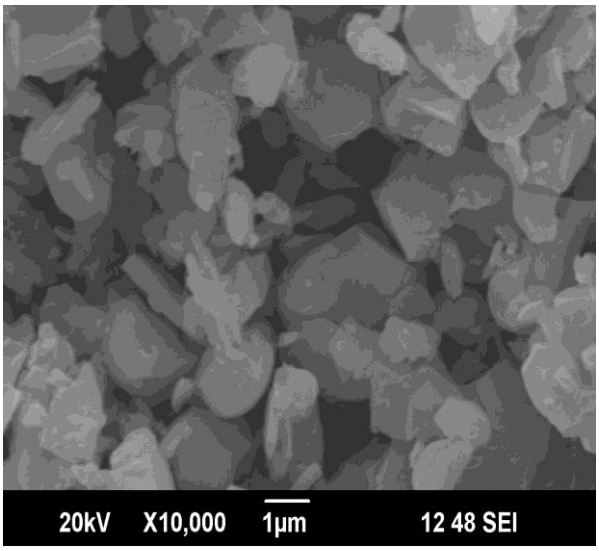

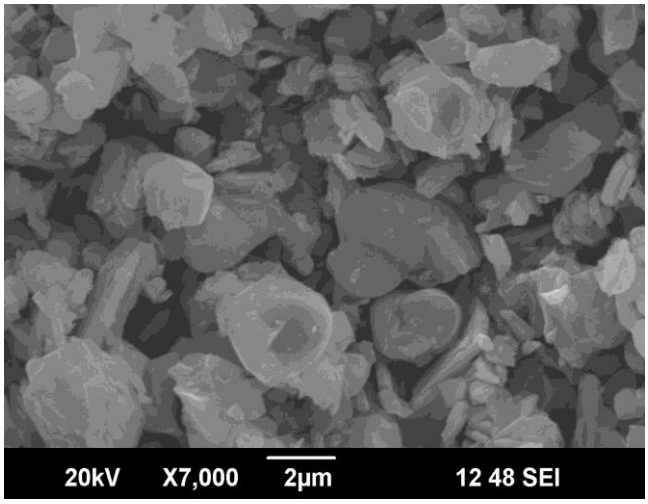

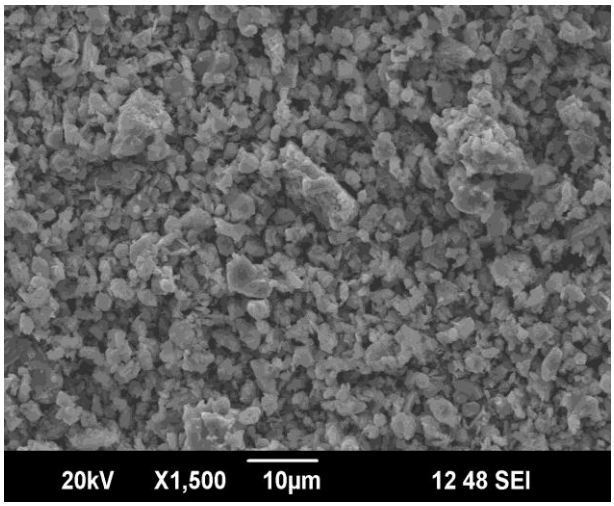

Figuer 2. SEM image of $CaAl_6Fe_6O_{19}$

Table 3. Observation table of $CaAl_6Fe_6O_{19}$

Sample	Grain size (nm)	Aspact factor
$CaAl_6Fe_6O_{19}$	376.7	2.05

IV. CONCLUSION

The ferrites $CaAl_6Fe_6O_{19}$ with Al Substituted were synthesized by Standard ceramic method. The X-ray diffraction studied confirm the formation of monophase M-type hexaferrite and the a and c value of the sample supports this confirmation. Structural studies have confirmed the space group of the sample to be P6/mnc. The nanorange of particle size of hexaferrites helps to improve many magnetic properties mentioned earlier. The substitution of Al^{3+}

ion for Fe^{3+} ion greatly improves the magnetic parameters.

V. ACKNOWLEDGEMENT

The authors thanks to sophisticated test and Instrumentation Centre, STIC, Cochin University Keral, India for giving us best result for X-ray Diffraction (XRD) and Scanning Electron Microscope (SEM) in needed hour. The authors are also thankful to the management, Principal Prof. Dr. K. P. Kariya of VMV College, Nagpur for providing the basic facilities of synthesis of the sample.

VI. REFERENCES

[1]. V. Adelskoled, X-ray studies on magnetoplumbite, Pob. 6FeO3 and other substances resembling. 'beta alumina' No2 O, Arkiv for kemi Mineralogioch Geologi, Series A-1229 (1938) 1-9.

[2]. R.C. Pullar, Hexagonal ferrites: a review of the synthesis, properties and applications of hexaferrite ceramics, Progress in Materials Science, 57 (2012) 1191-1334.

[3]. S.H. Mahmood, Properties and Synthesis of Hexaferrites, in: S.H. Mahmood, I. AbuAljarayesh (Eds.) Hexaferrite Permanent Magnetic Materials, Materials Research Forum LLC, Millersville, PA, 2016, pp. 74-110.

[4]. S.H. Mahmood, Permanent Magnet Applications, in: S.H. Mahmood, I. Abu-Aljarayesh (Eds.) Hexaferrite Permanent Magnetic Materials, Materials Research Forum LLC, Millersville, PA, 2016, pp. 153-165.

[5]. I. Bsoul, S. Mahmood, Structural and magnetic properties of BaFe12-xAlxO19 prepared by milling and calcination, Jordan Journal of Physics, 2 (2009) 171-179.

[6]. A. Awadallah, S.H. Mahmood, Y. Maswadeh, I. Bsoul, M. Awawdeh, Q.I. Mohaidat, H. Juwhari, Structural, magnetic, and Mossbauer spectroscopy of Cu substituted M-type hexaferrites, Materials Research Bulletin, 74 (2016) 192-201.

[7]. S.H. Mahmood, A. Awadallah, Y. Maswadeh, I. Bsoul, Structural and magnetic properties of Cu-V substituted M-type barium hexaferrites, IOP Conference Series: Materials Science and Engineering, IOP Publishing, 2015, pp. 012008.

[8]. A. Awadallah, S.H. Mahmood, Y. Maswadeh, I. Bsoul, A. Aloqaily, Structural and magnetic properties of Vanadium Doped M-Type Barium Hexaferrite (BaFe12-xVxO19), IOP Conference Series: Materials Science and Engineering, IOP Publishing, 2015, pp. 012006.

[9]. S.H. Mahmood, I. Bsoul, Hopkinson peak and superparamagnetic effects in BaFe12-xGaxO19 nanoparticles, EPJ Web of Conferences, 29 (2012) 00039.

[10]. J.A.Kohn, D.W.Eckart, and C.F.Cook, "Crystallography of the hexagonal ferrites," Science, vol. 172 , no.3983, pp.519-525 (1971).

[11]. K.G. Rewatker, C.S.Prakashand D.K.Kulkarni. Synthesis and characterization of a. CaAlx(CuTi)6-xO19hexaferrite system. Materials Letters 1997, 28, 365-368.

[12]. C.S.Prakash and Kulkarni D.K., Chromium substituted hexagonal calcium ferrites. a. Ind. J. Pure Applied Physics. 1994,32, 361-363.

[13]. C.S.Prakash, V.M.Nanoti, G.M. Rao and D.K. Kulkarni. Substitutional effect of magnetic behavior of calcium hexaferrite. J.Magn. Magn. Mater .1995, 140-144, 2089-2090.

[14]. C.S.Prakash, Nanoti V.M. and Kulkarni D.K.Magnetic Characterisation of calcium hexaferrites .Materials Letters ,1995, 24, 171-173.

[15]. Sanjay R. Gawali, Kishor G. Rewatkar and Vivek M. Nanoti Structural and Electrical properties of Mtype Nanocrystalline Aluminium substituted Calcium Hexaferrites. Advances in Applied Science Research, 2012, 3, 2672-2678.

[16]. Magnetic Characterisation of calcium hexaferrites. C. S. Prakash. V. M. Nanoti and D.K.Kulkarni Materials Letters , 1995, 24 p.171-173.

[17]. C.S.Prakash and D.K.Kulkarni, Variational Effect in Substituted Calcium Hexaferrite International Journal of Knowledge Engineering. 2012,3, 79-80.

[18]. Ch.Mamatha, M.Krishnaiah and C.S.Prakash Comparative Study of CaAl3Fe9O19 andCaAl4Fe8O19 Nanoparticles Synthesized by Solution Combustion Method. Proceedings ofthe Second National Seminar on New Materials Research and Nanotechnology OOTY,2013, 135-138. (ISBNNo.978-93- 81104-33-0).

National Conference on "Recent Trends in Mathematical Modeling, Simulation Methods, Computations, and Physical Sciences"
(MMSCP-2019), Organised by Hislop College, Nagpur, Maharashtra, India
International Journal of Scientific Research in Computer Science, Engineering and Information Technology
© 2019 IJSRCSEIT | Volume 4 | Issue 4 | ISSN : 2456-3307

Novel Method of Preparing CNF/$NiCo_2S_4$ by Electrospinning Method for High Performance Supercapacitor

Rounak R. Atram[1], Priya L. Shah[2], Tanushree S. Das[2], Sunil H. Ganatra[2], Subhash B. Kondawar[1]

[1]Department of Physics, Rashtrasant Tukdoji Maharaj Nagpur University, Nagpur, India

[2]Department of Chemistry, Institute of Science, Nagpur, India

ABSTRACT

In this paper, a novel CNF/ $NiCo_2S_4$ nanofibres were synthesized by simple one step inexpensive electrospinning process. CNF/$NiCo_2S_4$ material was used as electrode material for supercapacitor. The synthesized material was characterized for the study of surface morphology, elemental configuration and functional group identification by using scanning electron microscopy (SEM), energy dispersive X-ray spectroscopy (EDAX) and Fourier transform infrared spectroscopy (FTIR). The electrochemical performance of as synthesized material was further studied in 1M H_2SO_4 electrolyte by using cyclic voltametry (CV) with potential window of 1.4V, Galvanostatic charge-discharge from which the maximum specific capacitance of 370F/g with energy and power density of 12.85Wh/g and 124.92W/kg respectively at current density of 1A/g was obtained. The charge transfer mechanism was studied from electrochemical impedance spectroscopy (EIS). These results show that the CNF/$NiCo_2S_4$ electrode could be promising material for supercapacitor application.

I. INTRODUCTION

The global increase in human population has contributed to a requirement of high energy storage devices. Until now, petroleum based fuels have been widely used but due to limited petroleum resources their is a need for an alternate energy resource. An example of such an energy storage device is a supercapacitors which is also referred to as ultracapacitors or electrochemical capacitors have attracted a considerable attention [1]. Supercapacitors have high power density, fast recharging capability, high performance flexibility and long cycling stability [2]. Supercapacitors are compared with other energy storage devices by using ragon plot. This type of graph presents the power densities of various energy storage devices versus their energy densities. This graph reveals that supercapacitor occupy a region between batteries and conventional capacitors. However, the energy density of supercapacitor is lower than that of batteries and fuel cells. Therefore, their is requirement of increasing the energy density in supercapacitor to a level comparable to batteries. Supercapacitors are classified into three types, electrochemical double layer capacitor (EDLC), pseudocapacitor and hybrid capacitors. EDLC store charge electrostatically or non-faradaically and their is no direct transfer of charge between electrode and electrolyte. The electrode material used to store charge in EDLC are carbon materials. Some of the examples are activated carbon (AC), carbon nanotubes(CNTs) , carbon nanofibres(CNFs), templated carbon and graphene. Pseudocapacitors store charge faradaically through the transfer of charge between electrode and electrolyte. Two electrode materials are used to store charge in pseudocapacitors are metal oxides and conducting polymer. Hybrid capacitors consists of combined features of EDLCs and pseudocapacitors. It has greater energy and power densities and possess better performance characteristics [3]. Hybrid carbon nanofibres have superior electrochemical performance with high mass capacitance, good rate

capability and cycle stability[4]. Hybrid capacitors are further classified into three types: composite hybrids , asymmetric hybrids and battery type hybrids. In our present work, we have taken CNF/$NiCo_2S_4$ as a composite material and synthesized it by simple one – step inexpensive electrospinning process.

II. EXPERIMENT

2.1- Preparation of CNF/$NiCo_2S_4$

The electrospinning solution was prepared by dissolving 1gm PAN in 10ml DMF and stirred for 2hrs. at 70°C. After 2hrs nickel, cobalt, sulphur precursors were added in stiochiometric ratio of 2:4:8 and kept for magnetic stirring overnight. Then the stirred solution was transferred to 10ml syringe for electrospinning process. The distance between the needle tip and collector plate was 15cm, the voltage was maintained at 20KV and the flow rate of solution was 0.8ml/hr. After electrospinning process obtained nanofibres were transferred to oven for drying overnight. Further , the dried nanofibres were carbonized in horizontal quartz tube furnance in an inert atmosphere of N_2 .

III. RESULT AND DISCUSSION

The fabricated PAN and CNF/$NiCo_2S_4$ was analysed by SEM images for morphological studies at magnification of 5.40 KX and 8.46 KX respectively at a scale of 2μm.

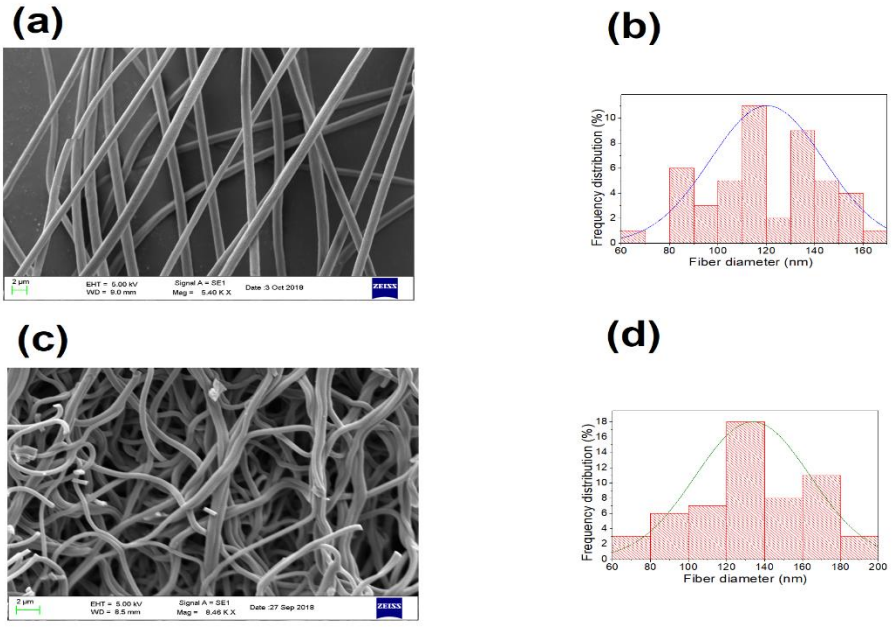

Figure 1. SEM Morphologies of (a) PAN/ $NiCo_2S_4$, (b) histogram for diameter range in nm, (c) CNF/$NiCo_2S_4$, (d) histogram for diameter range in nm

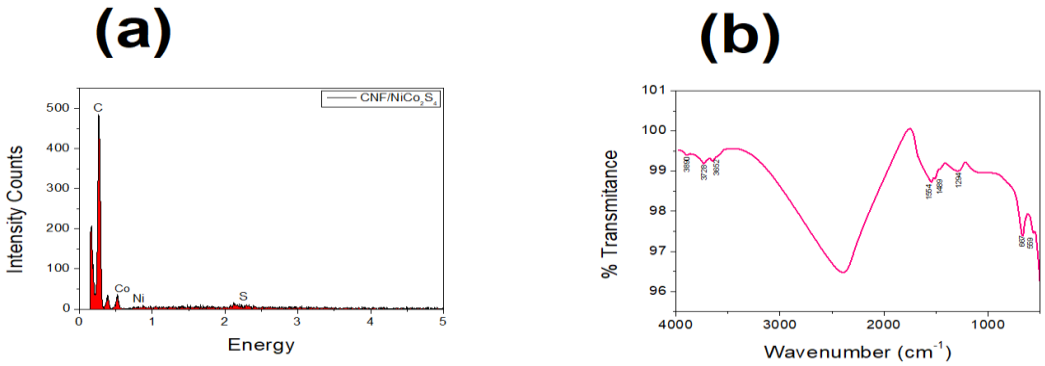

Figure 2. (a) Energy dispersive X-Ray spectroscopy of CNF/$NiCo_2S_4$, (b) FTIR for CNF/$NiCo_2S_4$,

The elemental configuration of Carbon, Nickel, Cobalt and Sulphur was confirmed by Energy Dispersive X-ray Spectroscopy (EDAX). The functional groups were determined by Fourier Transform Infrared Spectroscopy (FTIR) and the various peaks have a particular IR frequency which corresponds to different functional groups.

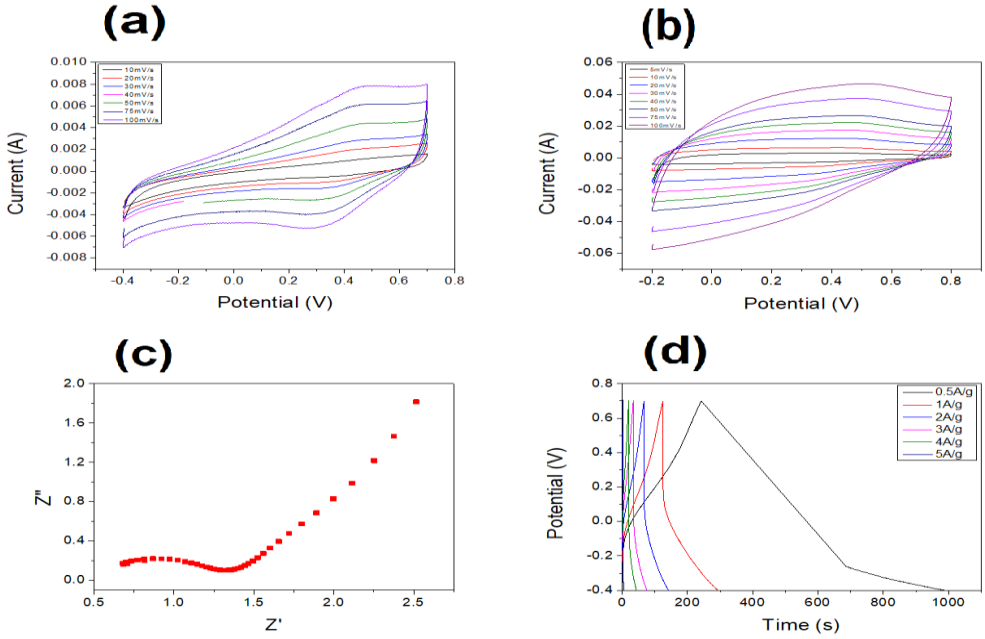

Figure 3. (a) (b) shows the CV curves for CNF/$NiCo_2O_4$ and CNF/$NiCo_2S_4$ respectively, (c) shows

the Nyquist plot for CNF/$NiCo_2S_4$, (d) Galvanostatic Charg-Discharge curves at various current densities

Figure 3 (a) illustrates the CV curves of the CNF/$NiCo_2O_4$ at various scan rates of 10,20,30,40,50,75,100 mV/s. 3b illustrates the CV curves of the CNF/$NiCo_2S_4$ at various scan rates of 5,10,20,30,40,50,75,100 mV/s. The area covered by CV curves of the CNF/$NiCo_2S_4$ was much larger than that of the CNF/ $NiCo_2O_4$, which indicates the outstanding electrochemical performance of CNF/$NiCo_2S_4$. From the CV curves the current obtained in $NiCo_2S_4$ is 9 times higher than the

$NiCo_2O_4$. Figure 3(c) EIS is typically used to investigate the performance of the electrochemical capacitors such as internal resistance, capacity. At high frequency the intercept on the real axis represents a combined resistance (R_s) which contains the intrinsic resistance of the electrode materials, ionic resistance of the electrolyte, and the contact resistance between the electrode and the current collector[5]. The present EIS plot exhibit R_s value of 0.056Ω. A semi-circle was observed and its diameter represents the charge transfer resistance(R_{CT})of approximately 0.7Ω. To determine the application potential of the CNF/$NiCo_2S_4$ as an electrode material , Figure 3(d) shows GCD curves, GCD measurements were performed at various current densities from 0.5 to 5 A/g as shown in figure . The maximum specific capacitance of 338.11F/g was obtained at 0.5A/g.

IV. REFERENCES

[1]. M. Vangari,T. Pryor,L. Jiang,supercapacitors:review of materials and fabrication methods journal of energy engineering june 2013.

[2]. D. Li,Y. Gong ,C. Pan ,facile synthesis of hybrid CNF/NiCo2S4 composite for high performances supercapacitor.

[3]. S.B.Kondawar, conducting polymer nanoconposites for supercapacitors.

[4]. Y. Liu, G. Jiang, S. Sun, B. Xu,J. Zhou, Y.zhang,J. Yao,growth of NiCo2S4 nanotubes on carbon fibres for high performance flexible supercapacitors, journal of electroanalytical chemistry 804(2017)212-219.

[5]. D.Y.kim,G.S.Ghodake,N.C.Maile,A.A.Kadam,D. S.Lee,V.J.Fulari,S.K.Shinde,chemical synthesis of hierarchical NiCo2S4 nanosheets like nanostructure on flexible foil for a high performance supercapacitor.

[6]. P. Xiong, J. Zhu, X. Wang, Recent advances on multi-component hybrid nanostructures for electrochemical capacitors, Journal of Power Sources 294 (2015), 31-50.

[7]. E. Azwar, W. Mahari, J. Chuah, D. Vo, N. Ma, W. Lam, S. Lam, Transformation of biomass into carbon nanofiber for supercapacitor application – A review, International Journal of Hydrogen Energy, Vol-43, Issue-45, Nov (2018), 20811-20821.

[8]. J. Libich, J. Maca, J. Vondrak, O. Cech, M. Sedlarikova, Supercapacitor: Properties and applications, Journal of Energy Storage 17 (2018), 224-227.

[9]. X. Zhao, H. Chen, F. Kong, Y. Zhang, S. Wang, S. Liu, L. Lucia, P. Fatehi, H. Pang, Fabrication, Characteristics and application of carbon materials with different morphologies and porous structures produced from wood liquefication: A review, Chemical Engineering Journal, Vol (364), May (2019), 226-243.

National Conference on "Recent Trends in Mathematical Modeling, Simulation Methods, Computations, and Physical Sciences"
(MMSCP-2019), Organised by Hislop College, Nagpur, Maharashtra, India
International Journal of Scientific Research in Computer Science, Engineering and Information Technology
© 2019 IJSRCSEIT | Volume 4 | Issue 4 | ISSN : 2456-3307

Effect of Cosmological Constant on the Periods of Vibrating System In the Reissner-Nordstrom Space-Time

Kalpana Pawar[1], Rishikumar Agrawal[2] , N. T. Katre[3]
[1]Department of Mathematics, Shri R.R.Lahoti Science College, Morshi, Affiliated to S.G.B. Amravati University, Amravati, Maharashtra, India
[2]Department of Mathematics, Hislop College, Nagpur, Maharashtra, India
[3]Department of Mathematics, Nabira Mahavidyalaya, Katol, Nagpur, Maharashtra, India

ABSTRACT

In this paper considering circular trajectory $r =$ constant in the plane $\theta = \frac{\pi}{2}$ in the Reissner-Nordstrom (anti) de-Sitter space-time, a relation analogous to a relation between perihelic shift is obtained by using Shirokov's technique. Thereby our result supports the conclusion that the cosmological constant term Λ on gravitating particle instead of helping the matter to curve the space-time mode, decurves the space-time which means that nature of gravitational fields due to the matter and charges matter with cosmological constant Λ may be of different type. In our case θ- vibrations lie further behind r or (ϕ) - vibrations as an effect of positive cosmological constant on the periods of vibrating system.

Keywords: Cosmological constant, R-N field, θ- vibrations, r or (ϕ) - vibrations.

I. INTRODUCTION

According to Einstein, all the forms of matter and energy are under the influence of gravitation and hence the universe filled with matter and energy is under the action of the attractive force of gravitation. Moreover, the universe is static; therefore it is bound to collapse under gravity. So to prevent the collapse, Einstein (1917) introduced a cosmological constant Λ having the dimensions of space curvature. In 1922, Friedmann solved the Einstein's gravitational field equations and found a cosmological solution, which prevents non-static model of an expanding universe.
In 1922, Edwin Hubble's observations convinced astrophysicists that the universe is not at all static by observing the red shift of distant galaxies. Therefore, Einstein rejected the term Λ , which does not have a direct physical meaning. The term $\Lambda g_{\mu\nu}$ which is added to the energy momentum tensor suggests an interpretation in terms of constant pressure. This pressure would be responsible for avoiding the cosmological collapse seen in the case of the non-zero density of matter. But then it is necessary to explain the existence of such universal pressure by some macroscopic phenomenon.

Sakharov, Wheeler, Landau, Pomeranchak and others have proposed number of such explanations. In their papers, the authors evaluate the constant Λ , as being of order of $10^{-56}cm^{-1}$. The value of Λ along with its physical interpretation is deduced by supposing that the vacuum is endowed with very high elasticity (of order Λ^{-1}), which is due to the quantum fluctuations of energy in the vacuum. Due to the physically plausible reasons Λ is retained in the modern cosmology.

Establishing the criteria for existence and stability of circular orbits, Howes (1981) has studied the effect of a positive cosmological constant Λ on the circular orbits in the R-N field and Kerr field, with the help of geodesic deviation equation.

Taking into account the importance of Λ in the modern cosmology, we have studied the effect of a positive cosmological constant Λ, on the periods of vibrating system in this paper. In the section 2.2, expressions for the frequencies of a vibrating system are derived in the R-N field with cosmological constant Λ. In the section 2.3, the periods of vibrating system in the Schl'd field with cosmological constant Λ on the periods of vibrations is discussed. In the section 2.4, conclusions are drawn.

II. FREQUENCIES OF VIBRATIONS

In the GTR, the equation of deviation from the geodesic is

$$\frac{d^2\xi^i}{ds^2} + 2\,\Gamma^i_{\mathrm{jk}}\,u^{\mathrm{j}}\,\frac{d\xi^k}{ds} + \frac{\partial\Gamma^i_{\mathrm{jk}}}{\partial x^l}\,u^{\mathrm{j}}\,u^k\xi^l = 0 \text{ , (2.1)}$$

where ξ^i is the infinitesimal 4-vector giving the deviation from the basic geodesic, $u^i = \frac{dx^i}{ds}$ is the 4-velocity vector tangential to the basic geodesic and Γ^i_{jk} are Christoffel symbols defined as

$$\Gamma^i_{\mathrm{jk}} = \frac{1}{2}\,g^{li}\left(\frac{\partial g_{\mathrm{lj}}}{\partial x^k} + \frac{\partial g_{lk}}{\partial x^{\mathrm{j}}} - \frac{\partial g_{\mathrm{jk}}}{\partial x^l}\right).$$

Reissner-Nordstrom field with cosmological constant Λ, known as Reissner-Nordstrom (anti) de-Sitter space-time is

$$ds^2 = -\left(1 - \frac{2m}{r} + \frac{e^2}{r^2} - \frac{\Lambda}{3}r^2\right)^{-1} dr^2 - r^2\,(d\theta^2 + \sin^2\theta\, d\phi^2) + \left(1 - \frac{2m}{r} + \frac{e^2}{r^2} - \frac{\Lambda}{3}r^2\right) dt^2 \text{ (2.2)}$$

where $r = x^1, \theta = x^2, \phi = x^3, t = x^4$.

For the field (2.2), metric tensors are

$$g_{11} = -\left(1 - \frac{2m}{r} + \frac{e^2}{r^2} - \frac{\Lambda}{3}r^2\right)^{-1}, g_{22} = -r^2,$$
$$g_{33} = -r^2\sin^2\theta,$$

$$g_{44} = \left(1 - \frac{2m}{r} + \frac{e^2}{r^2} - \frac{\Lambda}{3}r^2\right), g_{\mathrm{ij}} = 0 \text{ for } i \neq \mathrm{j} \text{ (2.3)}$$

and the non-vanishing components of the Christoffel symbols are

$$\Gamma^1_{11} = -\frac{1}{r}\left(\frac{m}{r} - \frac{e^2}{r^2} - \frac{\Lambda}{3}r^2\right)\left(1 - \frac{2m}{r} + \frac{e^2}{r^2} - \frac{\Lambda}{3}r^2\right)^{-1},$$

$$\Gamma^1_{22} = -r\left(1 - \frac{2m}{r} + \frac{e^2}{r^2} - \frac{\Lambda}{3}r^2\right)^{-1},$$

$$\Gamma^2_{21} = \frac{1}{r} = \Gamma^3_{31},$$

$$\Gamma^1_{33} = -r\sin^2\theta\left(1 - \frac{2m}{r} + \frac{e^2}{r^2} - \frac{\Lambda}{3}r^2\right),$$

$$\Gamma^4_{41} = \frac{1}{r}\left(\frac{m}{r} - \frac{e^2}{r^2} - \frac{\Lambda}{3}r^2\right)\left(1 - \frac{2m}{r} + \frac{e^2}{r^2} - \frac{\Lambda}{3}r^2\right)^{-1},$$

$$\Gamma^1_{44} = \frac{1}{r}\left(\frac{m}{r} - \frac{e^2}{r^2} - \frac{\Lambda}{3}r^2\right)\left(1 - \frac{2m}{r} + \frac{e^2}{r^2} - \frac{\Lambda}{3}r^2\right),$$

$$\Gamma^2_{33} = -\sin\theta\cos\theta,\ \Gamma^3_{23} = \cot\theta \text{ . (2.4)}$$

We suppose that the basic geodesic is a circular trajectory with radius $r =$ constant in the plane $\theta = \frac{\pi}{2}$ in the field (2.2). Following Howes (1981), if the basic geodesic are circular in the axisymmetric stationary field, θ-disturbances are independent of r, ϕ, and t-perturbations.

Therefore for $i = 2$, equation (2.1) assumes the form

$$\frac{d^2\xi^2}{ds^2} + \Gamma^2_{\mathrm{jk},2}\,u^{\mathrm{j}}\,u^k\,\xi^2 = 0 \text{ (2.5)}$$

If we suppose that,

$$\xi^2 = \xi^2_0\,e^{i\,\Omega\,s} \text{ (2.6)}$$

(ξ^2_0 is the amplitude of θ-vibrations) then from (2.5), we obtain

$$\Omega^2 = \Gamma^2_{\mathrm{jk},2}\,u^{\mathrm{j}}\,u^k \text{ , (2.7)}$$

where comma in the Christoffel symbol denotes the partial differentiation and Ω is the frequency of θ-vibrations.

For $i = 1, 3, 4$, from (2.1), we get

$$\frac{d^2\xi^1}{ds^2} + 2\,\Gamma^1_{\mathrm{j3}}\,u^{\mathrm{j}}\,\frac{d\xi^3}{ds} + 2\,\Gamma^1_{\mathrm{j4}}\,u^{\mathrm{j}}\,\frac{d\xi^4}{ds} + \Gamma^1_{\mathrm{jk},l}\,u^{\mathrm{j}}\,u^k\xi^l = 0,$$

$$\frac{d^2\xi^3}{ds^2} + 2\,\Gamma^3_{\mathrm{j1}}\,u^{\mathrm{j}}\,\frac{d\xi^1}{ds} = 0,$$

$$\text{and } \frac{d^2\xi^4}{ds^2} + 2\,\Gamma^4_{\mathrm{j1}}\,u^{\mathrm{j}}\,\frac{d\xi^1}{ds} = 0 \text{ (2.8)}$$

Further, if we suppose that

$$\xi^{\mathrm{j}} = \xi^{\mathrm{j}}_0\,e^{i\,\omega\,s},\ (\mathrm{j} = 1, 3, 4) \text{ (2.9)}$$

(ξ^{j}_0 is the amplitude of r, ϕ and t-vibrations), then from (2.8), we get

$$\left(\Gamma^1_{\mathrm{jk},1}\,u^{\mathrm{j}}\,u^k - \omega^2\right)\xi^1_0 + 2\,i\,\omega\,\Gamma^1_{\mathrm{j3}}\,u^{\mathrm{j}}\,\xi^3_0 + 2\,i\,\omega\,\Gamma^1_{\mathrm{j4}}\,u^{\mathrm{j}}\,\xi^4_0 = 0,$$

$$2\,i\,\omega\,\Gamma^3_{\mathrm{j1}}\,u^{\mathrm{j}}\,\xi^1_0 - \omega^2\,\xi^3_0 = 0,$$

$$\text{and } 2\,i\,\omega\,\Gamma^4_{\mathrm{j1}}\,u^{\mathrm{j}}\,\xi^1_0 - \omega^2\,\xi^4_0 = 0 \text{ (2.10)}$$

where ω is the frequency of r, ϕ and t-vibrations.

For non-trivial solution of (2.10), we equate the determinant of coefficients to zero and obtain

$$\omega^2 = u^{\mathrm{j}}\,u^k\,\Gamma^1_{\mathrm{jk},1} - 4\,u^{\mathrm{j}}\,u^k\,\Gamma^3_{\mathrm{j1}}\,\Gamma^1_{k3} - 4\,u^{\mathrm{j}}\,u^k\,\Gamma^4_{\mathrm{j1}}\,\Gamma^1_{k4}$$

$$\text{or } \omega^2 = \left(\Gamma^1_{33,1} - 4\,\Gamma^3_{31}\,\Gamma^1_{33}\right)(u^3)^2 + \left(\Gamma^1_{44,1} - 4\,\Gamma^4_{41}\,\Gamma^1_{44}\right)(u^4)^2 \text{ (2.11)}$$

where all the symbols Γ^i_{jk} and their derivatives are evaluated at $\theta = \frac{\pi}{2}$.

To determine u^3, consider geodesic equation

$\frac{du^i}{ds} + \Gamma^i_{jk}\, u^j\, u^k = 0$, ($i, j, k = 1, 2, 3, 4$) (2.12)

in the Einstein's theory of gravitation.

For circular orbits in the equatorial plane from (2.12) we find that

$\frac{dt}{d\phi} = \frac{u^4}{u^3} = \left(\frac{-\Gamma^1_{33}}{\Gamma^1_{44}}\right)^{\frac{1}{2}}$, (2.13)

which provides the angular velocity of the test particle as seen from the infinity.

Using (2.4) in (2.13), we get

$(u^4)^2 = \frac{r^2}{\left(\frac{m}{r} - \frac{e^2}{r^2} - \frac{\Lambda}{3} r^2\right)} (u^3)^2$. (2.14)

For the circular orbit in the equatorial plane, using (2.13) in (2.2), we get

$(u^3)^2 = \left(\frac{m}{r^3}\right)\left(1 - \frac{e^2}{m\,r} - \frac{\Lambda}{3}\frac{r^3}{m}\right)\left(1 - \frac{3m}{r} + \frac{2\,e^2}{r^2}\right)^{-1}$ (2.15)

Therefore expressions for the frequencies of θ-vibrations and r (or ϕ)-vibrations in (2.7) and (2.11) simplify to

$\Omega^2 = (u^3)^2 = \left(\frac{m}{r^3}\right)\left(1 - \frac{e^2}{m\,r} - \frac{\Lambda}{3}\frac{r^3}{m}\right)\left\{1 - \left(\frac{3m}{r} - \frac{2\,e^2}{r^2}\right)\right\}^{-1}$ (2.16)

$\& \ \omega^2 = (u^3)^2 \left\{1 - \frac{6m}{r} + \frac{3\,e^2}{r^2} + \frac{e^2}{m\,r} + \frac{e^4}{m^2 r^2} - \Lambda\left(\frac{4\,e^2 r}{m} + \frac{4\,r^3}{3\,m} - 5\,r^2\right)\right\}$

$\times \left\{1 - \left(\frac{e^2}{m\,r} + \frac{\Lambda}{3}\frac{r^3}{m}\right)\right\}^{-1} (u^3)^2$ (2.17)

respectively.

III. PERIODS OF VIBRATIONS

The corresponding period of θ-vibration is

$T_\theta = \frac{2\pi}{\Omega} = T_0\left(1 - \frac{3m}{2r} + \frac{e^2}{2mr} + \frac{\Lambda}{6}\frac{r^3}{m}\right) + o(\eta)$ (3.1)

and that of r (or ϕ)-vibration is

$T_r\ (or\ T_\phi) = T_0\left(1 + \frac{3m}{2r} + \frac{2}{3}\frac{\Lambda\, r^3}{m}\right) + o(\eta)$ (3.2)

in which $\frac{m}{r}, \frac{e}{r} = o(\eta)$, η is small and $T_0 = 2\pi\left(\frac{r^3}{m}\right)^{\frac{1}{2}}$ is the Newtonian period of test particle in the circular orbit of radius r.

The difference $\Delta T_{RN(\Lambda)}$ between the periods of θ-vibrations and r (or ϕ)-vibrations is

$\Delta T_{RN(\Lambda)} = T_\theta - T_r = T_0\left(-\frac{3m}{r} + \frac{e^2}{2mr} - \frac{\Lambda}{2}\frac{r^3}{m}\right)$ (3.3)

to the $1\frac{1}{2}$ order approximation.

For $\Lambda = 0$, (3.3) reduces to

$\Delta T_{RN} = T_\theta - T_r = T_0\left(-\frac{3m}{r} + \frac{e^2}{2mr}\right)$ (3.4)

Furthermore, for $e = 0$, (3.3) gives

$\Delta T_{Schl'd(\Lambda)} = T_0\left(-\frac{3m}{r} - \frac{\Lambda}{2}\frac{r^3}{m}\right)$ (3.5)

and for $\Lambda = 0$ from (3.5) we can recover the result

$\Delta T_{Schl'd} = T_0\left(-\frac{3m}{r}\right)$ (3.6)

which is analogous to the result obtained by Shirokov (1973) as a new effect of Einstein's Theory of Gravitation.

IV. CONCLUSION

From (3.3), (3.4), (3.5) and (3.6), we find relation between shifts in the periods of θ-vibration and r (or ϕ)-vibration in R-N field and Schwarzschild field with and without cosmological constant Λ, which is analogous to the relation between the perihelic shift in R-N field and Schwarzschild field obtained by H.J. Treder, H.H.V. Borzeszkowski, A.Van Der Merwe, W.Y.Yourgrau.

According to G.D. Rathod and T.M. Karade, the relation between perihelic shift $\delta\phi_{RN} < \delta\phi_{Schl'd}$ shows that charge on the gravitating particle instead of helping the matter to curve the space-time more, decurves the space-time.

Also according to Kalpana Pawar and G.D. Rathod, the similar relation between the periods of θ-vibration and r (or ϕ)-vibration is obtained which shows the effect of charge on gravitating particle is analogous to a relation obtained by using Shirokov's technique as $\Delta T_{RN} < \Delta T_{Schl'd}$.

In our case, from result (3.3), we observe that θ-vibrations lie further behind the r (or ϕ)-vibrations than the R-N field as an effect of positive cosmological constant Λ on the periods of vibrating system.

V. ACKNOWLEDGEMENT

Authors are grateful to Dr. T. M. Karade and Dr. G. D. Rathod for their fruitful discussion.

VI. REFERENCES

[1]. M.F. Shirokov, Gen. Rel. Grav. 4 (1973) 131.
[2]. Robert J. Howes, Gen. Rel. Grav. 13 (1981) 830.
[3]. H.J. Treder et al., Fundamental Principle of General Relativity Theory, NewYork/London: Plenum Press, 1980.
[4]. G.D. Rathod and T.M. Karade (1989), Analen der Physik, 7, Folge Band 46, Heft.
[5]. Kalpana Pawar and G.D. Rathod, Indian J. pure appl. Math., 32(8) : 1153-1156, August 2001.

National Conference on "Recent Trends in Mathematical Modeling, Simulation Methods, Computations, and Physical Sciences"
(MMSCP-2019), Organised by Hislop College, Nagpur, Maharashtra, India
International Journal of Scientific Research in Computer Science, Engineering and Information Technology
© 2019 IJSRCSEIT | Volume 4 | Issue 4 | ISSN : 2456-3307

Treatment of Ferroelectric Fatigue by Removal of Localized Impurities Structures in Lead Meta Niobate Single Crystal

Ajay Yoel
Department of Physics, Hislop College, Nagpur, Maharashtra, India

ABSTRACT

The present work provides an available way of enhancing optical quality of surface and trim down the fatigue properties of the ferroelectric lead meta niobate ($PbNb_2O_6$) single crystal, which will be helpful to use this material as ferroelectric storage device. This study provides a quantitative basis for imaging the local polarization dipoles at microscopic resolution, which are helpful for the investigation about domain wall motion under the application of electric field.

I. INTRODUCTION

Bulk ferroelectric domain inversion and differential etching processes have been used for fabricating the surface microstructures due to dependence of the etch rate and three fold y-direction symmetry in various ferroelectric materials [1]. The performance of many electro-optical devices is strongly based on stability of switchable ferroelectric polarization modes which involves the nucleation and growth of domain structures on crystal-surface under an external electric field, along with better optical quality of topography of crystal [2, 3]. The present article is an attempt to address such type of mechanism concerning domain wall nucleation and impurity-ion dipole interactions in achieving the preferred optical-quality at the surface of ferroelectric lead meta niobate ($PbNb_2O_6$) single crystal. The main objective of this study is to explore the crystal's surface with good optical ability, which will be helpful to eliminate the ferroelectric fatigue and localized behavior of impurities in $PbNb_2O_6$ single crystal at microscopic level. For improvisation of the optical quality of surface of $PbNb_2O_6$ single crystal, the domain wall nucleation and etching process is applied with external electric field, and underlying principle and mechanism of this technique is discussed with the evidences of surface micrographs of crystal.

II. MATERIALS AND METHODS

The single crystals of lead meta niobate ($PbNb_2O_6$ or PN) grown from melt by employing Goodman's technique in a slightly modified way [4]. The dried constituent oxides in molar composition 1:1 (22.3190gm of PbO and 26.5810gm of Nb_2O_5, analytical grade with 99.4% purity purchased from MERCK) grounded together and packed in to a 50cc platinum crucible. Programmable Gallenkamp furnace is set to melt the materials in crucible at temperature 1623°K for sufficient soaking time of about twelve hours. To avoid stray nucleation in crystal-growth process, a cooling and reheating process was performed in a suitable rate manner, through a program set in this furnace. It is observed that the obtained $PbNb_2O_6$ crystals are of pale yellow in color, oxygen deficient and containing platinum

ions as main impurity due to use of platinum crucible. By XRD-pattern of this grown material, the single orthorhombic phase at room temperature and lattice parameters with point group are calculated, while its ferroelectric nature and phase transition temperature (570ºC) is confirmed through hysteresis study [5].

The micro-structure surfaces of grown lead meta niobate ($PbNb_2O_6$ or PN) single crystal studied under reflection by microscope of METZER Company. The domain structure and its evolution during nucleation and polarization reversal processes has been investigated which offer full and direct information on the static and dynamic properties of this grown ferroelectric PN single crystal. The improvised optical quality of surface of PN crystal is observed through surface micrographs after the successive application of external electric field in forward/reverse direction followed by etching with dilute ammonium nitrate [$(NH_4)_2NO_3$], and microscopic changes in domain structures are discussed in the next section.

III. RESULTS AND DISCUSSION

Generally, the stabilized impurities in the form of dipole, cracks as the dislocation type of defects, roughness exponent of charges, space charges, grain boundaries, oxygen vacancies etc. are the realistic issues that always hindered the visibility of movements of domain walls, and consequently, are believed to be the causes of fatigue properties in ferroelectric materials. Domain wall dynamics, grain size effect on domain-transition, predominance of crystal-defects under external electric field have already been reported by us through the study of surface-micrographs for this ferroelectric $PbNb_2O_6$ single crystal [6, 7]. Less twinned and thin flake of about 0.1mm $PbNb_2O_6$ crystal is chosen for improvement of optical quality of its surface. The viewing direction is along the crystallographic [110] direction in Figure 1, where several impurity-segregation can be easily seen in the form of clusters with 90º and 180º domain walls, marked by arrows. Here, the impurities exist in the form of dipoles (made with nearby vacancies) stabilized themselves by forming micro-domains around the dipole in the crystal structure. The task to remove such type of impurities found difficult as they form dipole-clusters by interacting with electrons freed from the vacancies. Moreover, their behavior can be considered as relaxed dipoles shifting from their ionic states, getting more stabilized by accommodated themselves in various octahedral-voids in the structure when crystal was cooled in the growth process. Although, the impurity-ions (relaxed dipoles) are not visible in Figure 1, the impurity-aggregates and dislocation in the form of cracks present good picture of impurity-content on the surface of the $PbNb_2O_6$ crystal under study.

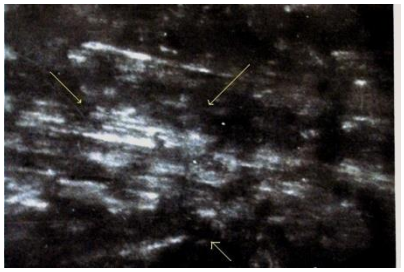

Figure 1. Surface of $PbNb_2O_6$ single crystal without application of electric field and etching.

The same piece of $PbNb_2O_6$ crystal whose surface is depicted in Figure 1, poled with *d.c.*electric field of 5000V/cm for twenty minutes. Figure 2 is the viewed surface of $PbNb_2O_6$ crystal after polling with such electric field of 5000V/cm in which the nucleation of fresh micro-domains of about (4-6) μm around the impurity-content can easily be observed, under the circle. It is pointed out here that the unfavorably oriented relaxed-dipoles in the cluster shown in Figure 1 are diffused in hopping process after the application of electric field, and remaining constituent freed charges are taking part in the nucleation of fresh micro-domains what are appeared in Figure 2. In this way, the relaxed dipoles are re-

excited from their ionic state to dipolar state. However, the anti-phase boundaries and the morphology of 90º domain walls, which influence the nucleation of new domains and the mobility of domains, and attributed the physical mechanism for polarization fatigue in ferroelectric $PbNb_2O_6$ crystal.

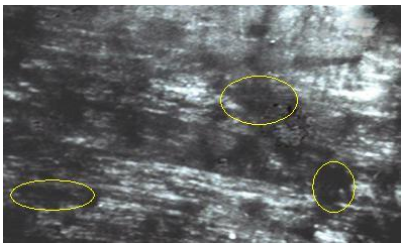

Figure 2. Surface of same piece of $PbNb_2O_6$ crystal after application of electric field 5000V/cm.

Further, the *d.c.*electric field of 15000V/cm in the *reverse direction* is again applied to same piece of $PbNb_2O_6$ crystal for only four minutes and its surface is shown in Figure 3. It can be observed in Figure 3; that the previously nucleated domain walls (Which were present in Figure 2.) are now evaporated from the viewing surface in Figure 3. This has happened because a large number of dipoles are being freed in this evaporation process of domains. Thus, by the application of forward and reverse electric field, the relaxed-dipoles are continuously excited and de-excited from their ionic state to dipolar state and vice-versa; subsequently a sufficient deposition of impurity-content at the surface of PN crystal can be seen in Figure 3.

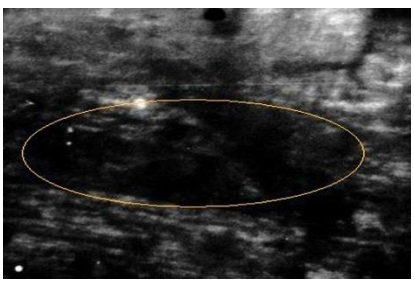

Figure 3. Surface of same piece of $PbNb_2O_6$ crystal after application of electric field 15000V/cm.

This accumulated deposition of impurities is now removed by washing with dilute ammonium-nitrate $[(NH_4)_2NO_3]$ and micrograph of washed surface of $PbNb_2O_6$ crystal is shown in Figure 4. Surface residues after etching were removed by post-etching cleaning solution. We can easily see the improvement of optical quality of surface of $PbNb_2O_6$ single crystal by comparing the Figure 1.and Figure 4. This whole process what is performed from Figure 1 to Figure 4 can be further repeated again and again to achieve better surface quality of crystal.

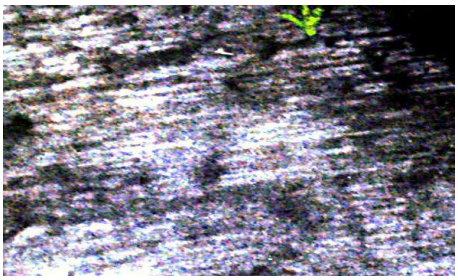

Figure 4. Surface of same piece of $PbNb_2O_6$ crystal after etching by Ammonium Nitrate.

Summarily, the whole process which has been discussed above is the attempt to reduce the ionic displacement consequential from the change of the lattice parameter resulted in octahedral distortion, improving the ferroelectric fatigue of the $PbNb_2O_6$ single crystal.

IV. CONCLUSION

In conclusion, a strong correlation found between the properties of ferroelectric fatigue and the behavior of localized impurity structures in ferroelectric lead meta niobate single crystal. Localized impurity structures are removable by a simple and low priced technique which involved etching and domain wall nucleation under the application of applied electric field to get better optical quality of the surface; it also confirms that lattice-defects can affect the crystal structure and width of domain walls.

V. REFERENCES

[1]. S. Mailis, C. L. Sones, and R. W. Eason, Micro-/Nanoengineering and Characterization of Ferroelectric Crystals for Photonic Applications Series: Springer Series in Materials Science, Vol. 91 ed. P. Ferraro, S. Grilli, P. De Natale, (2008).

[2]. Gysel, R., Stolichnov, I., Setter, N. & Pavius, M. Ferroelectric film switching via oblique domain growth observed by cross-sectional nanoscale imaging. Appl. Phys. Lett. 89, 082906 (2006).

[3]. Roelofs, A. et al. Depolarizing-field-mediated 180 degrees switching in ferroelectric thin films with 90 degrees domains. Appl. Phys. Lett. 80, 1424 (2001).

[4]. K.G.Deshmukh, S.G.Ingle, J.Phys.D: Appl. Phys. 4 124 (1971).

[5]. A.Yoel, P.E.P.Michael, M.V.Kokate and V.A.Tabhane, Phys. B. Cond. Matter. 407, 4 p.576 (2012).

[6]. A.Yoel, M.V.Kokate, V.A.Tabhane, Bio-Nano Front. Special issue 5, p.53 (2012).

[7]. A.Yoel, M.V.Kokate, V.A.Tabhane, Proceedings of National conference on Current Development in Nano-science: Challenges and Opportunities, K.N.College Nagpur, India, ISBN No. , p.101 (2013).

National Conference on "Recent Trends in Mathematical Modeling, Simulation Methods, Computations, and Physical Sciences"
(MMSCP-2019), Organised by Hislop College, Nagpur, Maharashtra, India
International Journal of Scientific Research in Computer Science, Engineering and Information Technology
© 2019 IJSRCSEIT | Volume 4 | Issue 4 | ISSN : 2456-3307

Design and Development of Intelligent System for Waste Collection and Handling I-SWaCH

M. C. Naidu[1], Dr. M. J. Hedau[2]
[1]Hislop College , Nagpur, Maharashtra, India
[2]Shri Shivaji Science college Nagpur, Maharashtra, India

ABSTRACT

Around the globe, more and more litter is being thrown away carelessly or dumped illegally in streets, in public spaces or in nature. Littering and the wrong waste disposal respectively affect adversely the public order, lead to higher costs for the cleaning teams and to a diminished quality of life for society. This project has been conceptualized to tackle situation against littering and the incorrect waste disposal. This innovative idea allows city authorities to tackle the problem more efficiently by the use of technology.

I. INTRODUCTION

An intelligent garbage collector and management system. Few sensors make the bin Interactive, Attractive, Intelligent and Efficient. Infrared sensor is used to detect a human presence in surrounding and to activate the garbage bin by flip open its flap for a small duration of time. A pressing mechanism ensures optimum usage of the garbage bin. Every time the bin detects new garbage put into it, it activates the pressing mechanism. Two electronic switches are employed for start and stop operation of pressing mechanism. The time period of the mechanism is calculated from start to stop every time it is activated which gives indication of the amount of garbage in the bin. It also has a GSM Modem installed in the waste containers that then send data to the concerning Authority. The Authorities can then calculate optimized collection schedules and routes based on the data sent by the GSM module in each container. Essentially, you always empty the waste containers exactly when needed, never wasting money on nearly empty containers. This is a small step toward Swach Bharat and Smart city Initiatives.

II. PART DESCRIPTION

IR SENSOR : An infrared sensor is an electronic device, that emits in order to sense some aspects of the surroundings. An IR sensor can measure the heat of an object as well as detects the motion. These types of sensors measures only infrared radiation, rather than emitting it that is called as a passive IR sensor. Usually in the infrared spectrum, all the objects radiate some form of thermal radiations. These types of radiations are invisible to our eyes, that can be detected by an infrared sensor. The emitter is simply an IR LED (Light Emitting Diode) and the detector is simply an IR photodiode which is sensitive to IR light of the same wavelength as that emitted by the IR LED. When IR light falls on the photodiode, The resistances and these output voltages, change in proportion to the magnitude of the IR light received. In this project two IR sensors are used one for detecting human presence and another for detecting

garbage being dumped into the bin and activating pressing mechanism.

GARBAGE BIN: In this project an closed bin is designed to provide hygienic surrounding environment. A small opening with flap is provided to put garbage inside the bin. A IR sensor is built and placed around the opening to detect garbage being dumped in the bin and activate the inbuilt pressing mechanism. The design of pressing mechanism consist of a rigid wooden board with gears and DC motor for its up and down movement and electronic switch placed at the bottom of it. The IR sensor at the opening of the bin provides necessary trigger signal to the microcontroller which starts the downward motion of pressing mechanism until all the garbage is compressed to the maximum. At this point the electronic switch beneath the pressing mechanism is on and triggers upward motion of the pressing mechanism up to the start point.

EMBEDDED SYSTEM : An Embedded System is a combination of piece of microcontroller based hardware and typical software to undertake specific task. Embedded systems uses microcontroller to perform its own task. Embedded system prefers microcontroller as it contains RAM, EPROM, OSCILATORS, TIMERS, COUNTERS are in built in microcontroller chip.So microcontroller reduces cost of product and space that gives more advantage in Embedded World..One of the most critical needs of an embedded system is to decrease the power consumption and space. This can be achieved by integrating more functions into the CPU chip. In this project an 8 bit Atmega microcontroller is used, which is triigered by the IR sensor. The microcontroller in trun activates the DC motor to start the downward motion of the pressing mechanism while the electronic switch beneath the pressing mechansim is used to trigger microcontroller and therefore the DC motor for upward movement of the mechanism. The microcotroller is programmed to monitor the time elapsed from start to stop of the mechanism movement every time it is initiated and compares with a predefined value which indicated that the bin is full. At this point the microcontroller closes the flap at the opening of the bin temporarily untill the bin is cleared , displays message on the LCD display that the bin is full and initiate communication with concerning autority through GSM module.

GSM MODULE : A GSM modem is a device which can be either a mobile phone or a modem device which can be used to make a computer or any other processor communicate over a network. A GSM modem requires a SIM card to be operated and operates over a network range subscribed by the network operator. It can be connected to a computer through serial, USB or Bluetooth connection. A GSM modem can also be a standard GSM mobile phone with the appropriate cable and software driver to connect to a serial port or USB port on your computer. GSM modem is usually preferable to a GSM mobile phone. The GSM modem has wide range of applications in transaction terminals, supply chain management, security applications, weather stations and GPRS mode remote data logging.

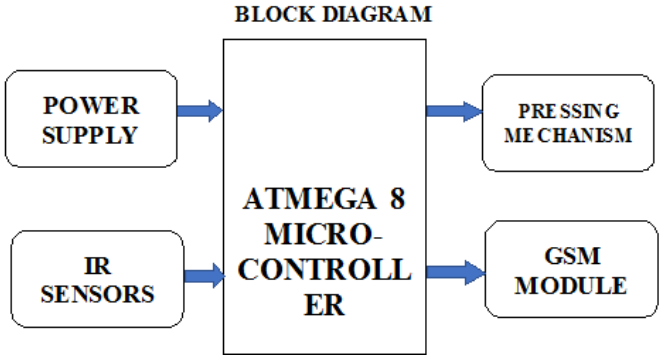

Figure 1

WORKING: The circuit consist of an individual with two infrared detector. One of this sensor senses human presence nearby and open up the flap of the garbage bin making it interactive with the user , the

other sensor is used to detect weather the waste has been delivered, after a time delay of 5 second the flap gets closed . the microcontroller Atmega 8 is programmed to start the Pressing mechanism for optimum use of dust bin space .Two switches at both ends of the pressing mechanism is employed to detect time dealy between start and stop of pressing mechanism, an counter counts the elapsed time and compare with the predefined value to check whether the dust bin is full and then in that case triggers the GSM module which in turn sends message containing dust bin ID and Address to the concerning authority indicating that it is full.

ADVANTAGES :

- User friendly interactive Garbage bin
- Complete utilization of space inside the dustbin by using pressing mechanism
- Closed bin with automated opening and closing mechanism
- Smart communication system between I-SWaCH and concerning authority.

III. CONCLUSION

This small idea ensures that there is proper cleanliness, no overflowing garbage, no foul smell ,optimum usage of the bin and very good management with the concerning authority.

IV. REFERENCES

[1]. Asang Dani, Yashavant Kanetkar , " Go Embedded ", BPB publications 1st edition 2008

[2]. Dhananjay Gadre , "Programming and customizing the AVR microcontroller", Tata Mc Graw- Hill Publishing company ltd 2003

[3]. International Journal of Advanced Research in Electrical, Electronics and Instrumentation Engineering"Infrared Sensor Rig in Detecting Various Object Shapes" Siti Asmah Daud1 , Nasrul Humaimi Mahmood2 , Pei Ling Leow3 , Fauzan Khairi Che Harun4 PhD Student,

[4]. Faculty of Bioscience and Medical Engineering, University Teknologi Malaysia, Johor, Malaysia.

[5]. Senior Lecturer, Department of Biotechnology and Medical Engineering, Faculty of Bioscience and Medical Engineering, University Teknologi Malaysia, Johor, Malaysia.

[6]. Senior Lecturer, Department of Engineering Control and Mechatronics, Faculty of Electrical Engineering, University Teknologi Malaysia, Johor, Malaysia.

National Conference on "Recent Trends in Mathematical Modeling, Simulation Methods, Computations, and Physical Sciences"
(MMSCP-2019), Organised by Hislop College, Nagpur, Maharashtra, India
International Journal of Scientific Research in Computer Science, Engineering and Information Technology
© 2019 IJSRCSEIT | Volume 4 | Issue 4 | ISSN : 2456-3307

Application of Manifold Sensors in Wireless Digital Thermometer

S. S. Shende[1], M. J. Hedau[1], K. Y. Rokde[2]

[1]Assistant Professor, Department of Electronics, Shivaji Science College, Nagpur, Maharashtra, India

[2]Assistant Professor, Department of Electronics, K. R. Pandav, Mahavidyalaya, Nagpur Maharashtra, India

ABSTRACT

This paper describes the application of a manifold sensors in wireless digital thermometer for measuring temperature from different sensors using single wireless digital thermometer. In this paper primarily temperature sensor LM35 is used. ADC0808 is used to convert analog signal obtained from temperature sensor into digital format so that the special parallel to serial encoder will transmit the signal using Tx module to remote receiving end. At the receiving end the transmitted signal is received by receiver module. Reverse action is carried out on the signal to what happed at the transmitting end and temperature detected by sensor is displayed on digital multi-meter on mV scale.

Keywords: Temperature Sensor, ADC, Encoder

I. INTRODUCTION

Temperature is certainly among the most commonly measured parameters in industry, science, and academia. Recently, the growth of wireless instrumentation technology, along with some clever innovations, has provided new ways to apply temperature measurement sensors combined with personal computers to collect, tabulate, and analyse the data obtained.

Wireless monitoring system is, as their name suggests, monitoring systems that can be installed without the need to run cabling or wires. Wireless monitoring systems are the ultimate in quick, easy and neat monitoring installation solutions. Because they are wireless they are very discreet and unobtrusive, there is no buildings' decoration spoiling nor is there an unsightly wire highway on wall surfaces. Wireless monitoring systems are more convenient than hard wired systems and it means that even the most unlikely places can have a wireless monitoring a system installed and in a fraction of the time.

Temperature measurement in today's industrial environment encompasses a wide variety of needs and applications. To meet this wide array of needs the process controls industry has developed a large number of sensors and devices to handle this demand. Temperature is a very critical and widely measured variable for most applications. Many processes must have either a monitored or controlled temperature. The paper deals with measurement of temperature using temperature sensor LM35. In all eight LM 35 sensors are been used in the current work.

II. METHODOLOGY

Temperature measurement can be done using temperature sensor LM35 but the problem arises when one has to measure more than one temperature at a time. To overcome this problem an approach has

been shown in the paper to sense temperature from eight sensors at a time.

At the transmitting end, we have temperature sensor LM35, ADC 0808, Encoder HT12E2, Sequential Data Selector and Transmitter Module. An 8 bit ADC continuously scans and converts signals from eight different temperature sensors. The sensors are selected sequentially by a 3 bit binary addressing system. At any instant of time an 8 bit ADC generates an 8 bit binary number equivalent to the analog signal obtained at the output of a particular temperature sensor, being selected by 3 bit binary addressing system. By using special parallel-to-serial encoders, this 8-bit data, along with the binary address of the sensor, is sent serially to the remote receiving end. Communication between the two ends are met with the help of a pair of 433MHz UHF transmitter and receiver modules operating in ASK/OOK mode. At the receiving end, the transmitted signal is received by a 433MHz ASK/OOK RF receiver module. The received 8-bit serial signal is then converted back to its original parallel form, by using special data decoders HT 12E. An equivalent analogue signal is then developed from this data by an 8-bit digital-to-analogue converter (DAC). A digital multimeter connected at the output of the DAC is used to show the temperature on mV scale.

III. EXPERIMENTAL SETUP & WORKING

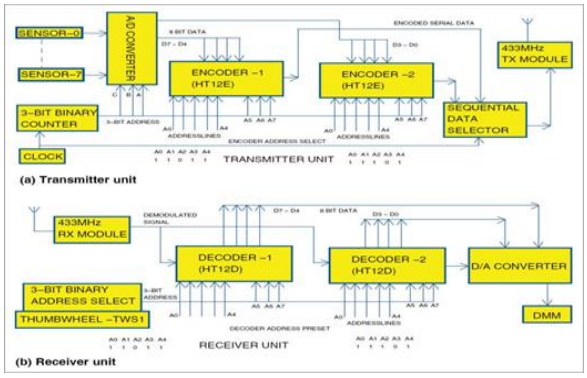

Figure 1. Block Diagram Of Manifold Sensors In Wireless Digital Thermometer

Figure **1.a** shows the block diagram of the transmitter unit for the wireless addressable digital thermometer. Eight LM35 IC temperature sensors are connected to ADC 0808. Although the ADC is capable of accepting a total number of eight sensors through its eight input lines, less number of sensors could be used as well as, whenever desired. IC 7404 configured as a CMOS oscillator with the help of resistors and capacitor feeds the ADC with necessary clock pulses required for conversion processes.

Output voltage of LM35 series IC temperature sensors follows linearly (@10mV/°C) the centigrade temperature of its surroundings, taking 0mV at 0°C temperature. The ADC continuously scans its eight input lines. The scanning process is governed by a 3-bit binary up counter built around CD4029. The counter places a continuously-changing 3-bit binary number on A-B-C input lines of the ADC. Scanning rate is dependent upon the clock constructed around timer NE555, and is 8Hz, approximately. Hence, each of the eight sensors is allowed to send data to the ADC for approximately one-eighth of a second, irrespective of whether all sensors are connected or not.

Here, IC 0808 is configured in continuous operational mode. So, whenever a particular sensor is addressed, output lines of the ADC reflect the present analogue output status of the sensor. Output of the ADC goes to data input lines of special encoders HT12E; higher nibble to first HT12E and lower nibble to second HT12E, respectively. As TE input of encoders is permanently grounded, the encoders are configured to produce encoded data continuously. These two encoded digital outputs are alternately steered to TX1 (TX-433MHz), a UHF RF transmitter module, to modulate UHF carrier wave generated by the module.

Encoder output: Whenever IC 555 output pulse goes high, output of HT12E is steered to TX1 through

diode. At the same time, due to the presence of transistor inverter, output of HT12E is inhibited to reach TX1 through the gate. As soon as the clock pulse returns to logic 0, output of HT12E gets its passage to TX1 through gate of 7408.

So, in essence, analogue data of a sensor is converted and the resultant 8-bit digital data is sent to the remote end using ASK/OOK modulation, in a complete clock cycle of IC 555.

Modulated signal is radiated into space through a wire, acting as an antenna, connected at the antenna point of the module.

Figure **1.b** shows the receiving unit of the wireless addressable digital thermometer. RX1, a 433MHz RF receiver module, is used to receive and demodulate ASK-modulated RF signal transmitted by TX1 of the transmitter unit. Demodulated output is a train of rectangular pulses comprising a 4-bit data nibble and destined for a particular decoder as explained earlier.
Transistor BC547 is used as a pulse amplifier to amplify the signal output from RX1 and, hence, raises the pulse height to CMOS compatible logic -1 (>3.5V at 5V). This compatible output is then fed to CMOS NAND gate 4011. NAND gate helps to get pulses of perfect rectangular-wave shape. Output of IC 4011 is fed to decoders HT12D. Address lines of the decoders are preset to receive data from two encoders HT12E, respectively.
LEDs connected at their outputs flicker to indicate reception of valid data. Decoding speed is 200kHz (approximately). Decoded data is then fed to DAC 0808. Analogue current output of the DAC is loaded. Voltage developed across it is fed to a digital multimeter, which shows the temperature on mV scale. A thumbwheel switch is used to change the preset address of the decoders. The switch changes the last three LSB of the address.

III. RESULT AND DISCUSSION

Table 1. Temperature recorded by different techniques and deviation

Sr. No	Actual	Experimental	Deviation
1.	37.4	37.2	0.2
2.	37.6	37.3	0.3
3.	37	37.1	-0.1
4.	36.8	36.9	-0.1
5.	37	36.8	0.2
6.	36.5	36.3	0.2
7.	37.5	37.3	0.2
8.	36.7	36.4	0.3
9.	37.5	37.3	0.2
10.	36.9	37	-0.1
11.	37.2	37	0.2
12.	37.6	37.4	0.2
13.	36.7	36.9	-0.2
14.	36.8	36.5	0.3
15.	37.5	37.3	0.2
16.	36.9	37	-0.1
17.	37	37.2	-0.2
18.	37.3	37.1	0.2
19.	37.4	37.2	0.2
20.	36.5	36.3	0.2

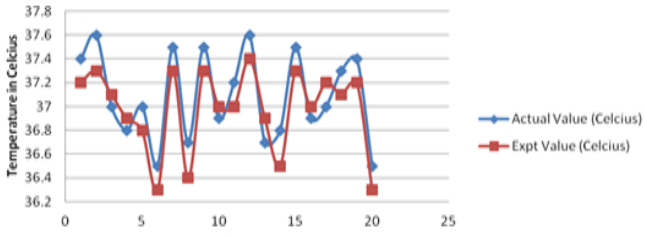

Figure 2. Graph representing the comparison of data for Temperature by different techniques.

For proper operation of this wireless thermometer, reference current (to pin 4 of DAC0808) of the receiver unit should be pre-adjusted. To do this, follow the steps below:

Connect a known voltage source (not exceeding +5V) to any input of the ADC, say, at pin 4 of the ADC.

Switch on the transmitter unit. Connect a DMM across Resistor of the receiver unit. Set the range switch to DC 200mV range, positive lead to ground and negative lead to top of Resistor. Switch on the receiver unit. LEDs at decoder outputs should start glowing to indicate the received voltage data. If source voltage is 1.5V, status of LEDs should be as listed in Table I. So, received voltage = (D× 5)/256 = (76×5)/256 = 1.50

where D is the weight of the binary numbers represented by LED7 through LED14. Now, adjust trim potmeter to get 150.00mV on the dial of the multimeter. Connect another voltage source at the input and see that the multimeter shows it correctly. If required, re-adjust the trim potmeter. After proper calibration, enclose the circuit in two separate boxes with suitable connections of input and LED indicators.

STATUS OF LEDS IN THE RECEIVER UNIT								
LED	7	8	9	10	11	12	13	14
Data	DB7	DB6	DB5	DB4	DB3	DB2	DB1	DB0
Weight	128	64	32	16	8	4	2	1
Status	OFF	ON	OFF	OFF	ON	ON	OFF	OFF

IV. CONCLUSION

Although the system can be used best to measure temperatures in hazardous or inaccessible areas (like a radioactive zone), the same can also be used by a hospital doctor to monitor, from a fixed location, the body temperatures of multiple patients lying in different rooms without visiting each patient in person.

A hotel control room can monitor temperatures of all the rooms at the same time by using multiple units. The unit can also be used (with certain modifications) as a wireless digital voltmeter.

V. REFERENCES

[1]. https://electronicsforu.com/electronics-projects/wireless-digital-thermometer-multiple-sensors

[2]. M. J. Hedau, M. P. Dhore, P. B. Dahikar, "Application of Wireless Signal Simulation Via Cell-Phone "International Conference on circuit system and simulation, , pp. 92–95, Vol.7, IACSIT Press, Singapore, 2011.

[3]. M. J. Hedau, M. P. Dhore, P. B. Dahikar, "Application of Microcontroller in Technical communication"International Journal of ETA and ETS, IACSIT ISSN No 0974-3588Vol.5Issue 1,2012.

[4]. P. B. Dahikar M. J. Hedau, S. C. Moholkar "Application of Microcontroller in Receiving Unit of the Technical Communication" International Journal of ETA and ETS, IACSIT ISSN No 0974-3588 Vol.5 Issue 2, 2012.

[5]. S.S.Shende, P.B.Dahikar, M.J.Hedau, K.Y.Rokde, "Alternative Technique to perform Surgeries in Hospital by Surgical Diathermy" International Journal of Innovative Research in Computer and Communication Engineering- IJIRCCE", of ISSN number is 2320-9798 on Vol.2, Issue 1, 2014.

National Conference on "Recent Trends in Mathematical Modeling, Simulation Methods, Computations, and Physical Sciences"
(MMSCP-2019), Organised by Hislop College, Nagpur, Maharashtra, India
International Journal of Scientific Research in Computer Science, Engineering and Information Technology
© 2019 IJSRCSEIT | Volume 4 | Issue 4 | ISSN : 2456-3307

Environmental Monitoring Using Wireless Sensor Networks(WSN) based on IOT

Madhav G Raut[1], Pradeep B. Dahikar[2]

[1]Department of Electronics, Hislop College, Nagpur, Maharashtra, India
[2] Department of Electronics, Kamla Nehru Mahavidayalya, Nagpur, Maharashtra, India

ABSTRACT

In recent years, we have seen a new era of short-range wireless technologies like Wi-Fi, Bluetooth , ZigBee, emerging in front of us. The project aims at building a system which can be used on universally at any scale to monitor the parameters in each environment. Raspberry-pi and sensors collects all the real-time data from environment and this real-time data is fetched by the web server and display it. User can access this data from anywhere through Internet. Raspberry Pi works as a base station which connects the number of distributed sensor nodes via zigbee protocol. Wireless Sensor Networks (WSN) has been employed to collect data about physical phenomenon in various applications such as habitat monitoring. The Internet of Things (IoTs) can be described as connecting everyday objects like smart-phones, Internet TVs, sensors and actuators to the Internet where the devices are intelligently linked together enabling new forms of communication between things and people, and between things themselves. In wireless sensor network system, the sensor node sense the data from the sensor and that data collects the end tags, end tags send its data to the router and router to coordinator.

Keywords : WSN, Arduino, Arm Microcontroller,WSN, Zigbee Module.

I. INTRODUCTION

The development in wireless sensor networks can be used in monitoring and con- trolling various parameters in the agriculture field, weather station field. The sensor network hardware platforms are basically low -power embedded systems with some different sensors such as onboard sensors and analog I/O ports to connect sensors. Like hardware, software should also be developed, including OS, sensor/hardware drivers, networking protocols and application-specific sensing and processing algorithms. The purpose or objective of environmental monitoring is different in different situations, but important aims to environmental monitoring to find risks to human and wildlife, scope to population migration from high density areas to low density areas and to restrict emission of gases. Wireless sensor network (WSN) is a low cost, low power wireless network made up of thousands of smart sensor nodes which monitor physical or environmental conditions, such as temperature, pressure, moisture, etc. at different area or different location. The Internet of Things (IoT) is an emerging key technology for future industries, and environmental monitoring. The Internet of Things (IoTs) can be described as connecting everyday objects like smart-phones, Internet TVs, sensors and actuators to the Internet where the devices are intelligently linked together enabling new forms of communication between things and people, and between things themselves. Building IoTs has

advanced significantly in the last couple of years since it has added a new dimension to the world of information and communication technologies.

II. INTERNET of TINGS (IOT)

The Internet of things (stylized Internet of Things or IoT) is the internetworking of physical devices, vehicles (also referred to as "connected devices" and "smart devices"), buildings, and other items—embedded with electronics, software, sensors, actuators, and network connectivity that enable these objects to collect and exchange data. In 2013 the Global Standards Initiative on Internet of Things (IoT-GSI) defined the IoT as "the infrastructure of the information society. “The IoT allows objects to be sensed and/or controlled remotely across existing network infrastructure, creating opportunities for more direct integration of the physical world into computer-based systems, and resulting in improved efficiency, accuracy and economic benefit in addition to reduced human intervention. Typically, IoT is expected to offer advanced connectivity of devices, systems, and services that goes beyond machine-to-machine (M2M) communications and covers a variety of protocols, domains, and applications. the vision of the Internet of things has evolved due to a convergence of multiple technologies, including ubiquitous wireless communication, real-time analytics, machine learning, commodity sensors, and embedded systems.

III. WIRELESS SENSOR NODE (WSN)

The main components of a sensor node are a microcontroller, transceiver, external memory, power source and one or more sensors. The controller performs tasks, processes data While the most common controller is a microcontroller, other alternatives that can be used as a controller are: a general-purpose desktop microprocessor, digital signal processors, FPGAs and ASICs. A microcontroller is often used in many embedded systems such as sensor nodes because of its low cost, flexibility to connect to other devices, ease of programming, and low power consumption. Transceiver Sensor nodes often make use of ISM band, which gives free radio, spectrum allocation and global availability. The possible choices of wireless transmission media are radio frequency (RF), optical communication (laser) and infrared. Radio frequency-based communication is the most relevant that fits most of the WSN applications. WSNs tend to use license-free communication frequencies: 173, 433, 868, and 915 MHz; and 2.4 GHz. The functionality of both transmitter and receiver are combined into a single device known as a transceiver. From an energy perspective, the most relevant kinds of memory are the on-chip memory of a microcontroller and Flash memory—off-chip RAM is rarely, if ever, used. Flash memories are used due to their cost and storage capacity. Memory requirements are very much application dependent. A wireless sensor node is a popular solution when it is difficult or impossible to run a mains supply to the sensor node. A wireless sensor node is a popular solution when it is difficult or impossible to run a mains supply to the sensornode.

IV. OVERALL ARCHITECTURE

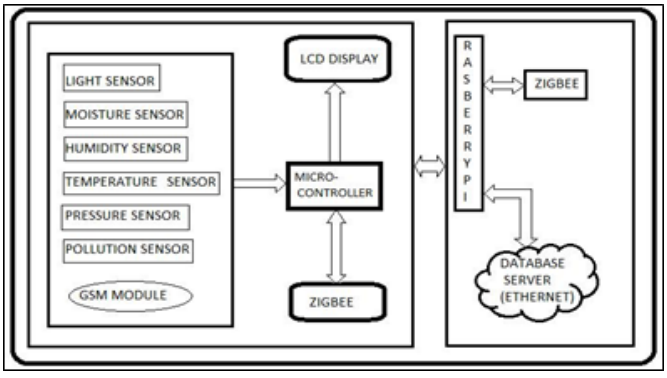

Figure 1

WORKING :

The figure shows the overall system architecture of environmental monitoring wireless sensor network

system Sensor node is a major part in this system it is responsible for information or sensor data. Raspberry pi manages multiple sensor nodes. Design and Implementation of Environment monitoring system using Raspberry-Pi which contains interfacing with various sensors (temperature, Humidity, CO2, Vibration). Real time data will be collected by all the sensors and will be fetched by the Webserver. the gateway node of wireless sensor network, that is raspberry pi (base station) consist of database server and web server in one single-board computer hardware platform, it reduces the cost and complexity of deployment. Sensor node sense the data from the sensor and that data receives the end tag, end tag search the nearest router if router in its range it immediately sends the data to the router, next router to coordinator, here coordinator is directly communicating with the base station. Base station sends all data to the cloud or Ethernet (Database server). The WSN is built using a coordinator node and several sensor nodes, a workstation and a database.

V. RASPBERRY PI

The Raspberry Pi is a low cost, credit-card sized computer that plugs into a computer monitor or TV, and uses a standard keyboard and mouse. The raspberry pi is the cheapest ARM11 powered Linux operating system single board computer board. This board runs an ARM11microcontroller @1GHz and comes with a 1GB of RAM memory [16,17], as this model has better specifications as compared to other raspberry pi models such as raspberry pi B and B+ model [4]. It is a capable little device that enables people of all ages to explore computing, and to learn how to program in languages like Scratch and Python. It's capable of doing everything you'd expect a desktop computer to do, from browsing the internet and playing high-definition video, to making spreadsheets, word-processing, and playing games. It supports 32GB external SD or micro SD card, the device consists a 4USB ports.

VI. ARDUINO PLATFORM

The Mega 2560 is a microcontroller board based on the ATmega2560. It has 54 digital input/output pins (of which 15 can be used as PWM outputs), 16 analog inputs, 4 UARTs (hardware serial ports), a 16 MHz crystal oscillator, a USB connection, a power jack, an ICSP header, and a reset button. It contains everything needed to support the microcontroller; simply connect it to a computer with a USB cable or power it with a AC-to-DC adapter or battery to get started. The Mega 2560 board is compatible with most shields designed for the Uno and the former boards Duemilanove or Diecimila. Arduino Mega, etc. I used Arduino Uno in this development. Arduino is based on ATmega328. The package contains a 16 MHz ceramic resonator, a USB connection, a power jack and ICSP header and a reset button. Instead of using the FTDI USB-to-serial driver chip our Arduino features the Atmega16U2 chip programmed as a USB-to-serial converter.

VII. XBEE MODULE

Zigbee is a high-level communication protocols used to create wireless networks. Transmission distances to 10–100 meters depending on power output and environmental characteristics, ZigBee devices can transmit data over long distances by passing data through a mesh network topology. The Zigbee transmission data rate is 250 Kbit/s [6]. Zigbee is an established set of specifications for wireless personal area networking (WPAN), i.e. digital radio connections between computers and related devices. For the wireless communication between sensor nodes and the gateway node ZigBee RF modules were used. All the ZigBee devices are based on ZigBee standard which has adopted IEEE 802.15.4 for its physical layer and MAC protocols. The wireless devices based on this standard operate in 868 MHz, 915 MHz and 2.4 GHz frequency bands having a

maximum data rate 250Kbps. ZigBee protocol layers are based on OSI model. When the pan is to use ZigBee, it is necessary to mention IEEE 802.15.4 standard. One of the finest characteristics about this standard is it allows user to use PHY and MAC layer defined by IEEE 802.15.4 and lets user to define the upper layers of the OSI model. Similarly, ZigBee also use the MAC and PHY layer of IEEE 802.15.14 standard.

VIII. CONCLUSIONS

Comparing with collection and forwarding information or data of traditional base station (gateway), this system has low-cost, low power consumption, and easy to maintain. This paper designs a wireless sensor network system using Raspberry Pi as a base station, XBee as a networking protocol, sensor node as combination of sensors, controller and zigbee. Hence, we can create sensor-logging application, location-tracking applications, and a social network of things with status updates, so that you could have your location parameter control itself based on your current location. One major advantage of the system lies in the integration of the gateway node of wireless sensor network, database server, and web server into one single compact, low - power, credit-card-sized computer Raspberry Pi, which can be easily configured to run without monitor, keyboard, and mouse. Such a system is very useful in many environmental monitoring and data collection

IX. REFERENCES

[1]. Kochlan, M.; Hodon, M.; Cechovic, L.; Kapitulik, J.; Jurecka, M., “WSN for traffic monitoring using Raspberry Pi board,” Computer Science and Information Systems

[2]. (FedCSIS), 2014 Federated Conference on, vol., no., pp.1023,1026, 7-10 Sept. 2014 C. Pfister, Getting Started with the Internet of Things. Sebastopol, CA: O'Reilly Media Inc., 2011.

National Conference on "Recent Trends in Mathematical Modeling, Simulation Methods, Computations, and Physical Sciences"
(MMSCP-2019), Organised by Hislop College, Nagpur, Maharashtra, India
International Journal of Scientific Research in Computer Science, Engineering and Information Technology
© 2019 IJSRCSEIT | Volume 4 | Issue 4 | ISSN : 2456-3307

Transparent Patch Antenna Development for Solar Cell Hybridisation

Anup P. Bhat[1], S. J. Dhoble[2], K. G. Rewatkar[3]

[1]Department of Electronics and Computer Scie, RTM Nagpur University, Nagpur, Maharashtra, India

[2]Department of Physics, RTM Nagpur University, Nagpur, Maharashtra, India

[3]Department of Physics, Dr. Ambedkar College, Deekshabhoomi, Nagpur, Maharashtra, India

ABSTRACT

Straightforward fix antennas are microstrip fix antennas that have a specific dimension of optical straightforwardness. Exceptionally straightforward fix antennas are possibly reasonable for incorporation with solar boards of little satellites, which are winding up progressively critical in space investigation. Conventional fix antennas utilized on little satellites rival solar cells for surface territory. Be that as it may, a straightforward fix antenna can be set legitimately over solar cells and resolve the issue of going after restricted surface land. For such coordination, a high optical straightforwardness of the fix antenna is required from the solar cells' perspective. Then again, the antenna ought to have at any rate adequate radiation properties in the meantime. Dynamic coordinated antenna structure strategy is reached out to coincided fix applications trying to improve the general power efficiency of the front end correspondence subsystem.

I. INTRODUCTION

There is a few probability of putting solar cells straightforwardly on the patches. Different mixes like putting solar cells behind reflect cluster antennas have likewise been contemplated. On account of fix antennas, the cells can't be near the patches' transmitting edges because of damaging collaborations. As innovation has been progressing quickly, a thought rose to incorporate the antenna and solar cell into (solid) building square units. These units may then be duplicated as wanted to make a structure whose transmitting gap is additionally utilized as the light – gathering territory. A tale half and half innovation where formless silicon solar cells are either coordinated or physically joined with printed space antennas is exhibited.

This fundamental thought is shown with the assistance of two inventive structures where the solar cells are legitimately developed on a hardened steel ground – plane or stuck onto a standard copper layer imprinted on a dielectric substrate. execution when contrasted and a straightforward juxtaposition of antennas and solar cells.

Straightforward fix antennas, as an uncommon kind of microstrip fix antennas have been considered for over two decades. Their normal structure comprises of a best layer conductive fix, base layer ground, and dielectric substrate in the middle. In this investigation, the best layer conveyor and the dielectric substrate of the fix antenna are should have been optically straightforward.

The conductor's straightforwardness can be accomplished by applying straightforward conductive

oxides films as strong strip and work structure where the conductive oxide, for example, indium tin oxides (ITO), by using coincided sheets on standard and hexagonal conductors sheet for the substrate, models incorporate ordinary glass, spread glass of solar boards, and so on.

An essential use of straightforward fix antennas is their joining with the solar boards for little satellites, where constrained surface zone is an issue for mounting antennas, solar cells, and space instruments. This is of incredible importance for little satellites. Other conceivable applications incorporate reconciliation of antennas with window glass or vehicle windshield or unpleasant best antenna, electrical vehicle following antenna.

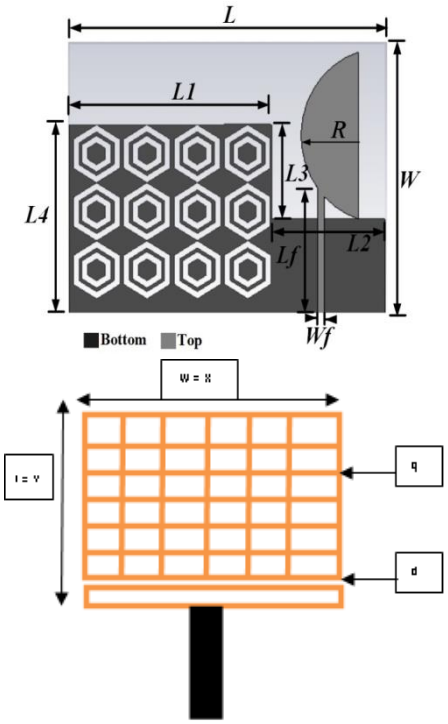

Figure 1 : Antenna design for ITO Glass in Hexagonal and rectangular pattern Mesh Deposition

Table 1: Antenna dimensional parameter

L	45	L3	12
W	35	L4	13
Lf	17	L5	32
Wf	1.2	L6	28
L1	30	a	8
L2	15	g	0.8

These antennas are electrically like customary fix antennas and have similar points of interest. Moreover, they give high optical straightforwardness, which is basic for the solar cells. In this manner, they can be set straightforwardly over the solar board without influencing the solar cells' usefulness. Huge space make expected to agree to the expanding interest for media transmission, interactive media and expanding logical goals. The need to actualize a few complex instruments on one single space make prompts an expansion in the number and size of antennas and solar generators.

For the above issue there is the choice to spare "land" by joining two capacities keeping up execution square with or to expand ability (e.g., to offer correspondence in a non-ostensible circumstance). SONTENNA could even be a mission empowering arrangement.

The physical antenna is organized with the length, width and thickness based arrangement with the assortment in the permittivity and vulnerability. The length and the width of a fix can be found by a mix of informative examination and accurate procedures. Fix width minorly influences the booming repeat and radiation case of the antenna. A greater fix width extends information transmission, and radiation efficiency. With genuine excitation one may pick a fix width W more noticeable than the fix length L without stimulating undesired modes. It might be seen that the width can be resolved from conditions as frail:

$$W = \frac{c}{2fr}\sqrt{\left(\frac{(\varepsilon r+1)}{2}\right)} \quad (1)$$

Additionally, the fix length decides the resounding recurrence, and is a basic parameter in structure on account of the inalienable restricted transmission capacity of the fix. The length is found by ascertaining the half-wavelength esteem and afterward subtracting a little length to display the bordering fields impact.

$$l = \frac{c}{2fr\sqrt{\varepsilon eff}} - 2\Delta l \quad (2)$$

$$\Delta l = 0.412h\frac{(\varepsilon eff+0.3)\left(\frac{W}{h}+0.264\right)}{(\varepsilon eff-0.258)\left(\frac{W}{h}+0.813\right)} \quad (3)$$

$$\varepsilon eff = \frac{\varepsilon r+1}{2} - \frac{\varepsilon r-1}{2}\sqrt{(1+\frac{12t}{W})} \quad (4)$$

$$\boldsymbol{Zo = \frac{120\pi}{\sqrt{\varepsilon reff}(1.393+\left(\frac{W}{h}\right)+\frac{2}{3}\ln(\frac{w}{h}+1.444)}} \quad (5)$$

Straightforward fix antennas can be coordinated with surface-mounted solar boards of little satellites [3] or window glass of structures or autos [4]. These applications require high optical straightforwardness just as great radiation properties of the antenna. Fix antennas produced using straightforward conductive film, for example, silver covered polyester and indium tin oxides (ITO) films, were accounted for [1, 5]. Be that as it may, the straightforwardness of these antennas isn't sufficiently high for viable applications. Reports on coincided fix antennas recommended an unpredictable exchange off between the antenna's properties: the transfer speed and cross-polarization level can be improved by sacrificing the increase [2]; a low radar cross segment (RCS) can be accomplished if the addition and transmission capacity are undermined [6].

Figure 2: transparent mesh design with solar cell and patch antenna

The polyimide substrate is secured by an aluminum layer (back contact) and by a ZnO layer, which forestalls aluminum dispersion. The layers referenced above additionally structure a mirror for the occurrence solar light so as to expand assimilation and therefore, produce increasingly current. The genuine solar cell is made of three silicon layers: a slight high conductivity phosphor doped n-layer, a natural (un doped) layer with a low imperfection thickness and an extremely meager exceptionally conductive p-layer. Most photons are invested in the natural layer, while the doped layers are in charge of the development of an electric field inside the solar cell itself. The gatherer layer over the cell must be straightforward and conductive and thus it is made of straightforward conductive oxides(TCOs)- either indium tin oxide or zinc oxide. Since TCOs have a somewhat low conductivity contrasted with metals, a finger design is stored on top made of a Cr grip layer secured by thicker Ag layer .Overall the cell thickness is under 5μm however normally a 50 μm thick polyimide substrate is utilized as a help in independent applications. In spite of the fact that this kind of cell is less proficient than Ga-As solar cells which are right now utilized in space applications, a-Si:H cells demonstrates a superior watt/kilogram proportion because of their light weight.

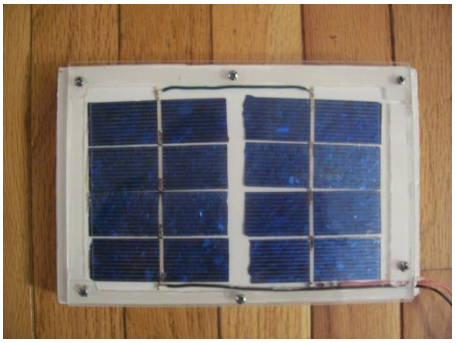

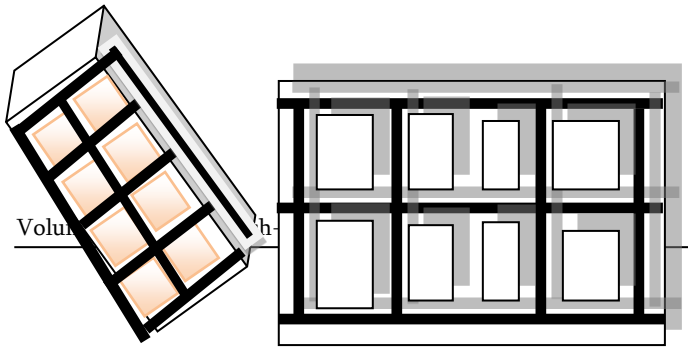

Figure 3 : developed solar cell antenna

Mesh structure

Hypothetically, the geometry of coincided fix antennas can be a self-assertive shape. As referenced before in this segment, nonetheless, the work example ought to be planned dependent on the present ways on the fix that are required for a specific radiation mode. This guarantees unsurprising antenna properties as well as concealment of undesired radiation modes. This paper for the most part centers around rectangular and roundabout fit patches, as delineated in Fig. 3, because of their generally basic work designs. It tends to be seen that a coincided fix antenna comprises of two arrangements of work lines. The first set of lines are in charge of conveying the ideal flows while the second gathering of lines are symmetrical to the present way lines with the end goal that a fix can be shaped.

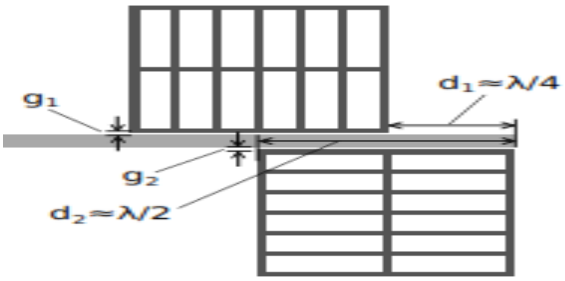

Figure 4: Mesh design for quarter$\lambda/4$ and $\lambda/2$ array antenna design

Table 2: antenna designed with frequency and dielectric basis

Freq Ghz	W um	L um	effective dielectric Ɛreff	Δ L	Lg um	Wg Um
1.227	97256392	83180172.61	2.160000035	0.841936	83180180	97256401.2
1.575	75767360	64801315.27	2.160000045	0.841936	64801323	75767369.9
1.72	83917190	80971803.68	1.160000022	1.05366	80971811	83917199.8
2.1	56825520	48600986.28	2.16000006	0.841936	48600994	56825529.8
2.4	49722330	42525862.91	2.160000069	0.841936	42525871	49722339.7
2.6	45897536	39254642.64	2.160000074	0.841936	39254650	45897545.1
3	39777864	34020690.2	2.160000086	0.841936	34020698	39777873.7

The optical transparency of such meshed patches is defined as the percentage of the see-through area of the patch. As an example, the formula to calculate the transparency (T) of a rectangular meshed patch which has a dimension of W (width) by L (length) is given as follows:

$$transparacy = \left[1 - \frac{Aconductor}{Apatch}\right] * 100 = \left[1 - \frac{q(NL+MW)-q2NM}{WL}\right] * 100\% \quad (6)$$

Feed technique

Among the most widely recognized bolstering procedures for microstrip fix antennas are test feed and inset feed. For solar board coordinated coincided patches, these two feed structures can just confound the plan. With the nearness of solar cells, making a

by means of through the solar board is wrong in reasonable structure. In the event that the inset feed line is picked, at that point the geometry of the fit fix must be balanced so as to help a progressively mind boggling current examples because of the abnormality of the fix shape. Because of such focal points, the T-coupling feed structure, was utilized in this investigation.

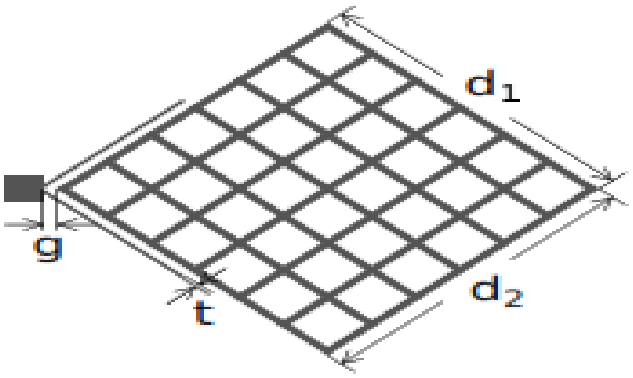

Figure 5 : mesh design with the T-Coupling axial feed point

As an upgraded sort of closeness line coupling, the T-coupling plan can be utilized to couple a ring resonator or to nourish a round or rectangular antenna [9– 11]. This encouraging technique possibly gives two degrees of opportunity to tuning: the branch thickness and the dividing s as set apart for both rectangular and hexagonal coincided fixes in Fig.

Impact of line width

A lot of test encouraged rectangular coincided fix antennas were structured on ITO , Zn and Glass plate (μ= 2.6, tanδ = 0.0037, h = 2.132 mm) and analyzed so as to think about the impact of line width and on the antenna properties. The substrate (roughly 100 mm × 170 mm) was supported with copper. These antennas have similar measurements (45 mm × 35 mm). To accelerate the recreation, the optical straightforwardness was picked to be 70%. It is conceivable to do a similar report with antennas of 90% straightforwardness and achieve a similar end. Be that as it may, the higher the straightforwardness, the smaller the work line width, and increment the proficiency

Impact of Orthogonal Lines

The flows primarily flow on the matrix lines parallel to the length of the fix (L), while the flows flow on the lines symmetrical to the length of the fix are negligible [13]. This marvel recommends that lessening the symmetrical lines ought not affect antenna properties in a vast sense and that one can accomplish additional optical straightforwardness by such decrease. The accompanying investigation was set up to break down the effect of the symmetrical lines on the antenna execution. The length and width of the fit fix antenna were stayed to be 37 mm and Table 2.1: Simulated feed point embed remove versus linewidth of rectangular fit patches (45 mm × 37 mm). he work geometry comprises of 25 to 50 lines parallel to the present ways, or length, of the fix and the quantity of lines symmetrical to the fix length changed from 20 to 6 with a fixed line width q of 0.3 mm; subsequently, the optical straightforwardness extended from 70% to 79%.

Table 3: transparency basis of the frequency application

Surface material	90% ITO Coated	85% Coated	70% Plastic Coated	72 Polymer doped	**Efficiency**

Surface resistance Ohm/Sqm	4.7	4.7	3.9	5.0	
freq	2.5	3.10	4.5	5.4	6.3
S11 dB	-5.7	-9.3	-13	-20	-18.8
Efficiency	22.1	39.5	65.9	75.6	89.4

As can be observed, decreasing the number of orthogonal lines does not hinder the performance of the meshed patch antenna, and the antenna transparency can be optimized without severely degrading its radiation properties.

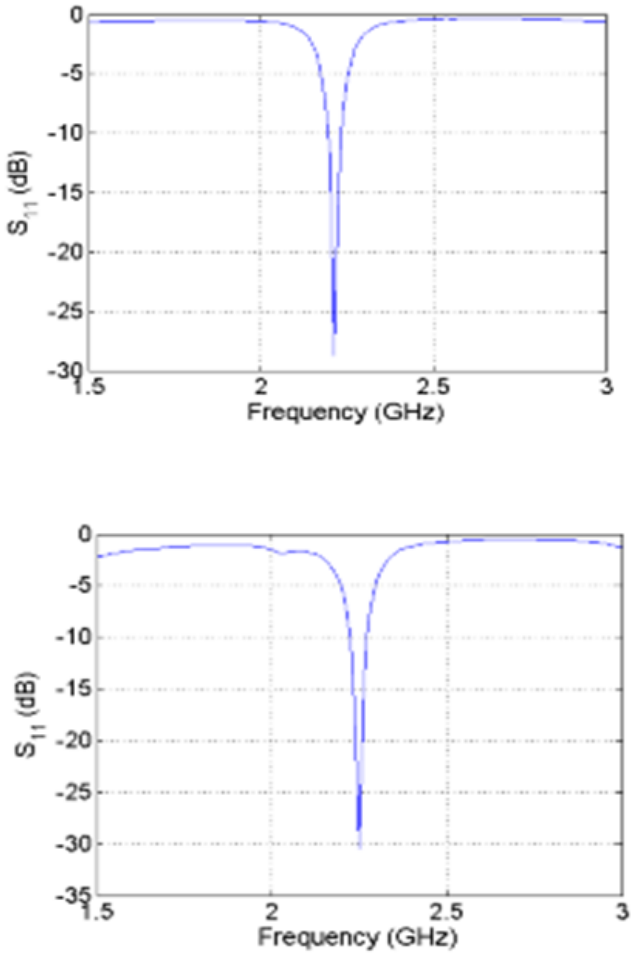

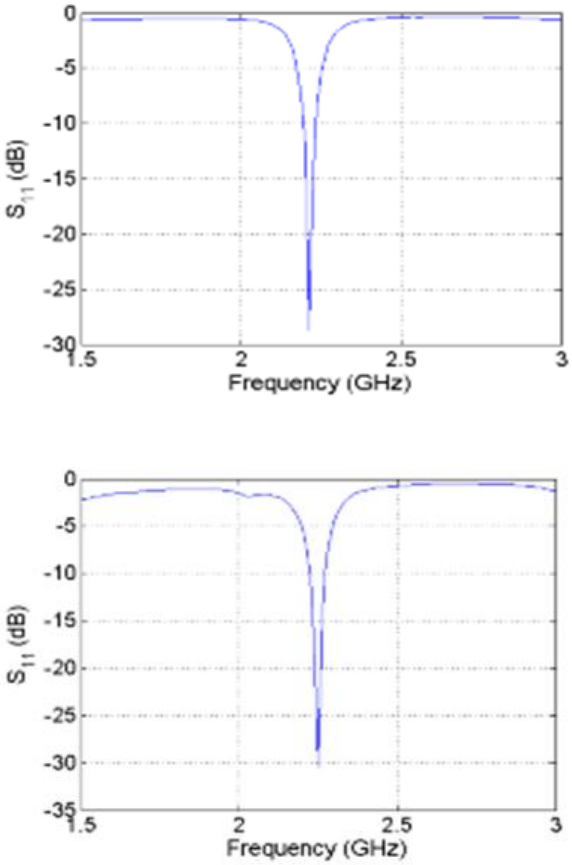

Figure 5 : Effect of feed point a on frequency and feed point

Table 4 : design patch frame

Antenna Parameter	Patch 1	Patch 2
Width	45 mm	45 mm
Length	35.4 mm	35.4 mm
Line Width (q)	1 mm	2 mm
Resonant Frequency	2.417 GHz	2.359 GHz
Input Impedance	226 Ω	262 Ω
Gain	5.471 dB	5.338 dB
Impedance Bandwidth	1.86 %	1.70 %

II. RESULTS AND DISCUSSION

Despite the fact that in the real execution of combination with solar cells, a straightforward

dielectric (for example spread glass) will be the substrate for fit fix antennas, the plan reasoning of the CP fit antennas is the equivalent for straightforward and non-straightforward substrates. Consequently, in the present research center approval, Roger's RO4003C cover (o= 3.55, h = 1.524 mm, tand = 0.0021) was picked to inspect the structure. The two coincided patches are straightforward to lights and the straightforwardness is defined as the proportion of the seethrough zone over the whole fix zone.

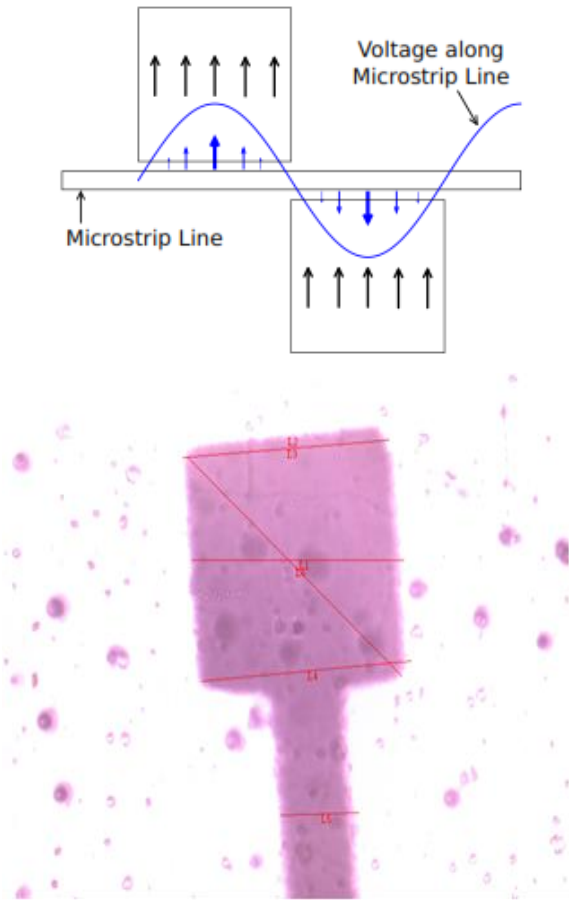

Figure 6 : current direction with the developed transparent rectangular mesh structure

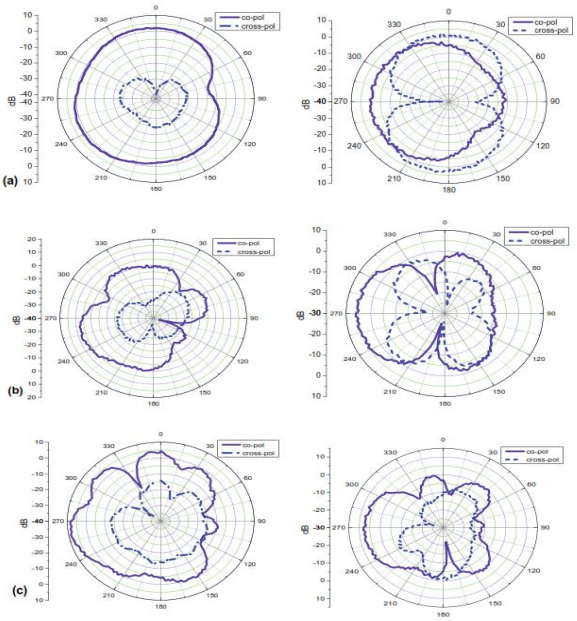

Figure 7 : radiation pattern measure with the antenna

The meshed patches can be placed on solar cells whereas the non-transparent feed line can be placed along the gap between solar cells. The transparency of the meshed antenna can be controlled by the width and the number of the mesh lines. The relation between the transparency and antenna properties has been found [15]. The operational frequency is chosen to be in S band, where the size of the meshed patch is realistic to be placed on top of a commercial triple-junction solar cells used in space applications.

Table 6 : antenna design with the frequency

Freq	2.5	3.10	4.5	5.4	6.3
Patch size	13.5x16.7	19.3x20.2	221.0x17.4	21.5x18	7.3x5.5
Line width	0.20	0.16	0.17	0.045	0.13
Loss tangent	0.000256	0.000256	0.000256	0.000256	0.000256

Data transmission Enhancement Mechanism

The proposed strategy to broaden the data transfer capacity in this paper is accomplished by utilizing three fit patches of somewhat different sizes The

three antennas utilize a similar feed line and such a configuration is exceedingly practical to be executed on a multi-U CubeSat (for example joining a few CubeSats together where each CubeSat has an element of 10 cm × 10 cm × 10 cm) for frequencies higher than S band. The holes between the fit patches and the feed line should be tuned all the while so as to accomplish an impedance coordinating. Furthermore, it is fundamental for all the three patches to create surface flows in stage, bringing about including bordering fields. Something else, the radiation would be extraordinarily diminished because of sources wavering in inverse ways. This can be acknowledged when the two nearby fixes are set on different sides of the feed line.

Table 7 : antenna dimension with the solar cell efficiency

	Antenna designe	Line width mm	No of Line in mesh x mm	No of Line in mesh y mm	S11 dB	Inner distance D mm	Feed line position	Efficiency %
47x36	Rectangular A	0.45	25	27	-23.0	13.2	20	78.2
45x35	Rectangular B	0.53	30	32	-22.4	13.5	22	78.9
40x30	Rectangular C	0.80	34	32	20.3	13.9	12	73.4
47x36	Hexagon A	0.60	22	42	21.3	14.5	12	73.5
45x35	Hexagon B	0.80	28	40	22.6	13.5	12	73.7
40x30	Hexagon C	1.10	30	45	21.3	13.2	12	76.1

III.CONCLUSION

In the moment the expanding voltage size, as theoretically is framed along the open-finished feed line, diminishing surface flows are incited, by means of capacitive coupling, flowing in a similar heading on both the patches. The purpose behind this is the positive voltage on the feed line drives "positive charges" on the upper fix far from the hole side while the negative voltage pulls "positive charges" on the fit antennas is the equivalent for straightforward and non-straightforward substrates. In this way, in the present research center approval,. As a source of perspective antenna, a solitary component square fix with 30 mm side length and 1 mm work line thickness, was intended to reverberate at about 2.48 GHz and manufactured utilizing a circuit board processing machine. The coupling hole and the situation of the fix regarding the tip of the feed line were tuned to get a decent impedance coordinate. Figure demonstrates the model of the antenna intended for impedance transmission capacity improvement. The transparencies of these patches, defined as the proportion of the region of the openings inside the fix to that of the whole fix, are around 70%. This straightforwardness isn't sufficiently high for the genuine applications from the solar cells' point of view, in any case, these parameters were picked for the simplicity of creation utilizing the processing machine and an extremely high straightforwardness can be accomplished by refining the work lines of the fix with an increasingly exact assembling office.

IV. REFERENCES

[1]. S. Vaccaro, C. Pereira, J. Mosig, and P. de Maagt, “In-flight experiment for combined planar antennas and solar cells (solant),” IET

Microwaves, Antennas & Propagation, vol. 3, no. 8, pp. 1279–1287, 2009.

[2]. A. P. Bhat, "smart instrumentation technology for nanostructure antenna and solar cell" Master's thesis, RTM Nagpur University Nagpur , India, 2017.

[3]. R. N. Simons and R. Q. Lee, "Feasibility study of optically transparent microstrip patch antenna," IEEE Antennas and Propagation Society International Symposium, vol. 4, pp. 2100–2103, 1997.

[4]. K. Ito and M. Wu, "See-through microstrip antennas constructed on a transparent substrate," 7th IET International Conference on Antennas and Propagation, pp. 133–136, 1991.

[5]. G. Clasen and R. Langley, "Meshed patch antenna integrated into car windscreen,"Electronics Letters, vol. 36, no. 9, pp. 781–782, 2000.

[6]. "Meshed patch antennas," IEEE Transactions on Antennas and Propagation, vol. 52, no. 6, pp. 1412–1416, 2004.

[7]. X. He, S. Gong, Y. Ji, and Q. Liu, "Meshed microstrip patch antennas with low RCS," Microwave and Optical Technology Letters, vol. 46, no. 2, pp. 117–120, 2005.

[8]. T. W. Turpin, "Meshed patch antennas integrated on solar cell - a feasibility study and optimization," Master's thesis, Utah State University, Logan, UT, 2009.

[9]. N. Outaleb, J. Pinel, M. Drissi, and O. Bonnaud, "Microwave planar antenna with RF sputtered indium tin oxide films," Microwave and Optical Technology Letters, vol. 24, no. 1, pp. 3–7, 2000.

[10]. P. Prajuabwan, S. Porntheeraphat, A. Klamchuen, and J. Nukeaw, "ITO thin films prepared by gas-timing RF magnetron sputtering for transparent flexible antenna," 2nd IEEE International Conference on Nano/Micro Engineered and Molecular Systems, pp. 647–650, 2007.

[11]. F. Colombel, X. Castel, M. Himdi, G. Legeay, S. Vigneron, and E. M. Cruz, "Ultrathin metal layer, ITO film and ITO/Cu/ITO multilayer towards transparent antenna," IET Science, Measurement & Technology, vol. 3, no. 3, pp. 229–234, 2009.

[12]. H. J. Song, T. Y. Hsu, D. F. Sievenpiper, H. P. Hsu, J. Schaffner, and E. Yasan, "A method for improving the efficiency of transparent film antennas," IEEE Antennas and Wireless Propagation Letters, vol. 7, pp. 753–756, 2008.

[13]. G. Clasen and R. Langley, "Gridded circular patch antennas," Microwave and Optical Technology Letters, vol. 21, no. 5, pp. 311–313, 1999.

[14]. S.Vaccaro, P.Torres, J.R.Mosig, A.Shah, "Integratesolar panel antennas," Electron. Lett., vol.36, no.5, pp. 390-391, Mar.2000

[15]. "Capabilities of printed reflectarray antennas," in Proc. IEEE Phased Array Systems and Technology Symp., Boston, MA,Oct.1996, pp. 131-134.

[16]. K. Ito and M. Wu, "See-through microstrip antennas constructed on a transparent substrate," 7th IET International Conference on Antennas and Propagation, pp. 133–136, 1991.

[17]. G. Clasen and R. Langley, "Meshed patch antennas," IEEE Transactions on Antennas and Propagation, vol. 52, no. 6, pp. 1412–1416, 2004.

[18]. T. W. Turpin and R. Baktur, "Meshed patch antennas integrated on solar cells," IEEE Antennas and Wireless Propagation Letters, vol. 8, pp. 693–696, 2009.

[19]. G. Clasen and R. Langley, "Meshed patch antenna integrated into car windscreen," Electronics Letters, vol. 36, no. 9, pp. 781–782, 2000.

[20]. R. N. Simons and R. Q. Lee, "Feasibility study of optically transparent microstrip patch antenna," IEEE Antennas and Propagation

Society International Symposium, vol. 4, pp. 2100–2103, 1997.

[21]. X. He, S. Gong, Y. Ji, and Q. Liu, "Meshed microstrip patch antennas with low RCS," Microwave and Optical Technology Letters, vol. 46, no. 2, pp. 117–120, 2005.

[22]. G. Clasen and R. Langley, "Gridded circular patch antennas," Microwave and Optical Technology Letters, vol. 21, no. 5, pp. 311–313, 1999.

[23]. D. Pozar, "Five novel feeding techniques for microstrip antennas," IEEE Antennas and Propagation Society International Symposium, vol. 25, pp. 920–923, 1987.

[24]. L. Zhu and K. Wu, "Line-to-ring coupling circuit model and its parametric effects for optimized design of microstrip ring circuits and antennas," IEEE MTT-S InternationalMicrowave Symposium Digest, vol. 1, pp. 289–292, 1997.

National Conference on "Recent Trends in Mathematical Modeling, Simulation Methods, Computations, and Physical Sciences"
(MMSCP-2019), Organised by Hislop College, Nagpur, Maharashtra, India
International Journal of Scientific Research in Computer Science, Engineering and Information Technology
© 2019 IJSRCSEIT | Volume 4 | Issue 4 | ISSN : 2456-3307

A Review of Identity Recognition System Based on Biometrics

A. A. Halder, Dr. S. R. Pande
Department of Computer Science, SSES Amt's Science College Congress Nagar, Nagpur, Maharashtra, India

ABSTRACT

Personal identity recognition system based on biometrics is an effective method to recognize any person automatically with great accuracy and confidence. Palmprint is one of the biometric traits which are used to identify any person with accuracy. There are two types of features in palmprint that is structural feature and statistical features, structural feature can be extracted easily. The statistical feature such as creases are there in palmprint in large number. These creases remain approximately stable in person's whole life and which qualifies as features in palmprint recognition. Here in this paper different approach to personal identification based on palmprint is studied.

I. INTRODUCTION

In last two decade a sequence of automated identification system based on biometric is evolved such as identification system based on fingerprint, palmprint, iris, voice, finger knuckle, pulse of vain etc. [1]. It is considered that all other kind of identification system is outstanding at their place but here in this paper emphasis is given on study of palmprint based identification system. Palmprint, as a new biometric feature, has several advantages compared with other ones; hence it draws more attention of researchers get attracted [5-8]. Palmprint based identification system and fingerprint based identification system has some extent of similarity in functionality and its features. But the most significant feature of palmprint is its creases which are insignificant in fingerprint though there is similarity in between pamprint and fingerprint features. The fingerprint also has creases but they are dense and jolt, extraction of these features in fingerprint is a bit difficult compared to minutiae detection [2]. Where as in palmprint, these creases remain nearly as it is throughout the life and easy to extract, hence it could be considered the best feature for identification of a person in palmprint based identification system [3].

II. METHODS AND MATERIAL

Extraction Method: There is no standard definition of crease exist neither in mathematical nor in algorithm form. Any point in the crease has two features:

1. The direction has deviation from neighbor pixels.
2. It's located at a long and narrow region whose width has a large deviation from the neighbours.

These two types of above-mentioned crease in palmprint is shown in the image below-

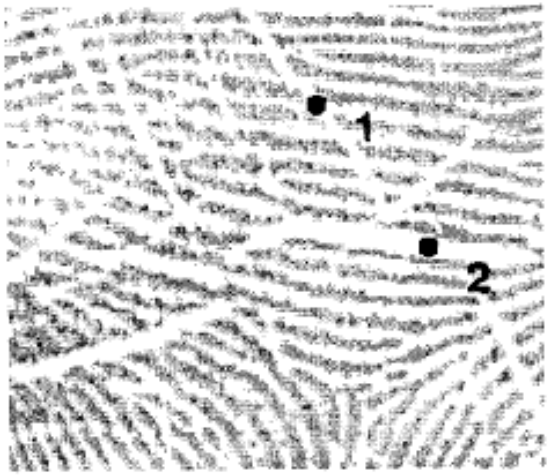

Fig. 1. The number 1 indicates a crease point of type I, the number 2 type 2[4].

To get crease points, an algorithm developed which takes use of a new direction map computing method and performs a twostep local analysis [4]. The palmprint features are classified as structural and statistical whereas texture energy belongs to statistical feature and lines in palmprint belongs to structural feature. The structural feature can recognize or discriminate palm strongly as the feature of it is lines in palm that remains almost same throughout the life [9]. But the line structure feature based palmprint system has many problems such as lines are very difficult to extract form blur palmprint image as shown in Fig.2, another problem is principal lines and wrinckles are not able to discriminate a person as there are many palmprint have similar line features as shown in Fig.3

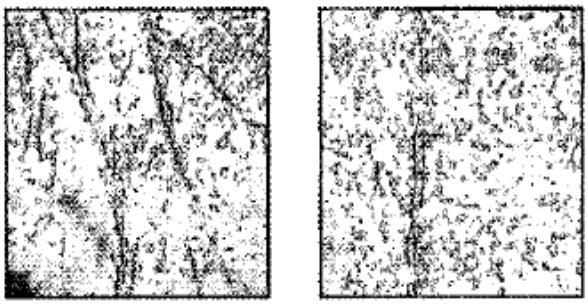

Fig.2- Some unclear lines palmprint images[10]

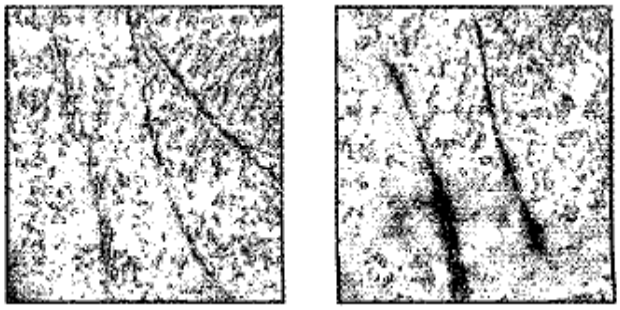

Fig.3- Some palmprints with similar lines[10]

The different feature of palmprint have different resolution and the principal lines are very thick hence they can be identified with low resolution and the wrinkles are thinner than principal line and then they can be analyzed in medium resolution and the ridges are thinnest and can be analyzed in high resolution. Hence, powerful multi-resolution analysis tool two-dimensional wavelet transformations can decompose the image in several directions and hence widely used [10].

III. RESULTS AND DISCUSSION

PALMPRINT RECOGNITION ALGORITHM: For simplicity line segments are compared which comprise the creases. Match finding algorithm in its first stage adjust the image for counteracting rotational and translational transforms. It generates the gray image then this gray image is compared and similarity coefficient is used for matching [4]. Here in this approach image line segments are adjusted and compare the line segments and count how many line segments are matched, the result is not satisfactory, it becomes had to decide one line segment matches the other, sometimes one segment matches the part of other and at sometime it is found that the two segments have the mutual sub-segments. To deal with this the gray image is generated from the crease line segment.

IMAGE MATCHING: Once the gray image is generated the pixels to pixels image matching is done.

If two pixels have the close direction then it is matched of hit. The summations of hits of two images show how similar two images are. In fuzzy directional energy based palmprint identification directional element based features are extracted through these stages such as contour extraction, dot orientation, vector construction after this line edge detection is done through these stages such as fuzzy dot orientation, fuzzy directional element energy feature construction.

IV.CONCLUSION

Research on palmprint based on crease shows that creases can be extracted correctly and more, based on the creases, the palmprint matching algorithm has great result. The crease will play an important role in palmprint analysis [4]. Fuzzy Directional Element Energy Feature can be extracted, represented and compared easily and has a strong ability to distinguish palms. Its rotation and translation robustness will be investigated in future work [9]. According to the fact that the different features have different resolution on palm, a novel palmprint feature; named wavelet energy feature**,** is defined based on wavelet. Wavelet Energy Feature can reflect the wavelet energy distribution of the principal lines, wrinkles and ridges at different scales, so it can discriminate palmprints effectively [10]. In this paper different approach of palmprint recognition is studied and the conclusion based on it is presented.

V. REFERENCES

[1]. Jain A K, Hong L, Pankanti S et al. An identityauthentication system using fingerprints. Proc. of IEEE, 1997,85(9): 1365-1388.

[2]. Miao D, Maltoni D. Direct gray-scale minutiae detection in fingerprints. IEEE Trans. PAMI, 1997, 19(1):27-39.

[3]. Shu,Wei, Research on Automatic Palmprint Recognition, PhD thesis,Tsinghua Univ., 1999.

[4]. Jun Chen, Changshui Zhang, Gang Rong,PALMPRINT RECOGNITION USING CREASE, 0-7803-6725- 110 1/$10.00 0200 1 EEE.

[5]. Dapeng Zhang and Wei Shu, “Two Novel Characteristics in Palmprint Verification: Datum Point Invariance and Line Feature Matching,” Pattern Recognition, vol. 32, pp. 691-702, 1999.

[6]. Shu Wei and D. Zhang, “Automated Personal Identification by Palmprint,” Optical Engineering, vol. 37, no. 8, pp. 2359-2362, 1998.

[7]. Shu Wei and D. Zhang, “Biometric Identification by Palmprint,” Proceedings of CISS’98, Princeton, New Jersey, USA, pp. 254-258, Mar. 1998.

[8]. Shu Wei and D. Zhang, “Palmprint Verification: an Implementationof Biometric Technology,” Proceedings of ICPR’98, Brisbane, Queensland, Australia, pp. 219-221, Aug. 1998.

[9]. Xiangqian Wu a, Kuanquan Wang a and David Zhang bFuzzy Directional Element Energy Feature (FDEEF) Based Palmprint Identification, 1051-4651/02 $17.00 (c) 2002 IEEE.

[10]. XIANG-QIAN wu (a! KUAN-QUAN WANG DAVID ZHANG,WAVELET BASED PALMPRINT RECOGNITION, Proceedqs of the First International Conference on Machine Learning and Cybernetics, Beijing, 4-5 November 2002, &7803-7508-4/02/$17.00 WO02 IEEE.

National Conference on "Recent Trends in Mathematical Modeling, Simulation Methods, Computations, and Physical Sciences"
(MMSCP-2019), Organised by Hislop College, Nagpur, Maharashtra, India
International Journal of Scientific Research in Computer Science, Engineering and Information Technology
© 2019 IJSRCSEIT | Volume 4 | Issue 4 | ISSN : 2456-3307

Need to Enact Stringent Laws on E -Waste Recycling for Sustainable Future

Namrata Babhulkar, Pallavi Bhave

Department of Psychology Hislop College, Civil Lines, Nagpur, Maharashtra, India

ABSTRACT

Electronic waste is one of the fastest growing waste streams in 21st century. India has taken a baby step in respect to e waste management but still there is lack of stringent laws on e –waste recycling laws. It is high time now India should work in direction of enacting stringent laws on e waste recycling and its implementation.

Keywords : E waste , Recycling.

"We share the earth not only with our fellow human beings

But with all the other creatures"

- By Dalai Lama

I. INTRODUCTION

Today we are living in 21st century and running a rat race in rapid developing technology world. Now time has came where robots and electronic machines are acting as servants of human being. Today almost any task can be done by a single click on smart phone which is one of awesome development in electronic world. All this technological development has definitely improved quality and quantity of human life but at the same time it is degrading our dear earth and its environment. We all can experience at every single minute of the day there is new invention of technology which is far better than existing and replaces the old technology. For Example just a few decades ago we all were using landline phone which was immediately replaced by simple basic mobile and which is now replaced by smart phone which is even getting smarter day by day which is a very good part but a coin has other side too. Every outdated mobile is being added in the list of e waste. E-waste is one of the fastest-growing waste streams.

E Waste (Electronic waste) refers to the disposal of broken electronic components and materials. E waste materials may be valuable and recyclable, such as random access memory and reusable laptops. Hazardous materials such as cathode ray tube monitor, requires special handling in disposals. Common discarded electronic products include computer, tv set, cell phones, radio, Microwaves, washing machines etc.

There are various sources of e waste such as e waste generated from household devices example vacuum cleaner, microwave oven, washing machine, air condition. waste generated from

communication devices like cell phone , landline phone, telegram , fax machine etc. waste generate from the products used for data processing such as computers, computer devices like monitor, speakers, keyboards, printers etc. the e waste generated from all the above sources has a bad effect both on environment and human being.

When we throw out our computers, they wind up in landfills, causing the possibility of toxic metal leaching into the groundwater. When e-waste is warmed up, toxic chemicals are released in to the air, damaging the atmosphere. Beside this e waste has worst effect on human beings. Electronic waste affects nearly every system in the human body because they contain a plethora of toxic components including **Mercury, Lead, Cadmium, Barium** and **Lithium**. Even the plastic casings of electronics products contain **Polyvinyl Chloride.** The health effects of these toxins on humans include birth defects, brain, heart, liver, kidney and skeletal system damage. They will also significantly affect the nervous and reproductive systems of the human body. To minimize the above harmful effects it is important to recycle it.

E waste recycling has a specific process and has following benefits.

- Reduces consumption of fresh raw material by making raw material available for re-use
- Reduces amount of e-waste going to landfills
- Reduces consumption of energy by minimizing product development lifecycle
- Reduces or stop pollution caused by informal processing of e-waste.
- Eliminate contamination of land and water by avoiding exposure of hazardous substance present in e-waste.

Laws on E-waste recycling in India

Indian Constitution has given both fundamental duty and fundamental right in relation to environment. Under Article 21 of the Constitution protection of life and personal liberty also includes right to live in pollution free environment. As Per part IV directive principles of state policy, Article 48 A states it is duty of state to issue direction for protection and improvement of environment and safeguarding of forest and wild life. Constitution in part IV A fundamental duties in Article 51 A (g) states that it is duty of every citizen of India to protect and improve environment including forest ,Lakes , Rivers and wild life and to have compassion for living creature .Following all above directions India introduces first e waste laws .

The various legislations enacted by the Government of India are:-

1) Guidelines for Environmentally Sound Management of E-waste, 2008; and
2) The e-waste (Management and Handling) Rules, 2011.

Under the Environment Protection Act 1986, the E waste (Management and Handling) Rules 2011were enacted and became effective from 1st

may 2012.E-waste (Management and Handling) Rules, 2011 including restrictions on usage of hazardous substances as per global best-practices and to prevent e-waste dumping in the country is a subject which is being dealt by Ministry of Environment and Forest (MoEF). This Department provides technical support to the MoEF in this regard. Thereafter, the e waste (Management) Rules 2016 were enacted in suppression of the 2011 rules and came into effect from 1st October 2016.However there is no provision of punishment for violation of any provision in the rule. Neither there is any body to ensure effective implementation of these guidelines and rules. in these guideline only space and amount of e waste to be recycled has been discussed but details about process and quality of recycling has not been discussed .As the given rules & Regulations does not provide any sanction or pecuniary punishment for its violation .It cannot be called as effective measure to cope up with the Problem.

Suggestion

1) Legal body should be established to supervised and keep a check on effective implementation of laws.
2) NGO's should be encouraged to work in the field of e waste recycling.
3) People and students should be educated about e waste recycling.
4) There should be uniform law on e waste recycling all over country .
5) There should be appropriate punishment for violation of these laws.

II. CONCLUSION

It is a high time now; India needs to enact stringent laws on e waste recycling. Which should give a detail guideline and process of recycling e waste in environment friendly way.

III. REFERENCES

[1]. https://www.britannica.com/technology/electronic-waste- article on topic electronic waste written by Gitanjali Nain Gill last accessed on 1 march 2019

[2]. http://www.yourarticlelibrary.com/waste-management/e-waste-sources-constituent-materials-and-problem-created-by-e-waste-notes/12344 last accessed on 1 march 2019

[3]. Singh Sankhla, Mahipal & Kumari, Mayuri & Nandan, Manisha & Mohril, Shriyash & Singh, Gaurav & Chaturvedi, Bhaskar & Kumar, Rajeev. (2016). Effect of Electronic waste on Environmental & Human health-A Review. IOSR Journal of Environmental Science, Toxicology and Food Technology (IOSR-JESTFT). 10. 2319-2399. 10.9790/2402-10090198104. last accessed on 2 march 2019

[4]. http://www.eemplindia.com/advantage-of-recycling.html Last accessed on 3/3/2019

[5]. www.technopedia.com last accessed on 4 march 2019

[6]. https://allgreenrecycling.com/effects-of-e-waste-on-our-environment/ last accessed on 5 march 2019

National Conference on "Recent Trends in Mathematical Modeling, Simulation Methods, Computations, and Physical Sciences"
(MMSCP-2019), Organised by Hislop College, Nagpur, Maharashtra, India
International Journal of Scientific Research in Computer Science, Engineering and Information Technology
© 2019 IJSRCSEIT | Volume 4 | Issue 4 | ISSN : 2456-3307

Green Chemistry : A Tool to Reducing Waste and Improving Sustainability In Chemical Industry

Jessie M. Moses[#]
[#]Assistant Professor, Hislop College, Temple Rd, Civil Lines, Nagpur, Maharashtra, India

ABSTRACT

Green Chemistry reflects the efforts of academia and industry to address the challenges related to sustainable development of the chemical industry and continuous progress is being made, both in academia and industry. Briefly, green chemistry is the utilization of a set of principles that reduce or eliminate the use and generation of hazardous substances.in the design, manufacture and application of chemical products. Many industries all over the world produce chemicals for their products that are harmful to the environment, human health and to all living species. Green Chemistry is the use of chemistry for the prevention of chemical pollution to the environment by using chemicals that are benign, or not harmful. Green Chemistry is often said to be a 'Cradle to grave approach'. This approach describes the need to consider all factors in the production of a chemical from the source of raw materials, to the disposal/recycle of the product once its useful lifetime has ended. The basic principle of green chemistry is that it is better to prevent waste than to treat or clean up waste after it is formed.

Keywords : Green Chemistry, Hazardous Substances, Disposal, Recycle

I. INTRODUCTION

The Green Chemistry revolution is providing an enormous number of challenges to those who practice chemistry in industry, education and research. With these challenges however, there are an equal number of opportunities to discover and apply new chemistry, to improve the economics of chemical manufacturing and to enhance the much tarnished image of chemistry. A reasonable working definition of green chemistry can be formulated as follows: Green chemistry efficiently utilizes (preferably renewable) raw materials, eliminates waste and avoids the use of toxic and/or hazardous reagents and solvents in the manufacture and application of chemical products (Sheldon,2000).

The goal of green chemistry solutions is to reduce or eliminate hazardous impacts of chemicals over a chemical product's life-cycle. Key guidelines associated with green chemistry are outlined in the Environmental Protection Agency's "Twelve Principles of Green Chemistry," which serves as the basis of creating and implementing chemicals and processes (Sheldon, 2007). Green Chemistry started after the Pollution Prevention Act of 1990 was passed. The Office of Pollution Prevention and Toxics (OPPT) began to develop ways to make chemical products and processes less hazardous to humans and the environment. There are many companies, foundations, clinics and individual chemists that are involved in Green Chemistry. The EPA and the Syracuse Research Corporation developed the Chemistry Expert System (GCES) which is used to develop and analyze the various principles of Green Chemistry. They find out sources of waste and evaluate the amount and risk produced and explore

opportunities to solve these problems. To achieve this, the Alternative Solvents Database (SolvDB) was constructed to help chemists and researchers so that they can efficiently find out alternatives to the harmful chemicals being used at the time.

Most manufactured products involve one or more chemical processes. We cannot imagine what our life will be like without the products by the chemical industry. Through the practice of green chemistry, we can create alternatives to hazardous substances we use as our raw materials. We can design chemical processes that reduce waste and reduce demand on diminishing natural resources. We can employ processes that use minimal amount of energy. Thus by using green chemistry, we can achieve all these and still maintain economic growth and opportunities while providing affordable products and services to a growing world population. This is a field open for innovation, new ideas and revolutionary progress. Over the years different principles have been proposed that can be used when thinking about the design, development and implementation of chemical products and processes. Paul Anastas of America coined the twelve principles of Green Chemistry in 1994 towards ideal synthetic methods to save natural resources [Anastas, 1998]. These principles enable scientists and engineers to protect and benefit the economy, people and the planet by finding creative and innovative ways to reduce waste, conserve energy, and discover replacements for hazardous substances. It is important to note that the scope of green chemistry and engineering principles go beyond concerns over hazards from chemical toxicity and include energy conservation, waste reduction, and life cycle considerations such as the use of more sustainable or renewable feedstock and designing for end of life or the final disposition of the product.

Principles of Green Chemistry:

There are twelve principles of Green Chemistry. These principles help to forge a path ahead in designing products and processes that would be less environmentally damaging while maintaining or enhancing product performance and economic cost. Designing processes to minimize environmental impact has become, in recent years, essential to industrial and engineering chemistry, and is likely to shape the field for the next 100 years (Jessop. et.al, 2009)

There are twelve principles of Green Chemistry are summarized as under.

1. **Prevention**: It is better to prevent waste than to treat or clean up waste after it is formed.
2. **Atom Economy**: Synthetic methods should be designed to maximize the incorporation of all materials used in the process into the final product.
3. **Less Hazardous Chemical syntheses**: Wherever practicable, synthetic methodologies should be designed to use and generate substances that possess little or no toxicity to human health and the environment.
4. **Designing safer Chemicals**: Chemical products should be designed to preserve efficacy of function while reducing toxicity.
5. **Safer solvents and Auxiliaries:** The use of auxiliary substances (e.g. solvents, separation agents, etc.) should be made unnecessary wherever possible and innocuous when used.
6. **Design for Energy Efficiency**: Energy requirements should be recognized for their environmental and economic impacts and should be minimized. Synthetic methods should be conducted at ambient temperature and pressure.
7. **Use of Renewable feedstocks**: A raw material or feedstock should be renewable rather than depleting wherever technically and economically practicable.

8. **Reduce Derivatives**: - Unnecessary derivatization (blocking group, protection/ deprotection, temporary modification) should be avoided whenever possible.
9. **Catalysis**: Catalytic reagents (as selective as possible) are superior to stoichiometric reagents.
10. **Designed for Degradation**: Chemical products should be designed so that at the end of their function they do not persist in the environment and break down into safe degradation products.
11. **Real time analysis for Pollution prevention**: Analytical methodologies need to be further developed to allow for real-time, in-process monitoring and control prior to the formation of hazardous substances.
12. **Inherently Safer Chemistry for Accident Prevention**: Substances and the form of a substance used in a chemical process should be chosen to minimize potential for chemical accidents, including releases, explosions, and fires.

By using the above principles of green chemistry in the design and manufacture of chemical products and processes, many industries in the world have been successful in lowering the overall costs associated with environmental safety and health.

Examples:

1. **Computer Chips**

Many chemicals, large amount of water, and energy are required to manufacture computer chips. In the study conducted in 2003, the industrial estimate of chemicals and fossil fuels required to make a computer chip was a 630:1. This means that it takes 630 times the weight of the chip in source materials just to make one chip. But it is a 2:1 ratio for the manufacture of an automobile.

1. Scientists at the Los Alamos National Laboratory (Voss, 2002) have developed a process that uses supercritical carbon dioxide in one of the steps of chip preparation, and it significantly reduces the quantities of chemicals, energy and water needed to produce chips.
2. Richard Wool, former director of the Affordable Composites from Renewable Sources (ACRES) program at the University of Delaware, found a way to use chicken feathers to make computer chips. The protein, keratin in the feathers was used to make a fiber form that is both light and tough enough to withstand mechanical and thermal stresses. The result is feather-based printed circuit board that actually works at twice the speed of traditional circuit boards. Although this technology is still under research for commercial purposes, this has led to other uses of feathers as source material, including biofuel .

2. **Paint**

Oil-based "alkyd" paints give off large amounts of volatile organic compounds (VOCs). These volatile compounds evaporate from the paint as it dries and cures and many have one or more environmental impacts. Carbon dioxide has also been successfully introduced into some dry-cleaning processes. So, various consumer formulations no longer contain a VOC solvent [Clarke, 2005].

- ✓ Procter & Gamble and; Cook Composites and Polymers created a mixture of soya oil and sugar that replaces fossil-fuel-derived paint resins and solvents, cutting hazardous volatiles by 50 percent. Chempol (R) MPS is an innovative, Sefose (R)-based alkyd resin technology that enables formulation of paints and coatings with less than half the Volatile Organic Compounds, or VOC's, of traditional, solvent-borne alkyd coatings. Sefose (R) technology from P&G is prepared from natural, renewable feedstock in a patented, solvent less process. Chempol (R) MPS

alkyd resins are specially-formulated to perform like traditional, petroleum-based solvents and create paint that is safer to use and produces less toxic waste

- ✓ Sherwin-Williams developed water-based acrylic alkyd paints with low VOCs that can be made from recycled soda bottle plastic (PET), acrylics and soybean oil. These paints combine the performance benefits of alkyds and low VOC content of acrylics. In 2010, Sherwin-Williams manufactured sufficient new paints to eliminate over 800,000 pounds, or 362,874 kilograms of VOCs.

3. Gold Nanoparticles

A simple, economic, and environmentally benign experimental route to synthesize gold nanoparticles using tea leaves in an aqueous media at room temperature was reported [Sharma, 2012]. The single-step method circumvents the use of surfactant, capping agent, or template and follows several principles of green chemistry.

4. Biodegradable Plastics

Several companies have been working to develop plastics that are made from renewable, biodegradable sources.

- ✓ Nature Works of Minnetonks, Minnesota, makes food containers from a polymer called polylactic acid branded as Ingeo. The scientists at Nature Works discovered a method where microorganisms convert cornstarch into a resin that is just as strong as the rigid petroleum-based plastic currently used for containers such as water bottles and yogurt pots. The company is working toward sourcing the raw material from agricultural waste.
- ✓ BASF developed a compostable polyester film that called “Ecoflex (R)”. They are manufacturing and marketing fully biodegradable bags, "Ecovio (R),"made of this film along with cassava starch and calcium carbonate. Certified by the Biodegradable Products Institute, the bags completely disintegrate into water, CO2 and biomass in industrial composting systems. The bags are tear-resistant, puncture-resistant, waterproof, printable and elastic. Instead of using conventional bags if these bags are used then kitchen and yard waste will be efficiently degrade in municipal composting systems.

II. CONCLUSION

Green Chemistry will be one of the most important fields in the future. Although this field has developed rapidly in the last 20 years, it is still at an early stage. Promoting ‘Green Chemistry’ is a long term task and many challenging scientific and technological issues need to be resolved; these are related to chemistry, material science, engineering, environmental science, physics and biology. Scientists, engineers and environmentalists should work together to promote the development of this field. There is no doubt that the development and implementation of green chemistry will contribute greatly to the sustainable development of our society.

In short, the benefits of Green Chemistry (USEPA,Washington 2017) can be summarized as follows :-

i) Cleaner air resulting from less release of hazardous chemicals to air leading to less damage to lungs.
ii) Cleaner water due to less release of hazardous chemical wastes to water leading to cleaner drinking and recreational water.
iii) Safer food because of elimination of persistent toxic chemicals that can enter the food chain.
iv) Safer consumer products of alltypes.
v) Lower potential for global warming, ozone depletion and smog formation.
vi) Less chemical disruption of ecosystems.

vii) Higher yields for chemical reactions consuming smaller amounts of feedstock.

viii) Reduced waste, eliminating costly remediation and hazardous waste disposal.

ix) Increased consumer sales by earning and displaying a safer product label (eg. Safer Choice Labeling)

x) Improved competitiveness of chemical manufactures and their customers.

III. REFERENCES

[1]. Sheldon, R.A.(2003) C.R. Acad. Sci. Paris, IIc, Chimie/Chemistry, 3, 541–551.

[2]. Sheldon R. A., Isabel W. C. E. Arends. and Hanefeld .Ulf., (2007) Introduction : Green Chemistry and Catalysis, Isabel Arends, Ulf Hanefeld, Wiley, 1.

[3]. Anastas, P. T. and Warner, J. C.,(1998) Green Chemistry: 12 Principles of Green Chemistry,Theory and Practice, Oxford University Press: New York,30.

[4]. Jessop, P. G., Trakhtenberg, S. and Warner, J.(2009) ACS Symposium Series, The Twelve Principles of Green Chemistry, 12, 401-436.

[5]. Voss, D. (2002) MIT Technology Review, Supercritical Carbon Dioxide: Carbon dioxide could make microchips smaller faster and cleaner to build.

[6]. Clarke, J. H. (2005) Part 1: Green Chemistry for Sustainable Development : Green Chemistry and Environmentally Friendly Technologies, Wiley ISBN 3-527-30985-3 : 12

[7]. Sharma, R. K., Gulati, S. and Mehta S., (2012) Preparation of Gold Nanoparticles Using Tea: A Green Chemistry Experiment, J. Chem. Educ. 89 (10), 1316–1318.

[8]. https : // www.epa.gov / benefits-green-chemistry

National Conference on "Recent Trends in Mathematical Modeling, Simulation Methods, Computations, and Physical Sciences"
(MMSCP-2019), Organised by Hislop College, Nagpur, Maharashtra, India
International Journal of Scientific Research in Computer Science, Engineering and Information Technology
© 2019 IJSRCSEIT | Volume 4 | Issue 4 | ISSN : 2456-3307

Smart Terpolymeric Materials : A Study of Thermal Degradation Behaviour

Pratik E. P. Michael+, Monali Trivedi, Karishma Khankule, Akshay Hedaoo, Anisha Michael
Department of Chemistry, Hislop College, Nagpur, Maharashtra, India

ABSTRACT

The new terpolymer abbreviated as (PBMF-I) was synthesized by polycondensation reaction of p-hydroxy benzoic acid - Melamine - Formaldehyde monomer in 1: 1: 2 molar proportion using acid catalyst in the temperature range of 120-160 ^{0}C for 6 hrs. The terpolymeric resin synthesized has been characterized by elemental analysis, UV-visible, IR and proton NMR spectral studies. Detailed study on thermal degradation behaviour of the newly synthesized terpolymer has been carried out in order to ascertain the mode of decomposition and kinetic parameters such as order of reaction (n), frequency factor (Z), entropy change (ΔS), free energy change (ΔF) and apparent entropy change (S*). Sharp-Wentworth and Freeman-Carroll methods are used to determine activation energy (Ea) and the thermodynamic parameters. The activation energy determined by these methods is found to be in good agreement with each other. The order of reaction is found out to be 0.9841.

Keywords : Synthesis, Thermal, Thermal degradation behaviour, PBMF-I, Kinetic parameters.

I. INTRODUCTION

Polymers, in performance and characteristics, offer a variety of unique properties, application prospects and diversity which cannot be matched by any other class of materials. Polymers, though introduced in the beginning of 19th century, still play a major role in our daily life. The terpolymers reported earlier are also said to have better acid resistance, better thermal stability and electrical properties. Thermogravimetric analysis of 8-hydroxyquinoline–melamine–formaldehyde resin has been carried out by Gurnule and his co-workers (1) and have also reported the thermal degradation of resin preparing from 4-hydroxyacetophenone, catechol with formaldehyde and calculated the various kinetic parameters. Thermogravimetric analysis of copolymer obtained from p-cresol, dithiooxamide with formaldehyde has also been reported (2). The study of thermal degradation of terpolymer resins has been carried out by numerous researchers across the world. Terpolymer and their chelates possess attractive applications in the field of environment pollution control, bioinorganic catalysts, hydrometallurgy, semiconducting devices and metal recovery from dilute solutions (3-7). Our previous work on thermal degradation of terpolymers synthesized from salicylic acid/8-hydroxyquinoline and guanidine with formaldehyde has also be documented (8, 9). The thermal stabilities of some newly synthesized terpolymers derived from p-cresol, melamine and formaldehyde were determined using Freeman–Carroll method (10). The thermal decomposition pattern of the terpolymer resins was evaluated by TGA and their kinetic parameters, such as activation energy (Ea), order of the reaction (n), entropy change (ΔS), free energy change (ΔF), apparent entropy (S*) and frequency factor (Z) determined by Freeman–

Carroll (FC) and Sharp–Wentworth (SW) methods (11, 12)

Experimental:

All the chemicals used were of AnalaR grade.

Synthesis

The terpolymeric resin was synthesized by refluxing a mixture of p-hydroxy benzoic acid (0.1 mol) and melamine (0.1 mol) with formaldehyde (0.2 mol) in an digital oil bath for 6 hours at 120 - 160 ^{0}C with occasional shaking. The yellowish coloured product obtained is repeatedly washed with cold and hot water to remove any soluble impurities. The resin was purified by dissolution in 8% NaOH solution and re-precipitated by drop-wise addition of 1:1 (v/v) of 2 M HCl. The terpolymer obtained was dried in an vacuum desicator over anhydrous calcium chloride. The reaction scheme in as given in the following:

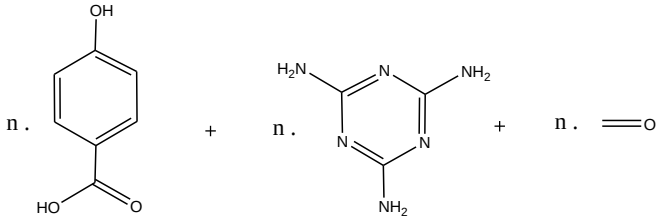

p-hydroxybenzoic acid **Melamine** **Formaldehyde**

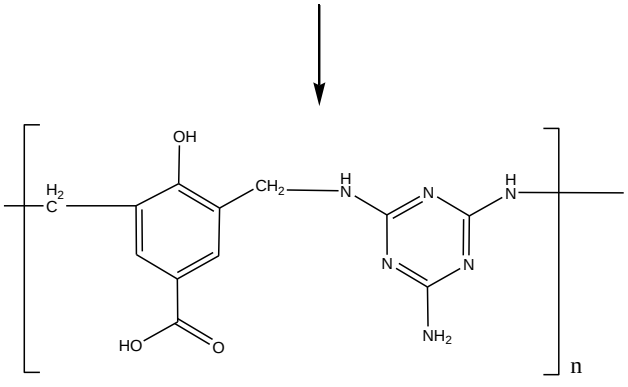

p-hydroxybenzoic acid - Melamine - Formaldehyde (PBMF I)

Terpolymer

Thermal Analysis

Theoretical Consideration. Thermogram was interpreted and analyzed to obtain information about the % weight loss at which gives information about polymer composition, product formed and kinetic parameters. Kinetics parameters have been determined using two different methods viz. Sharp-Wentworth (11), and Freeman-Carroll (12) methods as follows.

Sharp-Wentworth's:

$$\log [dc/dt] /[1 - c] = \log (A\beta) - [Ea/2.303R] \cdot [1/T], \quad (1)$$

where dc/dt is the rate of change of fraction of weight with change in temperature; β is linear heating rate, dT/dt; c is the fraction of polymer decomposed at time t. Thus, a linear plot of $\log((dc/dt)/(1 - c))$ versus $1/T$ is obtained whose slope gives the value of Ea and A may be evaluated from the intercept. The linear relationship confirmed that the assumed order is correct.

Freeman-Carroll's:

$$[\Delta \log (dw/dt)] /[\Delta \log Wr] = (-Ea /2.303R) \cdot [\Delta (1/T)] /[\Delta \log Wr]+ n, \quad \text{----------(2)}$$

where dw/dt is the rate of change of weight with time, $Wr = Wc - W$, Wc is the weight loss at the completion of reaction; W is the total weight loss up to time, Ea is the energy of activation, and n is the order of reaction. The $\Delta \log(dw/dt)$ and $\Delta \log Wr$ values were taken at regular intervals of $1/T$. In this case, $\Delta \log(dw/dt)/\Delta \log Wr$ versus $\Delta(1/T)/\Delta \log Wr$ gives a straight line. The slope and intercept are equal to $-(Ea/R)$ and n, respectively.

II. RESULTS AND DISCUSSION

The newly synthesized PBMF-I terpolymer is found out to be insoluble in almost all organic solvents but soluble in DMF and DMSO.

Thermogravimetric analyses of all the terpolymers has been studied. TGA of the terpolymers was carried out using a NETZSCH4 thermal analyzer along with a NETZSCH STA 409 PC/PG computing system. The samples were scanned in the temperature range of 20 – 1000°C under continuous flow of nitrogen gas at a linear heating rate of 10 °C/ min using a Pt-Pt-Rh thermocouple.

The thermal degradation curve for the PBMF- I is shown in figure.1. The thermogram of the PBMF- I terpolymer exhibited three-stage decomposition in the temperature range 90–1000°C. The first-stage decomposition started at 210°C and ended at 360°C, which may have been due to the loss of the side attached to aromatic ring and carboxyl group (COOH; 55.42% Cal. and 56.8% Found). The second-step decomposition started at 405 –498°C, corresponding to a 65.96% loss, which may have been due to the degradation of hydroxyl group, calculated as 64.59%. The third-step decomposition started from 524 – 883 °C, which may have been a result of the complete decomposition of the polymer ring (100% Cal. and 99.66% Found). The half-decomposition temperature of the PBMF- I terpolymer is also given in table 2. The thermodynamic parameters for the polymers were calculated on the basis thermal *Ea* values, which are shown in table 3.

Table 1. Thermoanalytical data and decomposition data of PBMF- I terpolymer

Terpolymer	Temperature Range (°C)	Decomposition Stage	Species Degraded	% Weight Loss	
				Found	Calculated
PBMF - I	210 – 360	First	Loss of the side chain attached to aromatic ring and carboxyl group	55.42	56.8
	405 – 498	Second	Degradation of the hydroxyl group	64.59	64.59
	524 - 883	Third	Complete decomposition of the polymer ring	99.66	100

Table 2. Activation Energy & Decomposition Temperature of PBMF- I terpolymer

Terpolymer	Decomp. Temp. ^{0}c	Activation Energy (KJ / mole)	
		FC	SW
PBMF - I	498	19.35	17.39

FC- Freeman-Carroll, SW- Sharp Wentworth

1) Table No. 3 Kinetic Parameter of PBMF- I terpolymer

Terpolymer	Entropy Change ΔS (J)	Free Energy Change ΔF (kJ)	Frequency Factor Z (sec^{-1})	Apparent Entropy Change S*(kJ)	Order of Reaction n
PBMF - I	-251.45	130.27	406.31	-23.91	0.9841

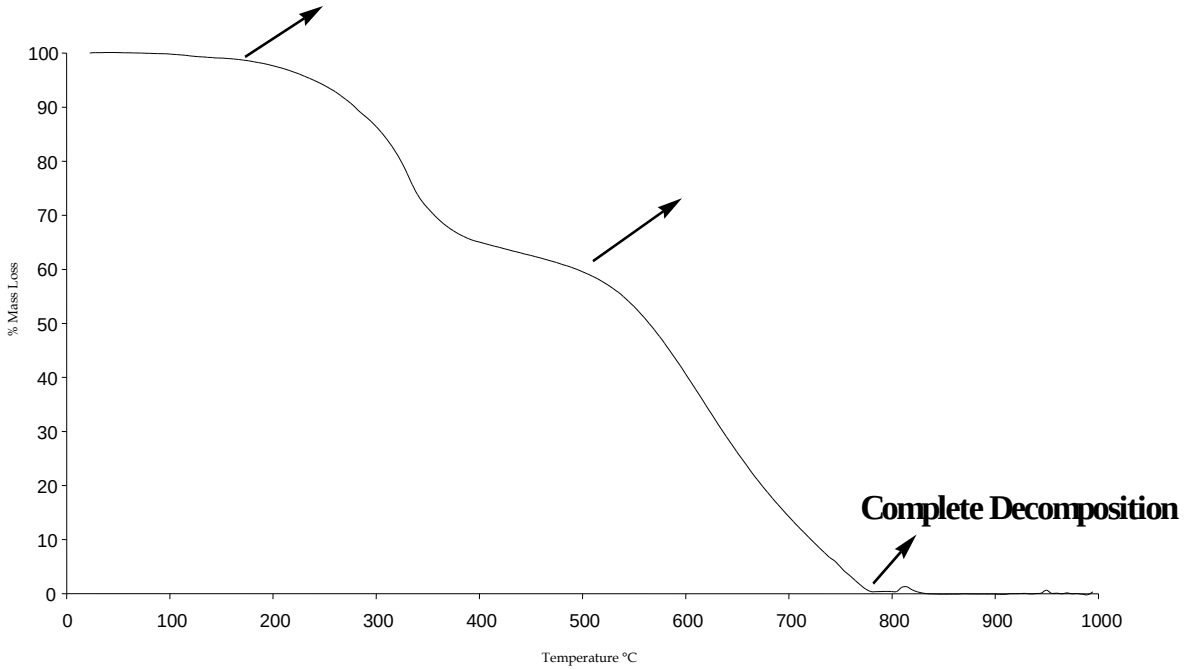

Fig. 1 Thermogram of p-hydroxybenzoic acid , melamine , formaldehyde terpolymer

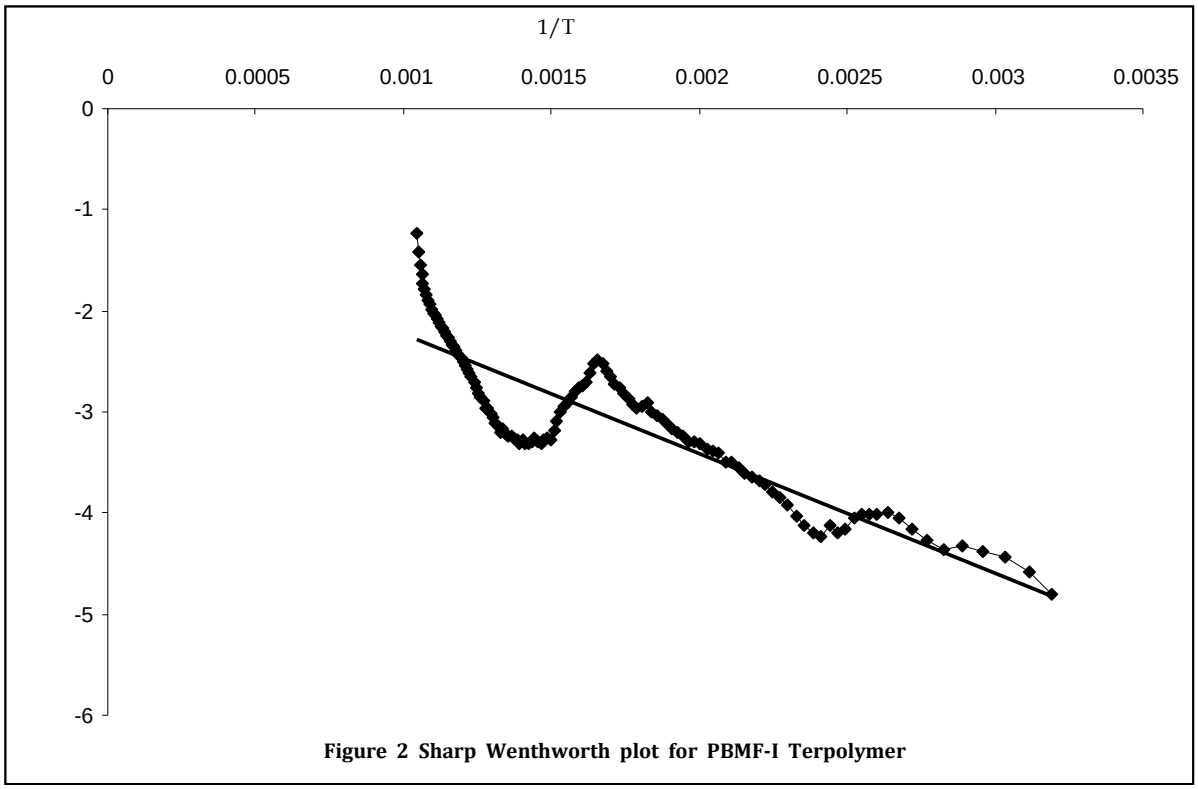

Figure 2 Sharp Wenthworth plot for PBMF-I Terpolymer

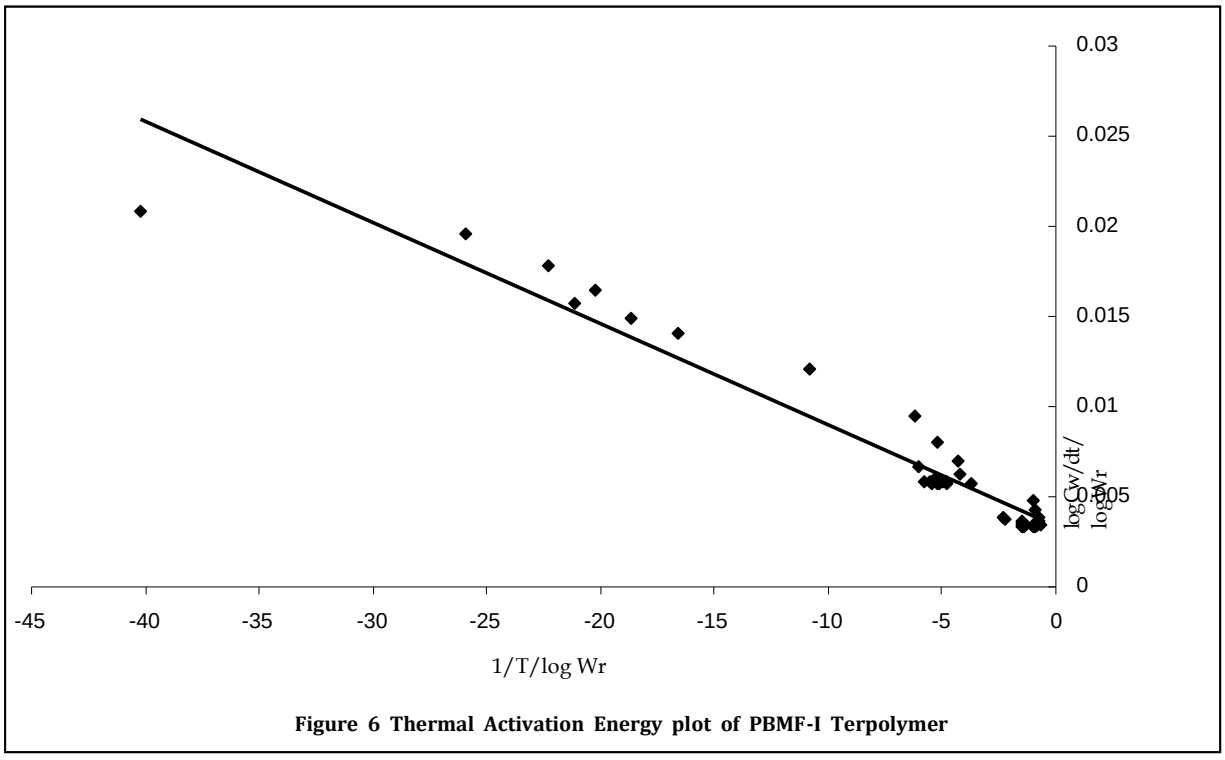

Figure 6 Thermal Activation Energy plot of PBMF-I Terpolymer

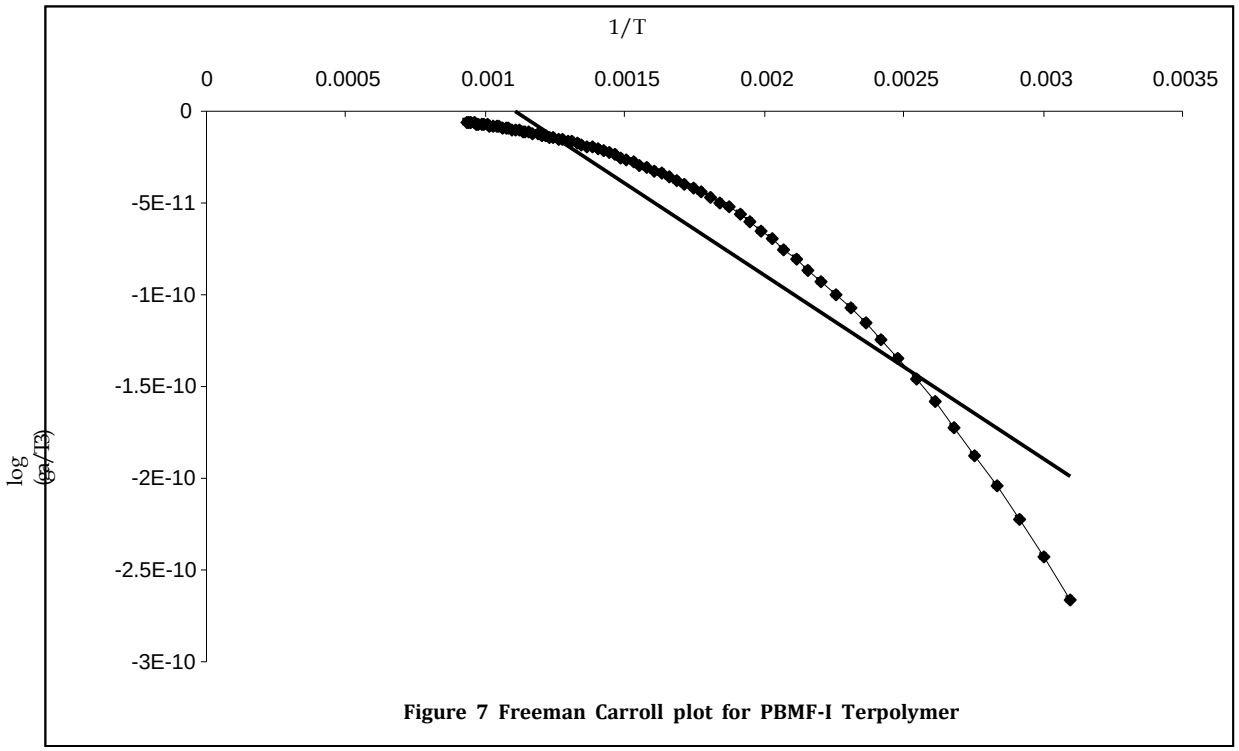

Figure 7 Freeman Carroll plot for PBMF-I Terpolymer

III.CONCLUSION

The thermogram of PBMF- I shows three degradation steps and the terpolymer molecule degrades completely at around 883 ^{0}C.

The TGA pattern indicates that the terpolymer has good thermal stability. The Ea (activation energy) calculated are found to be in good correlation with each other.

The negative entropy and low values of frequency factor calculated by Freeman Caroll method is indicative of the fact that the thermal stability of the terpolymer is a slow reaction.

The decomposition of the PBMF- I terpolymer almost follows first order kinetics but not completely.

IV.Acknowledgment

The authors are gratified to the Principal, Hislop College, Nagpur for the constant support, encouragement and for providing laboratory facilities. The corresponding author wish to acknowledge the financial support provided by University Grants Commission, New Delhi to carry out the work.

V. REFERENCES

[1]. W. B. Gurnule, H. D. Juneja and L. J. Paliwal, Orient J. Chem., 15, 283, 1999.

[2]. W. B. Gurnule, S. S. Katkamwar, E-Journal of Chemistry, 7(4), 1380-1390, 2010.

[3]. M. Drage, K. R. Czewinski, Sci., Techol., 35, 1117, 2010.
[4]. A. Burkanudeen and M. Karunakaran, Orient J. Chem., 19, 225, 2003.
[5]. S. A Patel, B. S. Shah and R. M. Patel., Iran. Polym. J., 13, 445, 2004.
[6]. M. Karunakaran and A. Burkanudeen, Orient. J. Chem., 18, 65, 2002.
[7]. A. I. Isamil, K. A. K. Ebraheem, M. S. Mubarak and F.I. Khalili, Solvent Extra. Ion. Exch., 21 125, 2003.
[8]. P. E. P. Michael, P. S. Lingala, H. D. Juneja, and L. J. Paliwal, JAPS, 92, 4, 2278–2283, 2004.
[9]. P. E. P. Michael, J. M. Barbe, H. D. Juneja, and L. J. Paliwal, Euro. Poly. J. 43, 12, 4995–5000, 2007.
[10]. R. N. Singru, A. B. Zade, W. B. Gurnule, JAPS, 109, 859, 2008..
[11]. E. S. Freeman and B. Carroll, The J. Phy. Chem., 62, 4, 394–397, 1958.
[12]. J. H. Sharp and S. A. Wentworth, Anal. Chem.. 41, 14, 2060–2062, 1969.

National Conference on "Recent Trends in Mathematical Modeling, Simulation Methods, Computations, and Physical Sciences"
(MMSCP-2019), Organised by Hislop College, Nagpur, Maharashtra, India
International Journal of Scientific Research in Computer Science, Engineering and Information Technology
© 2019 IJSRCSEIT | Volume 4 | Issue 4 | ISSN : 2456-3307

Luminescence in Ca8Mg (SiO4) 4Cl2 : Eu2+

Khushbu Sharma[1], S.V. Moharil[2], Gurjeet Talwar[3], K.B. Ghormare[4]
[1]Department of Physics, G.H. Raisoni Institute of Engineering. and Technology, Nagpur, Maharashtra, India
[2]Department of Physics, R.T.M Nagpur University, Maharashtra, India
[3]Department of Physics, Hislop College, Nagpur, Maharashtra, India
[4]Department of Physics, VMV arts JMT commerce and JJP science College, Maharashtra, India

ABSTRACT

In this paper $Ca_8Mg(SiO_4)_4Cl_2:Eu^{2+}$ prepared through solid state reaction. Obtained compound characterized by photoluminescence emission and excitation and to confirm the crystal structure X ray diffraction pattern is recorded

Keywords : Photoluminescence, Chlorosilicate, Eu^{2+}

I. INTRODUCTION

During recent years, scientists have turned their attention towards chlorosilicates to get good chemical, physical and thermal stability. Silicate based phosphors are widely used in display devices. There are some problems with synthesis and long term use of silicates. Silicates need temperatures higher than 1000 C, even up to 1400 C for synthesis. . They may get converted to glassy form. At high synthesis temperatures they can also react with low cost crucible materials such as porcelain and china clay.

For tuning the emission and excitation spectra, several substitutions have been tried. E.g. the substitution of Ca by Sr and Cl by F enhanced the green emission [1]in $Ca_3SiO_4Cl_2:Eu^{2+}$. In the same host Zhao et al [2] used sulfur co-doping for obtaining red emission. In $Sr_4Si_3O_8Cl_4$, the emission bands of the phosphors on uv excitation at room temperature shifted to longer wavelength with increasing Ca^{2+} content[3]. Some intermediate phases have been explored in more details as a result of such efforts.

In this paper $Ca_8Mg(SiO_4)_4Cl_2$ is prepared and photoluminescence characteristic are studied.

Though this compound was known for quite some time, it attracted attention of phosphor researchers as late as 1987[i] when Ye et al noted its good chemical and thermal stability. In 1992, PL of Eu^{2+} was reported[ii]. Lin et studied emission of Ce^{3+} which could also act as a sensitizer for Eu^{2+}[iii iv]. 427 nm emission of Ce^{3+} shows good overlap with Eu^{2+} excitation. Owing to green emission and near UV/blue excitation.

$Ca_8Mg(SiO_4)_4Cl_2:Eu^{2+}$ in solid-state lighting (SSL) was also proposed[v]. Luminescence of several rare earths such as Ce^{3+}[vi], Eu^{2+}[vii viii], Dy^{3+} [ix x] was studied with the objective of finding phosphors for solid state lighting.

Long lasting luminescence in $Ca_8Mg\ (SiO_4)_4\ Cl_2$: Eu^{2+},Nd^{3+} was first reported by Wang et al[xi] and due to better stability of this phosphor compared to the commercial $SrAl_2O_4$:Eu, the interest continues to date[xii].

Preparation

$Ca_8Mg(SiO_4)_4Cl_2:Eu^{2+}$ is prepared through solid state reaction. Ingredients used were $CaCO_3$, MgO, $CaCl_2$,

Eu_2O_3 and silicic acid ($SiO_2.1.5\ H_2O$). The mixtures of corresponding raw materials with a mole ratio of $CaCO_3$: MgO : SiO_2 : $CaCl_2$ = 7 : 1 : 4 : 1.5. All constituents in the required proportions were mixed together. The mixture on thoroughly grinding was transferred to furnace for heating at 700 C for 4 hrs. The powder so obtained was reduced at 900 C in a covered crucible under burning atmosphere provided by burning charcoal to convert Eu^{3+} to Eu^{2+}.

II. RESULT AND DISCUSSION

Fig 1 shows XRD pattern of $Ca_8Mg(SiO_4)_4Cl_2$. It shows an excellent match with ICDD file 41-0248. $Ca_8Mg(SiO_4)_4Cl_2$ has a cubic crystal structure with space group of Fd-3m.

PL spectra of Eu^{2+} activated $Ca_8Mg(SiO_4)_4Cl_2$ are shown in Fig. 2. Various Eu^{2+} concentrations ranging between 0.1-2.0 mol % were tried. Maximum emission was obtained for 1 mol.%. These results only are shown. Earlier, Guo et al viii also observed maximum emission for 0.9 mol.%. We observed an emission band around 505 nm. In the excitation spectrum three broad overlapping bands can be seen around 275, 332 and 367 nm, besides a shoulder around 430 nm. The positions of these bands are in good agreement with those reported earlier [xi]. In earlier works, a weak emission band had been observed around 426 nm [xi].

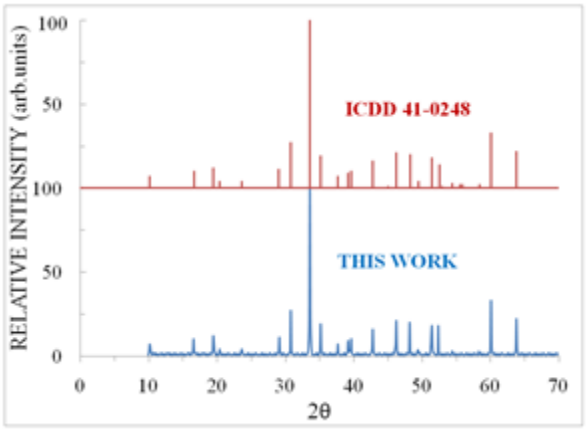

Figure 1: XRD pattern for $Ca_8Mg(SiO_4)_4Cl_2$compared with ICDD data

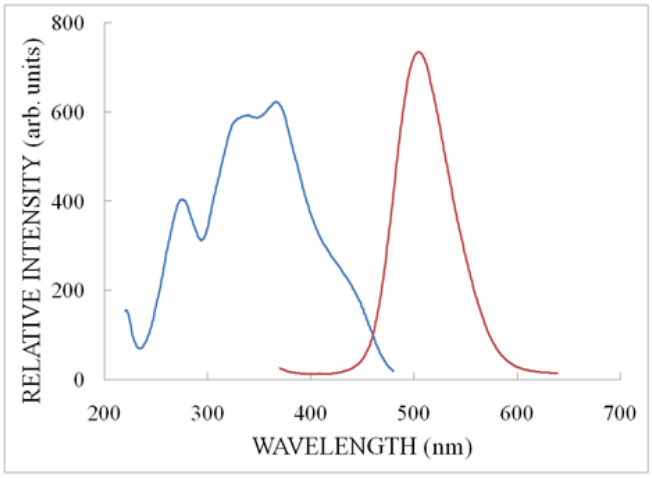

Figure 2: Photoluminescence spectra of $Ca_8Mg(SiO_4)_4Cl_2:Eu^{2+}$

a> Emission for 387 nm excitation
b> Excitation for 500 nm emission

It is therefore expected that Eu^{2+} ions occupy the Ca sites. Eu^{2+} ions at Ca2 sites are responsible for emission at 505 nm, while those at Ca1 sites lead to blue emission peaking around 426 nm. Among other things, the site occupancy will also depend on the method of preparation and thermal treatments received during the synthesis. Apparently, in the procedure we have followed, all the Eu^{2+} ions are occupying Ca2 sites.

that for Ca (CN = 6 and 8) are 1.14 and 1.26, respectively. It is therefore expected that Eu^{2+} ions occupy the Ca sites. Eu^{2+} ions at Ca2 sites are responsible for emission at 505 nm, while those at Ca1 sites lead to blue emission peaking around 426 nm. Among other things, the site occupancy will also depend on the method of preparation and thermal treatments received during the synthesis. Apparently, in the procedure we have followed, all the Eu^{2+} ions are occupying Ca2 sites.

Fig 3shows TL emission spectrum for $Ca_8Mg(SiO_4)_4Cl_2:Eu^{2+}$exposed to UV radiations. The sample was held at 100 C and the emission spectra

were recorded using Ocean Optics model USB 2000 spectrometer. As it employs CCD array as a detector, the spectra could be recorded in a fraction of second. PL is recorded at room temperature while TL emission spectrum at 100 C therefore the emission maximum is at slightly longer wavelengths (510 nm) and the peak is somewhat broader. Also, the resolution of USB 2000 spectrometer (10 nm) is not as good as that of spectrofluorimeter (1 nm).

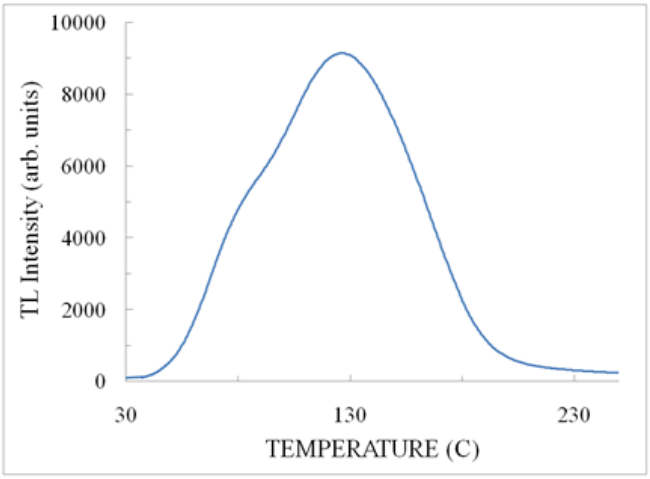

Figure 1: TL Glow Curve of $Ca_8Mg(SiO_4)_4Cl_2:Eu^{2+}$

III. CONCLUSION

$Ca_8Mg(SiO_4)_4Cl_2:Eu^{2+}$prepared through solid state reaction. XRD pattern of obtained compound is good agreement with ICDD data. Single emission band observed at visible range at 505nm. with excitation around 270 and 330 nm. Our results are in good agreement with reported work. First time we have recorded glow curve and the compound exhibited glow peak at 100C.

IV. REFERENCES

[1]. J.Wang, Z.Liu, W.Ding and Q. Su J. Appl. Ceram.. Technol 6 (2009) 447

[2]. Xin Zhao, Zhaosheng Li, Tao Yua and Zhigang Zouac RSC Adv.3 (2013) 1965

[3]. H. Wang, J. Huang, X. Yu, Jianguo Hu and Xianfen He J. Lumin. 40–41 (1988) 893K.

[4]. Edward S. Grew, Andrew J. Locock, Stuart J. Mills, Irina O. Galuskina, Evgeny V. Galuskin and Ulf Halenius Am. Mineralogist, 98 (2013) 785

[5]. H.Y. Jiao and Y.H. Wang, J. Electrochem. Soc. 156 (2009) J117

[6]. Zhiguo Xia , Peng Du, Libing Liao, Guowu Li and Shuai Jin Current Appl. Phys. 10 (2010) 1087

[7]. Wei Lu, Zhendong Hao, Xia Zhang, Xingyuan Liu, Xiaojun Wang and Jiahu Zhang Opt. Mater 33 (2011) 126

[8]. Jianfeng Sun, Youmin Shi, Wenlin Zhang, Dezhong Shen and Jiayue Sun Mater.Res.Bull. 47 (2012) 400

[9]. Jianfeng Sun, Wenlin Zhang, Youmin Shi, Dezhong Shen and Jiayue Sun J. Electrochem. Soc. 159 (2012) J5

[10]. Zhaomei Li, Shaokang Gao, Xiuxia Chen and Qun Yu J.Lumin 132 (2012) 1497

[11]. Stemmermann, H. Pollmann, H. Kuzel ICDD file 43-0085, it may be noted that ICDD citation Eur. J. Mineral. 3 (1991) 259 is wrong.

[12]. R.L. Ye, X.R. Wang and Z.Y. Zhang, J. Chin. Cer. Soc. 15 (1987) 309

[13]. X. Zhang and X.R. Liu, J. Electrochem. Soc. 139 (1992) 622

[14]. H. Lin, X.R. Liu and W.L. Xu, J. Chin. Cer. Soc. 25 (1997) 494

[15]. H. Lin, X.R. Liu and E.Y.B. Pun, Opt. Mater. 18 (2002) 397

[16]. Y. Fang, W.D. Zhuang, Y.M. Sun, X.M. Teng, H.Q. He and X.W. Huang, J. Rare Earths 22 (2004) 122

[17]. P.Yang, J.H.Lin and G.Q.Yao J.Rare Earths 23 (2005) 633

[18]. H.Y.Koo, S.K.Hong, J.M.Han and Y.C.Kang, J.Alloys Compd. 457 (2008) 429.

[19]. C.F.Guo, M.Li, Y.Xu, T.Li, Z.Y.Ren and J.T.Bai Appl.Surf.Sci. 257 (2011) 8836

[20]. Y.Fang, W.D.Zhang, Y.S.Hu, X.Y.Ye, H.Q.He and X.W.Huang J.Alloys Compd. 455 (2008) 420

[21]. Y.Fang, W.D.Zhang, Y.S.Hu, X.M.Xiao, H.Q.He and X.W.Huang J.Rare Earths 25 (2007) 573

[22]. J. Wang , M. Zhang, Q. Zhang, W. Ding and Q. Su Appl. Phys. B 87 (2007) 249

National Conference on "Recent Trends in Mathematical Modeling, Simulation Methods, Computations, and Physical Sciences"
(MMSCP-2019), Organised by Hislop College, Nagpur, Maharashtra, India
International Journal of Scientific Research in Computer Science, Engineering and Information Technology
© 2019 IJSRCSEIT | Volume 4 | Issue 4 | ISSN : 2456-3307

Removal of Heavy Metals from Waste Water using Low Cost Natural Adsorbents

Yamini Kawadkar[1], Anshita Mehar[1], Shubhajit Halder[2]
[1]Post Graduate Department of Chemistry, Hislop College, Nagpur, Maharashtra, India
[2]Department of Chemistry, Hislop College, Nagpur, Maharashtra, India

ABSTRACT

The main objective of the present work is the synthesis of adsorbent by using natural mustard and fenugreek seeds which is low cost adsorbent . the synthesis is carried out by chemical treatment followed by carbonization at 60°C . the synthesis adsorbent is studied for adsorption of Cr(VI) from industrial waste water for various concentration and doses. It is concluded that the adsorbent developed in the work fairly effective for removing Cr(VI) from industrial waste water.

Keywords : Adsorption, Heavy Metals, Adsorbent, Natural Seeds.

I. INTRODUCTION

Pollution is the one of the serious problem now days. Environmental problems are increasing day by day and are threatening the survival of mankind of earth. Discharge of industrial wastewater has increased, with rapid increase in population and growth of industrialization, quality of both surface and ground water is changing day by day. Waste water contains so many metal ions which are harmful for human being. The most common heavy metals are Cd,Cr,Cu,Hg etc. Chromium is one of the major metal ions hazardous for human; it causes skin ulcers, lung, nasal and sinus cancer. When Chromium is inhaled its compounds are respiratory track irritants and can cause sensitization. Several treatments are used for removing metals from waste water includes Reduction, precipitation, ion exchange, electrochemical reduction and reverse osmosis. These are very expensive, not to ecofriendly, high power requirement and incomplete metal removal.

Adsorption technique is successively alternative process that utilized for removing heavy metals from industrial waste water, which can be performed in batch mode or continuous process. Adsorption processes have offered flexibility in design and operation in design and operation and in many cases will produce high quality treated effluent. activated mustard, fenugreek seed and Kulta seed. This work is an overview of these low-cost alternative adsorbents (LCAs) comprising natural, industrial as well as synthetic materials wastes and their application for heavy metal removal. In view of its efficiency, simplicity, low cost, and reliability, this technique has very good potential for heavy metals removal from high-volume industrial wastewaters.

II. METHODS AND MATERIAL

Material for adsorbent : The conversion of seeds into adsorbent has been carried out using chemical treatment. The material used for the adsorbent

synthesis is mustard seeds/fenugreek seed/ kulta seeds,etc.

- Naturals seeds firstly washed and dried and crushed into fine size using grinder.
- The crushed material had given a chemical treatment by dilute acids like sulphuric acid, dilute nitric acid,dilute hydrochloric acid, etc. Then stirred for 6 hours on magnetic stirrer at room temperature.
- Filtered and several time washing with distilled water anf then carbonised in a oven at 250 °C for 2 hours.
- Adsorbents stored in air tight containers.The adsorbents obtained is used for the further analysis and experimentation.

Analysis methodology:

The concentration of chromium (VI) in indusrial wastewater is determined by colorimeter. The standradization of colorimeter is carried out by observing the colorimeter readings for various water solution containing different concentration .

Adsorption study:

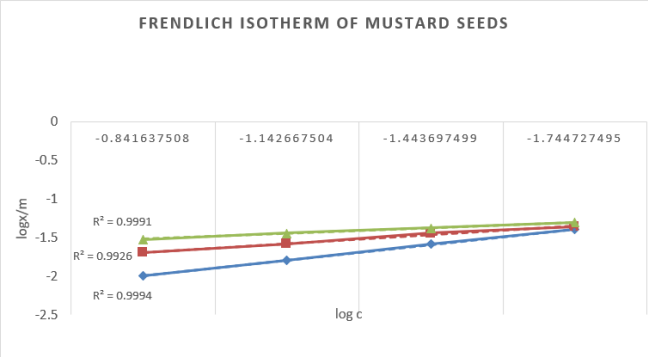

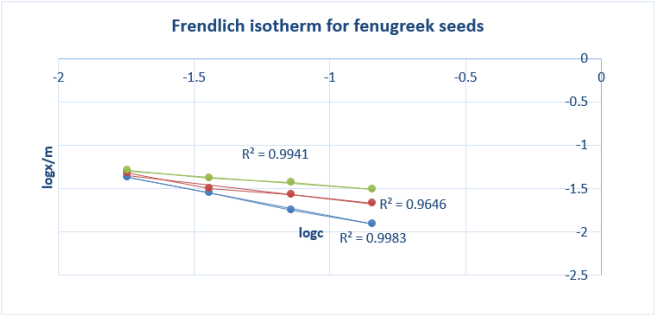

ADSORPTION EXPERIMENT:

The adsorption capacities of Cr from industrial wastewater solution of the Activated carbon were investigated by a batch method. Activated carbon with was thoroughly mixed conical flask, and the suspensions was shaken by an automatic shaker in a water bath at room temperature (25 ± 2 °C). Adsorption experiments were conducted by varying the pH (1-6 or 1-8), contact time (12 min to 8 h or 12 h), sorbent dosage (0.1-1.3g). The pH of each solution was adjusted by using 0.1N NaOH and 0.1N HNO_3.

Adsorption isotherms of Cr(VI) onto Activated carbon were measured at varying initial Cr concentration.

Following each adsorption experiment, the suspension containing Activated carbon and the above standard solution was filtered through Whattman filter paper to remove Cr(III) or Cr(VI) that have been adsorbed into the Activated carbon. Then the concentration of this metal in the filtrate was determined using calorimeter.

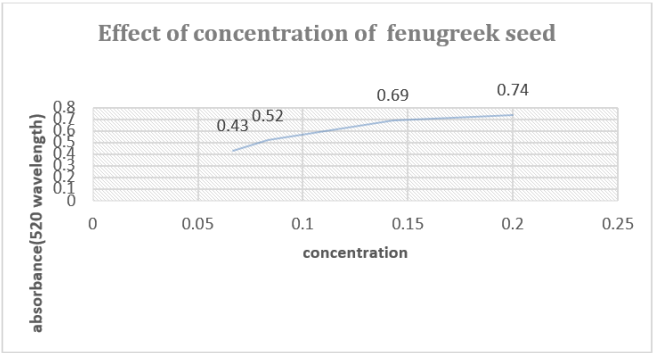

Fig 7: Effect of dosage of fenugreek seed at Chromium solution

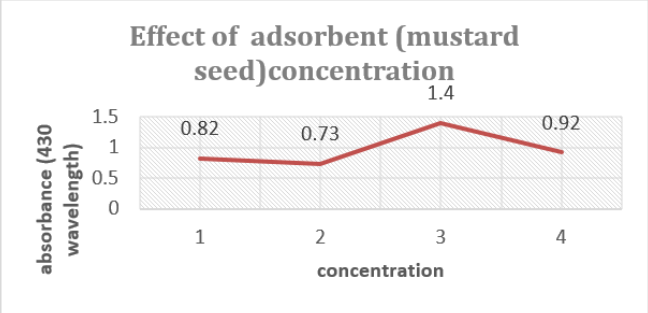

Fig 8: Effect of dosage of mustard seed at Chromium solution

III.CONCLUSION

The adsorption studies have indicated that 30% o Cr(VI) can be removed effectively . The yield of mustard/fenugreek/ kulta seed adsorbent in present work is 36% having surface area is satisfactory which is resembles with literature value for similar materials.Thus it can be concluded that the present work has demonstrated effectively that the snythesised adsorbent from seeds has potential as a low cost adsorbent and can be used effectively to adsorb heavy metal ion Cr(VI) from industrial wastewater.

IV. REFERENCES

[1]. C H. Huang, K. P. Chang, H. D. Ou, Y. C. Chiang, C. F. Wang, Adsorption of cationic dyes onto mesoporous silica. Microporous and Mesoporous Materials, Vol. 141, no. 1, pp.102-109, 2011.

[2]. N Chiron, R. Guilet, E. Deydier, "Adsorption of Cu(II) and Pb(II) onto a grafted silica:isotherms and kinetic models," Water Research, Vol. 37, no. 13, pp. 3079-3086, 2003.

[3]. Z Guo, D. D. Li, X. K. Luo, Ya. H. Li, Q. N. Zhao, M. M. Li, " Simultaneous determination of trace Cd(II), Pb(II) and Cu(II) by differential pulse anodic stripping voltammetry using are reduced graphene oxide-chitosan/poly-L-lysine nanocomposite modified glassy carbon electrode," Journal of Colloid and Interface Science, Vol. 490, no. 5, pp.11-22, 2017.

[4]. F Fu, Q. Wang, "Removal of heavy metal ions from wastewater: A Review." Journal of Environmental Management, Vol. 92, pp. 407-418, 2011.

[5]. R M. Ali, H. A. Hamad, M. M. Hussein, G. F. Malash, "Potential of using green adsorbent of heavy metal removal from aqueous solutions: Adsorption kinetics, isotherm, thermodynamic,mechanism and economic analysis," Ecological Engineering, Vol. 91, pp. 317-332, 2016.

[6]. J H. Park, Y. S. Ok, S. H. Kim, J. S. Cho, J.S. Heo, R. D. Delaune, D. C. Seo, "Competitive adsorption of heavy metals onto sesame straw biochar in aqueous solutions," Chemosphere,Vol. 142, pp. 77-83, 2016.

[7]. A E. El-Enany, A. A. Issa, "Cyanobacteria as a biosorbent of heavy metals in sewage water," Environmental toxicology and pharmacology, Vol.8, no. 2, pp. 95-101, 2000.

[8]. M N. Nourbakhsh, S. Kiliçarslan, S. Ilhan and H. Ozdag, "Biosorption of Cr6+, Pb2+ and Cu2+ions in industrial waste water on Bacillus," Chemical Engineering Journal, Vol. 85, no. 2, pp.351-355, 2002.

[9]. A B. Albadarin, C. Mangwandi, G. M. Walker and S. J. Allen, "Influence of solutionchemistry on Cr(VI) reduction and complexation onto date-pits/tea-waste biomaterials,"Journal of Environmental Management, Vol. 114, pp. 190-201, 2012.

National Conference on "Recent Trends in Mathematical Modeling, Simulation Methods, Computations, and Physical Sciences"
(MMSCP-2019), Organised by Hislop College, Nagpur, Maharashtra, India
International Journal of Scientific Research in Computer Science, Engineering and Information Technology
© 2019 IJSRCSEIT | Volume 4 | Issue 4 | ISSN : 2456-3307

Deep Learning for Mind Wave Electroencephalographic Biometric Security

Nagsen S Bansod[1], Siddharth Dabahade[2], M M Kazi[3], Jitendra Dongre[4], Prapti Deshmukh[5], K V Kale[6]
[1,2,3,5]MGM'S Dr. G. Y. Pathrikar College of Computer Science and Inforation Technology, Aurangabad. India
[4]Psychiatry Department, Byramjee Jeejeebhoy Government Medical Collegeand Sassoon General Hospitals, Pune, India
[6]Department of Computer Science and Information Technology, Dr. Babasaheb Ambedkar Marathwada University, Aurangabad, Maharashtra, India

ABSTRACT

Brain generates various signals according to the situation and activates. The frequency of the brain is different as per the level of action taken place by the person it may be either imaginary or motor imagery activities. From the brain signals imaginary signals are captured using MindWave Mobile Portable device. Frequency wise channels are separated and categories as Delta, Theta, Alpha and Beta. These channels are indicated emotions, movement, sensations, vision, etc. Features are extracted of each channel using Power Spectral Density (PSD) function. Feature level fusion is used for pattern matching. The Novelty of this work is a single electrode device is used to capture an Electroencephalography (EEG) imaginary data & feature level fusion of channels. The results are proven that these EEG imaginary signals could be used as better biometrics based authentication system.

Keywords : EEG, Mindwave, Identification, Verification, Biometric

I. INTRODUCTION

An electroencephalography (EEG) is a branch of Neuroscience. Recently, researchers in a Neuroscience and computer science attracted towards novel and innovative type of biometric based on neural activity of brain signals, such as EEG signals instead of the biological traits of the human body like face, fingerprint, iris, retina, voice, etc. EEG Signal biometric trait are very difficult to duplicate, break or guess. A novel approach is used for processing brain signal data through an EEG. The EEG gives various types of information about a person that is emotional, mediation and sad state. We can analyze EEG Signal and find out the human Concentration, Mathematical solution power, Letter Composition method, Rotational style. These parameters are considered to person identification and verification purpose. This research work is divided into mainly Introduction, Related research work, Proposed Methodology, Experimental Result and Conclusion.

II. RELATED RESEARCH WORK

An EEG signals, data feature measurement through two types of algorithm these are Discrete Fourier Transform (DFT) and Wavelet packet decomposition (WPD). The distinct features of EEG signal are consider with four feature set. The EEG signal data result was 93%, 87% and 93% classification rates of three feature set. By using Multilayer Perceptron Neural Network classifies EEG signal feature data gives 100% recognition rate but limited subjects only three. In this experiment subject has to seat normally with calm and quiet with closed eyes without any physical activity while collecting the datasets 4 channels are used [1].

In the recent research, identification & prediction of Motion Sickness (MS) of a driver in real life while driving the vehicle is very interesting and very important task because it can save the life of so many peoples in traveling. MS provide one type of security to the drive as well as passengers. Prediction of emotions in real time through EEG signals is a challenging task, while performing any activity human brain produces signals and the signals are coming from various parts of our brain. In case of emotions which is comes from occipital, parietal, somatosensory, etc. identification of generating signals according to the power of signals such as alpha, theta bands. Identification of emotions from the signals in a certain band as per the frequency level is possible through various feature extraction techniques and classification algorithm such as PCA, LDA, BFS, FFS, KNN, SVM, NWFE, ML, etc. apart from that LDA and ML gives 95%. Therefore, it can be used more or less robust techniques for the prediction of MS very effectively [2].

This work presents a novel approach for biometric identification using electroencephalogram (EEG) signals using Hilbert-Huang Transform (HHT). The amplitude and frequency were computed immediately after the HHT produce for the classification using salient characteristics. The proposed system was evaluated using two publicly available databases in these scenarios, single electrode of an EEG device which used for biometric data acquisition. A first database consists of 122 subjects and second having total 109 subjects, at the time of collecting the database were subject had shown with a sequence of images on the screen and some mechanical activity or screening works got the 96% and 99% success rate respectively. These results are compared favorably with recent research articles by the various algorithm and classification [3]. A research on biometric using motor imagery EEG signals and Auto Regressive Moving Average (ARMA) are used to construct an estimated model. From that they have used ARMA based classification system on the basis of Artificial Neural Network (ANN) approach. The extracted features are stored in the specific vector for the identification & verification on the basis of classification. Three persons, four types of the motor imagery EEG data signals were captured & perform the comparative results. Therefore, on the basis of the outcomes of [4] shows that it can be successfully exploited for purpose of person authentication and identification.

Therefore, an EEG data signal which belongs to motor imagery strongly provides a strong biometric based authentication and identification system will be used for security purpose. At the time of EEG based development of the system, classification played a vital role. They have compared the results of the system for the identification of imaginary movements of the persons using 3 different classifiers. H. Jian-Feng has compared Linear Discrimination Analysis (LDA), Artificial Neural Network (ANN) and Support Vector Machine (SVM) for classification of EEG signals, in this result LDA outperforms well as a better classifier than other algorithms [5]. The analysis of EEG data for the biometrics is concentrated on functional connectivity and measurement of time-domain statistical data which is co-dependent on each other. These two approaches are complex relations in EEG data measurement [6]. M. Abo-Zahad, et. al.[7] discusses challenges facing while practical implementation of biometric system based on the signals received from the brain for the identification of the person in a real life application.

Database acquisition is a time consuming procedure, in device setup time is varying when selecting no. of channels in the devices. In this case 64 channels were used to collect 109 people's data; it passes the signals in the middle range called as band pass filtering for the establishing functional connection amongst the sensors is calculated by the Phase based Lag Index system. From this connection data matrix is used to build the network to train the system and calculated

Eigenvectors. Brain resting state in performing well, but functional connectivity gives proper results, hence it can be a next generation technique for the classification of the data. EEG based biometric systems and biometric systems based on high-frequency scalp EEG features should be interpreted with caution [8].An explicitly investigated and assessed the permanence of the non-volitional EEG brainwaves over the course of time. Specifically, we analyzed how much the EEG signal changes over a period of six months, since any drastic change would make it unusable as an authentication method. The results are very encouraging, yielding high accuracy throughout the six-month period [9]. The amplitude of the brain signals is the indication of circadian rhythm which is tactless of the random changes for measuring features bi-variant measure Magnitude Squared Coherence (MSC) are used and reduced the number of channels of EEG signals for identification without any affect on the accuracy of the system.

The multidimensional data classification accuracy is better for fewest numbers of samples per person by using distance based classifier like KNN (K-Nearest Neighbor). In the previous literature, it is found that 64 channel data of 108 subjects gives 100% accuracy, in this case instead of 64 channels only 10 channels are used and also gives 100% recognition rate using 109 subjects' data with eye open resting position, environment for biometric identification [10].

III. PROPOSED METHODOLOGY

3.1 EEG Signal

In this research database is developed using a cost effective device that is Mindwave mobile and Micromax Canvas A114 mobile phone. The aged isomer programming LLC, free downloadable software in Android OS utilized. It is a portable system used for record database of the forehead with ear reference for database developers. The imaginary activity of letter Composition is captured with 5 iterations of 30 second.

Table 1. KVKRG Database Specification [13][14]

Database	Specification
Name	KVKRG EEG database
# Subject	200
Language	Marathi, English
Type	.csv
Session	3 (Morning, Afternoon, Evening)
Season	3 (Summer, Winter, Rainy)
Sampling Frequency	150 Hz
Activity (Task)	Imaginary closed eye: Baseline, Imaginary Mathematical, Geometric Figure Rotation , Mental Letter Composition Actity
Region	Maharashtra
Subjects Age	16-40
Gender	Male and Female
Environment	Controlled (Laboratories)

3.2 Feature Extraction

In this research work we used EEG Raw Value, eegRawValueVolts, Attention Level, meditation level, Blink strength, Delta (1-3Hz),Theta (4 -7 Hz), AlphaLow (8-9Hz), Alpha High (10-12 Hz), BetaLow (13-17 Hz), Gamma Low (31-40 Hz), Gamma mid (41- 50 Hz) these 7 features .

Apart from above features 5 features are selected for experiment because we are dealing with normal subject database these features are accept), Gamma Low (31-40 Hz), Gamma mid (41- 50 Hz).

Mean sample value (MSV)

Mean of all sample values

$$\text{MSV} = \frac{1}{N} \times \sum_{1=n}^{N} \quad x_n \qquad (1)$$

Signal consisting of a discrete-time sinusoid with an angular frequency of π/4 radians/sample with additive N (0,1) white noise. Create a sine wave with an angular frequency of π/4 radians/sample with additive N (0, 1) white noise. The signal is 320 samples in

length. Obtain the Welch PSD estimate using the default Hamming window and DFT length. The default segment length is 71 samples and the DFT length is the 256 points, yielding a frequency resolution of 2π/256 radians/sample. Because the signal is real-valued, the period gram is one-sided and there are 256/2+1 points [11].

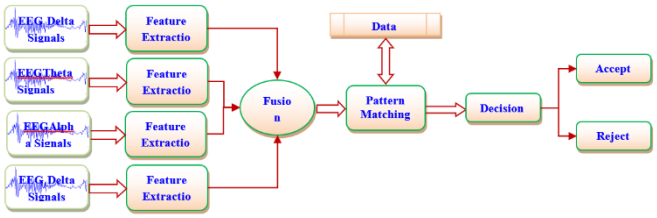

Fig 1: Proposed Methodology

Power Spectral Density (PSD)

The Power Spectral Density (PSD) to each frequency band is extracted from EEG signals as shown in the following. Wavelet translate of 4 levels was applied to decompose the filtered EEG data into five frequency bands, as shown in Table I, which reflect the physical activities. For each second (128 sampIes) in all channels and bands, a Fast Fourier Transform (FFT) with non-overlapping window was applied to find the PSD per band. Then the PSD is estimated as the average of the squared absolute value of the magnitude of the FFTs, as in equation (2)

$$PSD = \frac{1}{Nyq}\sum_{f=1}^{Nyq} |FFT|^{\wedge 2} \quad (2)$$

(2), Nyq is the Nyquist frequency (sampling frequency/2), and fis the frequency in Hz. To investigate the influence of use windowing with FFT, Hamming window with length 128 was applied before FFT producing another type of PSD named PSD with hamming Because Mindwave device has 1 electrode wish gives Delta (1-3Hz),Theta (4 -7 Hz), AlphaLow (8-9Hz), Alpha High (10-12 Hz), BetaLow (13-17 Hz), Gamma Low (31-40 Hz), Gamma mid (41- 50 Hz) these 7 features channels, obtained (5 bands * 1 electrode) .Obtain the Welch PSD estimate of an input

Feature level fusion Σ

Concatenate the feature set of multiple channel of EEG signal. In this research work the Delta, Theta, Alpha, Beta signal channel of EEG biometric. Let δ= {δ1, δ2, δ3…….. δn} an extracted feature of Delta signal, θ= {θ1, θ2, θ3…… θn} an extracted feature of Theta signal, α= {α1, α2, α3,….. αn} an extracted feature of Alpha signal and β= {β1, β2, β3,…… βn} an extracted feature of Beta signal obtained by concatenating augmenting normalize feature vector and performing feature selection on resultant fused feature vectors. We conduct extensive experiments to evaluate the effectiveness and robustness of the proposed system [13][14][15][16].
Convolution Neural Network (CNN)

Convolution Neural Network (CNN)

After normalization of EEG signal we have provided input to the CNN, i.e. NE X NT where NE is electrode (1) NT is time

NT = time * sampling rate.

Convolution Neural Network (CNN) consist of multilayer neural network perceptron (MLP) it has a special topology with multiple hidden layers. We can use for feature extraction and pattern classification like biological neural network like small cell input can be proceed. It can be used to process the row information without processing the row data.

Network Topology (NT)

It is the model which is used for prominent feature extraction as well as pattern classification. There are five layers included in the network topology which are two convolutional layer, two pooling layer and one fully connected layer [12]. The input data matrix has structure of 1* 150. The Convolutional layers convolve that input data matrix via six 5-by-5 filter and output the filtered data map.

The filtered data maps are then entered into the average pooling layer, which divides the input-filtered data maps into sets of 2- by-2 rectangles. For

each of these sub-regions, the average-pooling layer outputs the average value. The filtered data maps are then down-sampled and feature maps are obtained. During this step the computational complexity for upper layers is reduced. - The second convolutional layer uses the feature maps as input data. Through this and the second average-pooling layer, the first two steps are repeated. As a result, the features become more abstract and the computational complexity is further reduced. - Finally, the features obtained by the second average pooling layer are transferred to the fully connected layer. Ultimate classification is based on these features, Softmax activation function is used.

TABLE NO. 1. EEG DATA FEATURE SET

eegRawValue	Delta	Theta	Alpha		Beta		gammaLow	gammaMid
			alphaLow	alphaHigh	betaLow	betaHigh		
51	16745434	16750096	10235	9371	6354	4364	4869	3224
102	665851	91047	30130	7637	7995	25956	16752974	12957
19	206082	51834	4173	24355	14860	16748314	24462	18314
28	301085	38758	8633	24707	16746703	16759024	16537	17825
-279	1992969	99204	15682	68362	26465	27213	16761920	13203
89	483475	46766	68636	70677	16752442	83017	16597	6303
-349	16759164	16756526	16770661	12770	5000	18091	30031	8256
-300	285723	23618	2533	8622	4811	4421	3809	3397
24	16765681	28861	16745500	9428	17691	23362	16747113	16853
77	206582	10057	1356	5975	6416	5912	11819	4438
48	60769	16746334	16744346	16767015	15636	26680	23915	6900
51	364775	16773343	16749070	16756417	8894	22048	16496	10577
17	1446025	16769628	24715	14403	16756180	16766368	22151	8556
-264	97468	12890	10171	5712	8070	6106	10326	8207
34	273061	158117	83732	26191	8947	22988	25866	6478
17	616108	19593	14400	16751418	16755278	30792	15253	12013
39	75894	103275	16749335	23289	21902	22061	17374	8294

TABLE NO 2. DISTANCE MATRIX

0	7730991.949	6116394.356	737027 3.39	785323 6.593	119857 46.02	140892 20.78	868260 5.441	127443 09.83	9393457
7730991.949	0	6763899.424	5456663.712	8466063.153	9447346.576	11974204.53	7077255.627	8097867.78	8597073.966
611639	676389	0	924612	794019	700349	141643	880819	106202	967513

4.356	9.424		3.441	9.695	3.119	68.76	3.254	65.41	7.186
7370273.39	5456663.712	9246123.441	0	6404288.186	9653996.695	11183944.17	9126478.661	9998291.153	6559131.78
7853236.593	8466063.153	7940199.695	6404288.186	0	5306736.475	6803723.034	5317973.017	7220363.339	8087028.678
11985746.02	9447346.576	7003493.119	9653996.695	5306736.475	0	8348019.847	6841051.085	7160480.356	9936828.949
14089220.78	11974204.53	14164368.76	11183944.17	6803723.034	8348019.847	0	7079411.068	9844532.915	14272766.22
8682605.441	7077255.627	8808193.254	9126478.661	5317973.017	6841051.085	7079411.068	0	8326343.407	11133325.08
12744309.83	8097867.78	10620265.41	9998291.153	7220363.339	7160480.356	9844532.915	8326343.407	0	8998864.424
9393457	8597073.966	9675137.186	6559131.78	8087028.678	9936828.949	14272766.22	11133325.08	8998864.424	0

3.3 Pattern Matching

Manhattan Distance Metric

Distance is measured of two points X (x1, y1) and Y(x2, y2) along with the axes of the plane with right angles, it is

$$\text{Distance} = |x1 - x2| + |y1 - y2| \quad (2)$$

3.4 Data Model

The extracted features of the data are stored in the data model using .mat file for pattern matching.

3.5 Decision

After pattern matching here used accept or reject decision on the basis of data available in the data model.

In this experiment we have used 200 subjects with two sessions, but here we show only 10 subjects data in the above table because of space limitations [15][16].

IV. RESULT AND DISCUSSION

In this experiment the KVKRG EEG database consist of 200 Subject with 5 iterations and two session i.e. summer and rainy. Calculated 13 EEG features which are shown in the Table No.1 & 2. i.e EEG Raw Value, eegRawValueVolts, Attention Level, meditation level, Blink strength, Delta (1-3Hz),Theta (4 -7 Hz), Alpha Low (8-9Hz), Alpha High (10-12 Hz), Beta Low (13-17 Hz), Gamma Low (31-40 Hz) and Gamma mid (41- 50 Hz),all these channels are considered as a feature. At the first time we have selected Delta (1-3 Hz) for the training of each subject and one of the single subjects to test but the result is not satisfactory. In the second experiment the Theta(4-7Hz) signal is considered for training features and one by one Theta signal is measured in testing but result not so good.

In the third experiment the alphaLow (8-9 Hz) signal is considered for training features and one by one alphaLow signal is considered for testing it gives good performance. In the successive experiment alphaHigh (10-12 Hz) uses for training feature it sounds better result as compare to earlier experiment. BetaLow (13-17 Hz), Gamma Low (31-40 Hz), Gamma mid (41- 50 Hz) is also exploit on same experiment but not considerable result.

In experiment no. 8 fusion of low alphaLow and alphaHigh features give better performance, therefore it is suitable for biometric.

Classification of the EEG feature is most important to biometric security. The pattern recognition is the best technique for this EEG feature classification. In this experiment the Manhattan Distance Metric gives 61% classification and recognition rate, i.e. shown in table Table No 3. Distance Matrix.

V. CONCLUSION

The innovative is in this novel area, developed EEG data using cost effective mindwave mobile device for biometric purpose. Developed our own database of 200 people in two sessions. Features are extracted of EEG channels using PSD. Feature level fusion of Delta, Theta, Alpha and Beta channels. Manhattan distance measurement is used for classification gives 61% accuracy of classification of distinct personalities. CNN Provide better feature extraction and classification rate that Manhattan. In future we will increase the data size and one winter session data, and again we will find the unique pattern from that data to person identification.

VI. FUTURE WORK

The fusion of many electrodes or features may increase the recognition rate for biometric identification and verification purposes. We can perform the fusion approach for fusion of multichannel it may increase the recognition rate.

VII. ACKNOWLEDGMENTS

The Author would like to acknowledge and thanks to the Program Coordinator for providing me all necessary facilities and access to Multimodal Biometrics System Development Laboratory to complete this work under UGC SAP (II) DRS Phase-I & II F. No. -3-42/2009&No.F.4-15/2015/DRS-II(SAP-II), One Time Research Grant No.F.19-132/2014 (BSR). We would like to acknowledge and thank to University Grants Commission (UGC), New Delhi for awarding me “UGC Rajiv Gandhi & BSR & MANF National Fellowship”.

VIII. REFERENCES

[1]. H. A. Shedeed, "A new method for person identification in a biometric security system based on brain EEG signal processing," Information and Communication Technologies (WICT), 2011 World Congress on, Mumbai, 2011, pp. 1205-1210.2.

[2]. Y. H. Yu, P. C. Lai, L. W. Ko, C. H. Chuang, B. C. Kuo and C. T. Lin, "An EEG-based classification system of Passenger's motion sickness level by using feature extraction/selection technologies," The 2010 International Joint Conference on Neural Networks (IJCNN), Barcelona, 2010, pp. 1-6. doi: 10.1109/IJCNN.2010.5596739.

[3]. S. Yang and F. Deravi, "Novel HHT-Based Features for Biometric Identification Using EEG Signals," Pattern Recognition (ICPR), 2014 22nd International Conference on, Stockholm, 2014, pp. 1922-1927.

[4]. J. f. Hu, "Biometric System Based on EEG Signals: A Nonlinear Model Approach," Machine Vision and Human-Machine Interface (MVHI), 2010 International Conference on, Kaifeng, China, 2010, pp. 48-51.

[5]. H. Jian-feng, "Comparison of Different Classifiers for Biometric System Based on EEG Signals," Information Technology and Computer Science (ITCS), 2010 Second

[6]. M. Garau, M. Fraschini, L. Didaci and G. L. Marcialis, "Experimental results on multi-modal fusion of EEG-based personal verification algorithms," 2016 International Conference on Biometrics (ICB), Halmstad, 2016, pp. 1-6. doi: 10.1109/ICB.2016.7550080

[7]. M. Abo-Zahhad, S. M. Ahmed and S. N. Abbas, "State-of-the-art methods and future perspectives for personal recognition based on electroencephalogram signals," in IET Biometrics, vol. 4, no. 3, pp. 179-190, 9 2015.

[8]. doi: 10.1049/iet-bmt.2014.0040

[9]. M. Fraschini, A. Hillebrand, M. Demuru, L. Didaci and G. L. Marcialis, "An EEG-Based Biometric System Using Eigenvector Centrality in Resting State Brain Networks," in IEEE

Signal Processing Letters, vol. 22, no. 6, pp. 666-670, June 2015. doi: 10.1109/LSP.2014.2367091

[10]. M. V. Ruiz Blondet, S. Laszlo and Z. Jin, "Assessment of permanence of non-volitional EEG brainwaves as a biometric," Identity, Security and Behavior Analysis (ISBA), 2015 IEEE International Conference on, Hong Kong, 2015, pp. 1-6. doi: 10.1109/ISBA.2015.7126359

[11]. B. Singh, S. Mishra and U. S. Tiwary, "EEG based biometric identification with reduced number of channels," 2015 17th International Conference on Advanced Communication Technology (ICACT), Seoul, 2015, pp. 687-691.doi: 10.1109/ICACT.2015.7224883

[12]. Mashail Alsolamy, Anas Fattouh, "Emotion estimation from EEG signals during listening to Quran using PSD features", 2016 7th International Conference on Computer Science and Information Technology (CSIT), vol. 00, no. , pp. 1-5, 2016, doi:10.1109/CSIT.2016.7549457

[13]. L. Ma, J. W. Minett, T. Blu and W. S. Y. Wang, "Resting State EEG-based biometrics for individual identification using convolutional neural networks," 2015 37th Annual International Conference of the IEEE Engineering in Medicine and Biology Society (EMBC), Milan, 2015, pp. 2848-2851.doi: 10.1109/EMBC.2015.7318985

[14]. N. S. Bansod, S. B. Dabhade, M. M. Kazi, Y. S. Rode and K. V. Kale, "Single electrode brain signal data fusion for security," 2016 International Conference on Global Trends in Signal Processing, Information Computing and Communication (ICGTSPICC), Jalgaon, 2016, pp. 108-112.doi: 10.1109/ICGTSPICC.2016.7955279

[15]. N. S. Bansod, S. B. Dadhade, S. S. Kawathekar and K. V. Kale, "Speaker Recognition Using Marathi (Varhadi) Language," 2014 International Conference on Intelligent Computing Applications, Coimbatore, 2014, pp. 421-425.doi: 10.1109/ICICA.2014.92

[16]. S. B. Dabhade, N. S. Bansod, Y. S. Rode, M. M. Kazi and K. V. Kale, "Hyper spectral face image based biometric recognition," 2016 International Conference on Global Trends in Signal Processing, Information Computing and Communication (ICGTSPICC), Jalgaon, 2016, pp. 559-561.doi: 10.1109/ICGTSPICC.2016.7955363

[17]. S. B. Dabhade, N. S. Bansod, Y. S. Rode, M. M. Kazi and K. V. Kale, "Multi sensor, multi algorithm based face recognition & performance evaluation," 2016 International Conference on Global Trends in Signal Processing, Information Computing and Communication (ICGTSPICC), Jalgaon, 2016, pp. 113-118.doi: 10.1109/ICGTSPICC.2016.7955280

National Conference on "Recent Trends in Mathematical Modeling, Simulation Methods, Computations, and Physical Sciences"
(MMSCP-2019), Organised by Hislop College, Nagpur, Maharashtra, India
International Journal of Scientific Research in Computer Science, Engineering and Information Technology
© 2019 IJSRCSEIT | Volume 4 | Issue 4 | ISSN : 2456-3307

Dye Sensitized Solar Cell Using Basella Alba (Red Vine Spinach) Sensitizer Nanocrystalline TiO2 Photoanode

M. S. Dixit, Khadija Sofi, P. Sonone, G. T. Tayade, A. U. Ubale*

Nanostructured Thin Film Materials Laboratory, Department of Physics, Govt. Vidharba Institute of Science and Humanities, VMV Road, Amravati, Maharashtra, India

ABSTRACT

In the present work, dye sensitized solar cell is fabricated using Basella Alba (Red Vine Spinach) as sensitizer on nanocrystalline TiO_2 photoanode. TiO_2 photoanode film is deposited on transparent fluorine doped tin oxide (FTO) substrate using doctor blade method. Using UV- Vis spectrometer, optical absorption analyses is carried out for Basella Alba .The DSSC is fabricated by assembling Basella Alba sensitized photoanode and graphite coated counter electrode. The photoelectrochemical performance of the Basella Alba fruit dye extract showed an open ciorcuit voltage(Voc) of 0.8 mV, Short circuit current 10 mA Fill factor 0.63, and conversion efficiency 0.50%.

Keywords : Dye sensitized solar cell(DSSC), Titanium dioxide, Basella Alba dye.

I. INTRODUCTION

Among all other renewable energy sources, solar energy is safer and inexhaustible source of energy and it has greatest potential [1]. Photovoltaic's convert sunlight directly into electricity [2]. from the last three decades, The solar cell market is dominated by silicon based devices [3].However, recently DSSC have gained increasing interest due to its simple and low cost manufacturing process[4].A DSSC constitutes a photoelectrode and a catalytic electrode with an electrolyte between them. In 1991, O'Regan and Gratzel developed DSSC that work on the principle of plant photosynthesis and the efficiency of these cell was reported as 7.1% and 7.9% [5]. Usually, dye sensitized solar cells consist of a mesoporous titanium dioxide film, which is sensitized by a dye, in combination with a liquid or solid-state material. In hybrid solar cells the acceptor-type material is replaced by inorganic semiconductors like TiO_2, CdS, CdSe, PbS, PbSe, ZnO, or SnO_2 [6-12] .The DSSC sensitized by Ru compound absorbed onto nanoscale TiO_2 is most efficient and has efficiency 11-12% [13].

But ruthenium dye, including N3 and N719 are costly and hazardous to environment, thus other numerous metal free organic dyes have been used in DSSC [14]. Thus the natural dyes extracted from different parts of plant like leaves, fruits, flower, root, seed have been used as a sensitizer for DSSCs.

G. Calogero et al. [15] reported that Betaline pigment containing red turnip has highest efficiency of 1.70% . H. Zou et al. [16] have studied mangosteep pericap as a sensitizer with efficiency 1.17%. W. Lai et al.[17] have used Rhoeo Spathacea as a natural sensitizer and reported its efficiency as 1.02%. Bayron Cerda et al.[18] have used Maqui, Black Myrtle, Spinach and spinach black myrtle as natural sensitizer to increase the efficiency of DSSC and concluded that black myrtle has more efficiency as 0.040% among them.

Lawrence Amadi et al.[19] have studied the creation of natural dye sensitizer solar cell using vegetable dye from Red Cabbage, Green Cabbage, Spinach, Red Potato, Radish and concluded that green cabbage give the cell efficiency as 0.1% while red cabbage as 0.09% and radish and Potato as 0.06%. S.Rajkumar and K. Suguna [20] used Beet root and Pomegranate fruit to enhance the efficiency of DSSC. Monzir S et al. [21] used fifteen different dyes to study DSSC and found that schinus Terebinthifolis Leaves shows best performance for DSSC with photoelectrochemical parameter of J_{sc}= 2.40mA/cm^2,V_{oc}=0.68, FF=0.44 and efficiency ŋ= 0.73%.

It has been observed that there is a lot of work to be done in order to improve quantum efficiency of dye-sensitized solar cell. The advantages of natural dyes as photosensitizers are large absorption coefficients, high light-harvesting efficiency, no resource limitations, low cost, simple preparation techniques and no harm to the environment.

Fig.1 B.Alba Vine

Fig.2 Fruits of B.Alba

In the present work we used Basella Alba (Red Vine Spinach) as a sensitizer. . Basella Alba (Figure 1), bearing deep-green leaves, is commonly grown and harvested as a novel leafy vegetable in tropical and non tropical region, particularly during the summer season when the production of other leafy vegetables is short. Grown into the fall and winter seasons, the vines produce a substantial quantity of fleshy and dark blue fruits, which are usually discarded by farmers. The estimated production of fresh fruits is approximately 2 kg per plant. Value-added use of the natural pigments from the fruits as colorants and bioactive ingredient in related product development deserves research interest.

Basella Alba Fruit Red Pigment Analysis at Various Maturities concluded that three red-violet pigments were detected in ripe B. alba fruits. Gomphrenin I was identified as the major pigment [22]. The structural formula for Gomphrein I ($C_{24}H_{26}N_2O_{13}$) is shown below.

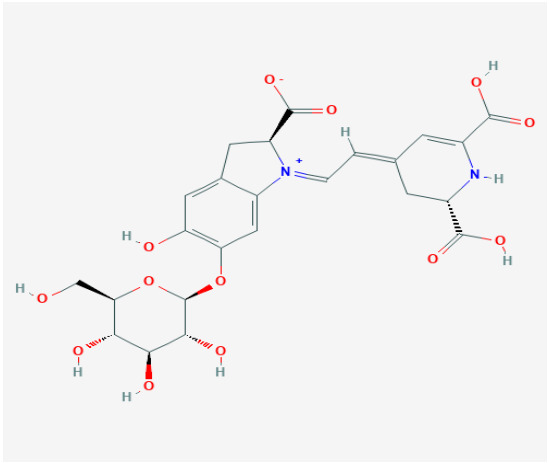

In addition to gomphrenin I, betanidin-dihexose and isobetanidindihexose were also detected. B. alba fruits could be regarded as a potent source of natural colorant[22].

Experimental Section

A. Preparation of TiO_2 paste

TiO_2 paste was prepared from homogeneous mixture of TiO_2 nanopowder and Ethyl cellulose. TiO_2 nanopowder and ethyl cellulose was mixed in morter for about 30 min to make the homogeneous mixture and α-terpnol and ethanol was added gradually. Few drops of acetyl acetone were added to the mixture. The slurry obtained is then kept for ultrasonication for 1h.

B. Extraction of dye

The fresh fruits of basella Alba(Red Vine spinach) were rinsed in distilled water to remove dust and

soluble impurities. 30g of the fruits were kept in 30mL of ethanol the beaker is covered with aluminum foil and kept it for 24 hrs. After that the fruits were filtered out and filtrate obtain was stored in a sample bottle covered with aluminium foil.

C. Preparation of TiO_2 photoanode

The photoanode is composed of conducting glass substrate of sheet resistance 15Ω/cm² (20 x20 mm²) coated with FTO (fluorine doped tin oxide). The 10 x10 mm² active area of substrate was coated with titanium dioxide with the help of Doctor blade method. The coated film of TiO_2 on FTO glass was annealed for 1 h at 450 °C. After that the glass slide is left dipped into dye for 24 hr so that the adequate adsoption of dye occure into the TiO_2 film. The electrode was then taken out of dye solution and rinsed with distilled water and ethanol, and used as photoanode for solar cell.

D. Assembling complete Dye sensitizrd solar cell

TiO_2 coated glass Slide was used as photoanode while graphite coated FTO glass slide was used as counter electrode. The counter electrode was kept on working electrode and to avoid the direct contact between them, the spacer was inserted between them. The space between working and counter electrode is filled with electrolyte. To couple the electrode the binder clips on opposite sides were used.

II. RESULT AND DISCUSSION

A. UV-VIS Analysis of Natural sensitizer

The extracted Basella Alba (Red vine spinach) was characterized using UV-Vis. UV-Vis spectra that provide the information about frequencies at which the dye absorb photon. Fig.1 shows the absorbtion wavelength Basella Alba dye is from 450nm to 580nm, which falls in the visible region.

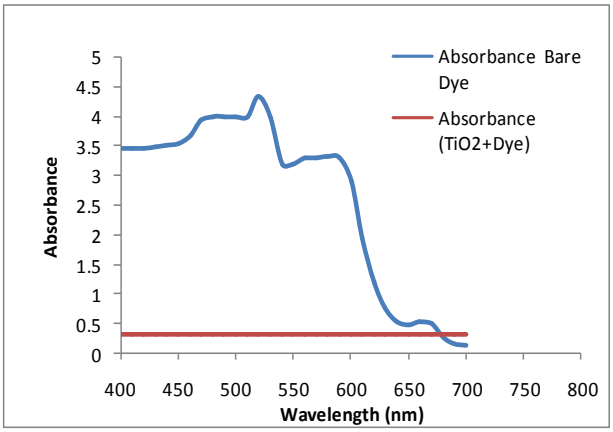

Fig. 3 Absorption spectrum of dye extract from Basella Alba (Red vine spinach) and TiO_2+dye

It is observed that the spectra of TiO_2 photoanode does not absorb visible light, but the absorbtion for Basella Alba sensitized TiO_2 photoanode is extended in the wavelength region 450-600nm.

B. Photovoltaic performance of DSSC.

The photovoltaic performance of the fabricated DSSCs employing metal free natural dye Basella Alba as photo-sensitizers are evaluated by recording the current and photovoltage (IV) . The sample was illuminated direct to sunlight and active area of the cell is exposed to light was 1cm x 1cm. From the recorded IV curve, the photovoltaic parameters such as open circuit voltage (V_{oc}), short circuit current (Isc), fill factor (FF) and the photo-conversion efficiency (ŋ) were calculated using the following empirical relation

$$\text{PCE, } \eta = \frac{Voc \times Isc \times FF}{Pin} \text{ x } 100$$

The fill factor of the assembled stack calculated using

$$FF = \frac{P\,\max}{Voc \times Isc}$$

Fig.5 represent the I-V characteristic of DSSC sensitized by Basella Alba(red Vine Spinach) .

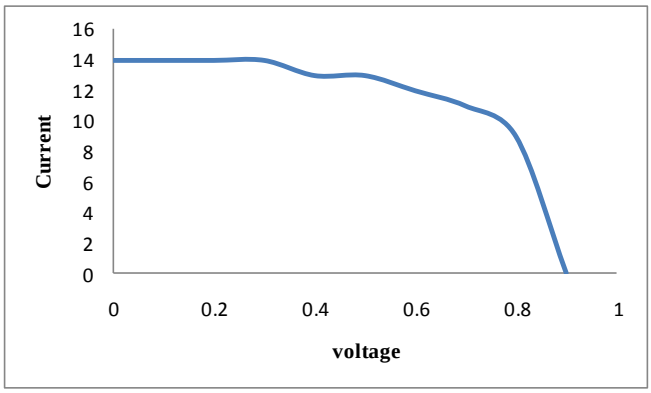

Fig.4- I-V characteristic of DSSC with Basella Alba (Red Vine spinach) extract Dye

Dye solution	I_{max} (mA)	V_{max} (mV)	I_{sc} (mA)	V_{oc} (mV)	FF	Ɗ (%)
Basella Alba	14	0.9	10	0.8	0.63	0.504

III.CONCLUSION

We have successfully fabricated DSSCs using cost effective and naturally abundant metal free photo-sensitizer extracted from Basella Alba (Red Vine Spinach). The absorbance property of the extracted natural sensitizers was examined using UV-Visible spectroscopy. From the photovoltaic studies, it showed the Photovoltaic parameter such as V_{max}, I_{max}, Voc, Isc, FF, PCE (ŋ) was O.9mV,14mA, 0.8mV, 10mA, 0.63, 0.5% respectively. High efficiency may be attributed to rich adsorption of dye molecule on to TiO_2 particle. For the betterment of the device, further optimization of various parameter is required which is future challenge in the field of DSSC.

IV. REFERENCES

[1]. A Evans, V. Strezov,T.J.Evans, Renew.Sust.Energ.Rev.13(2009)1082.

[2]. MDArcher,R.Hill,Clean Electricity fromPhotovoltaics,Vol.1,imperial College press(2001).

[3]. R Banos, M.Agugliaro, F. Montoya, F.,Gil,C.,Alcayde,A.,Gomez, J.G Renew. Sust.Ener Rev., 15 (2011)1753

[4]. M D. Archer, R. Hill, Clean Electricity from Photovoltaics, Vol.1, Imperial College Press(2001)

[5]. BO,Regan, M.Gratzel, Nature, 353,(1991) 737

[6]. T L. Benanti, D. Venkataraman, Photosynth. Res. 87,73 (2006) 91

[7]. M D. Archer, A. J. Nozik, Nanostructured and Photoelectrochemical System for Solar Photon Conversion. Imperial College Press(2008).

[8]. C Y. Kwong, A. B. Djurisic, P. C. Chui, K. W. Cheng, W. K. Chan, Chem..Phys. Lett. 384(2004)372

[9]. L Wonjoo, S. Seunghoon, H. Sung-Hwan, C. Byung Won, Appl. Phys.Lett. 92(2008) 193307

[10]. I Gur, N. A. Fromer, C.-P. Chen, A. G. Kanaras, A. P. Alivisatos, Nano Lett.7(2006) 409.

[11]. A R. W. Andrew et al., J. Phys D: Appl. Phys. 38(2005) 2006.

[12]. C Dehu, X, Jian, Z.Ting, P.Gary,AshokS,Gerhold, Michael., Appl. Phys. Lett.88(18),(2006)183111.

[13]. YChiba,A.Islam,Y Watanabe,R.Komiya, N.Koide,L.Han, J.Appl.Phy.45(2006)

[14]. JYum,E.Baranoff,S.Wenger,M..K.Nazeeruddin, M.Gratzel.,Ener,Envior.Sci.4, (2011)842

[15]. G. Calogero, G. D. Marco, S. Cazzanti, S. Caramori, R. Argazzi, A. D. Carlo, C. A. Bignozzi, Int. J. Mol. Sci. 11 (2010)254.

[16]. H Zhou, L. Wu, Y. Gao, T. Ma, J. Photochem. Photobiol. A: Chem. 219(2011) 188.

[17]. W H. Lai, Y. H. Su, L. G. Teoh, M. H. Hon, J. Photochem. Photobiol. A: Chem. 195(2008)307

[18]. Bayron Cerda, R. Sivakumar, M. Paulraj, J. Phy: Conf.720 (2016) 012030

[19]. Lawrence Amadi, Shaichisen Jenny, Asif Ahmad, N. Brown, S.Yadav, Destiny Brown, W.Ghann, A.Gayrama, Mintesinot Jiru, J.Uddin, Nanosci. Nanoeng. 3(3)(2015)25.

[20]. S Rajkumar, K. Suguna, Int. J. Engg . Res. Pub. 6(5) (2016) 93.
[21]. Monzir S. Abdel Latif,Mahmouud B. Abuiriban, Sci. Tech. Deve. 34(2015)135.
[22]. SH.lin,B.H.lin, W.M.Hsieh, H.J.Ko, CD Liu, LG Chen, Robin Y, YY Chiou, J.Agric. Food Chem. 58 (2010) 10364.

National Conference on "Recent Trends in Mathematical Modeling, Simulation Methods, Computations, and Physical Sciences"
(MMSCP-2019), Organised by Hislop College, Nagpur, Maharashtra, India
International Journal of Scientific Research in Computer Science, Engineering and Information Technology
© 2019 IJSRCSEIT | Volume 4 | Issue 4 | ISSN : 2456-3307

Copper and Copper Oxide Nanoparticles : Applications in Catalysis

Mayur Khedkar, Pratik E. P. Michael, Shoeb R. Khan*
Department of Chemistry, Hislop College, Nagpur, Maharashtra, India

ABSTRACT

Copper and Copper oxide nanoparticles (Cu NPs) have attracted considerable interest because of their catalytic, optical, mechanical and electrical conducting properties. The earth-abundant and inexpensive copper metal, have generated a great deal of interest specially in the field of catalysis. This paper discusses the uses of Cu and Cu-oxide NPs as catalysts for Ullmann type reactions and Gas Phase Reactions. We believe that this article will provide the necessary background information for further study and applications of Cu-based nanoparticles in catalysis.

Keywords : Copper, Nanoparticles, Ullmann reaction, Gas Phase Reaction

I. INTRODUCTION

Metal and metal oxide nanoparticles exhibit special properties and potential applications. Nanoparticles offer high surface to volume ratio and its size, dispersal, and morphology are the main reason for the novel and enriched properties.[1] Among various metal nanoparticles, inexpensive copper nanoparticles have attracted considerable interest because of their catalytic, optical, mechanical and electrical conducting properties.[2] Cu is relatively non-toxic to human beings, but is toxic towards many micro-organisms and hence can be used for antimicrobial treatments.[3] Because of their variable oxidation states (Cu^0, Cu^I, Cu^{II}, and Cu^{III}), it has a great scope in photo catalytic degradation of organic pollutants and catalytic organic transformations.[4]

Cu nanoparticles are initially formed and subsequently oxidized to form highly crystalline and stable Cu_2O. Copper (I) oxide (Cu_2O) also called cuprous oxide is a *p*-type metal oxide semiconductor with promising applications in solar energy conversion and catalysis.[5] In addition to this copper has high melting and boiling point which makes it thermally stable. Hence, Cu is compatible with high temperature and high pressure chemical reactions, like vaporphase reactions, microwave-assisted reactions, continuous flow reactions, and various organic transformations.[6]

II. METHOD OF PREPARATION of Cu-NPs

Preparation of highly active, selective, stable, robust, and inexpensive Cu nanoparticles is always a challenge in the field of research. The technique for the synthesis of Cu NPs are rely on the same methods that have been used to prepare other metal NPs,[7] which mainly include either "bottom-up" or "top-down" approach. In bottom-up approach atomic level precursors are used to synthesize nanoparticles sized materials, whereas in top-down method a bulk solid is broken down into nanosized materials. NPs are highly structure sensitive and their catalytic efficiency and selectivity mainly depend on the shape,

size, and composition of the nanoparticle. While both approaches have their pros and cons, the bottom-up approach has become more prominent as it offers greater scope for controlling the shape and size of the resulting nanomaterial.[8]

Generally physical and chemical methods have been used to synthesize copper nanoparticles. The most common approach for synthesizing Cu NPs is by creating microemulsions. However, this method requires large amounts of surfactants and organic solvents which increases the cost of production.[9] Microwave irradiation,[10] aerosol techniques, laser ablation, and radiolysis are common physical methods to synthesize nanoparticles but the use of expensive instruments and excessive energy consumption limits their application.[11] Chemical treatment for the synthesis of Cu NPs involves wet chemical, reverse micelle, biosynthesis and ionic liquid assisted methods.[12] In comparison to above methods, green synthesis of the Cu NPs is more safer and environmental friendly technique. Existing literature reports the use of *Terminalia arjuna* bark,[10] leaf broth of *Azadirachta indica*,[13] *Capparious zeylanica*[14] and *vitis vinifera*[15] as well as various other plant extract, were used as reducing and capping agent for the successful synthesis of Cu NPs. The uses of microorganism like *Pseudomonas stutzeri* bacteria and *Aspergillus* fugi have also been reported in the literature for the Cu NPs synthesis.[16]

III. APPLICATIONS OF Cu-NPs IN CATALYSIS

The catalytic activity of Cu NPs depends on composition of the nanoparticles as either the pure copper or the oxides; copper oxide nanoparticles have lower catalytic activity as compared to pure Cu NPs.[5] The activity is also affected by the method and condition of its preparation and the size of nanoparticles, smaller the particle size, greater the catalytic activity.[17] They are quit striking for this purpose because they often allow reactions to be carried out under green and sustainable reaction conditions. This section primarily focused on catalytic applications in Ullmann coupling reaction and gas phase reactions.

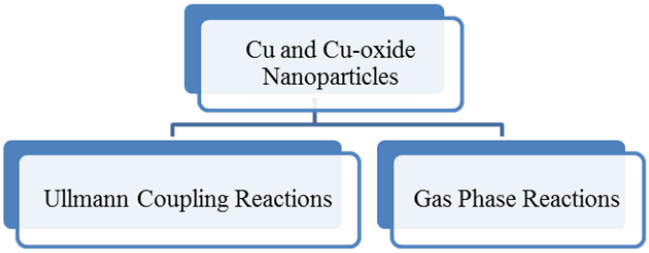

IV. ULLMANN COUPLING REACTIONS

Coupling reactions such as Suzuki, Heck and Sonogashira reactions, and C–S, C–O, C–B, and C–Se bond formation reactions are some of the important coupling reactions in organic synthesis. Several transition metal catalysts have been developed and employed for these conversions. Cu and Cu-based NPs emerged as an efficient, cost-effective and reliable option for many reported methods, and can be used for green and sustainable chemistry.[18]

The classical Ullmann reaction involves the conversion of iodobenzene to biaryl compound using various Cu nanoparticles (C-C bond formation reaction) (Figure 1). In 1998, Gedanken pointing out that different particle size of Cu NPs led to different catalytic activity, which could be due to the different surface areas, which decreases with increasing the particle size.[19]

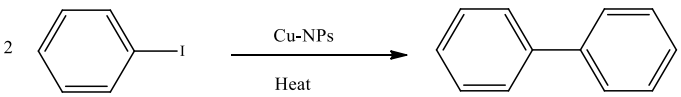

Figure 1. Classical Ullmann coupling reaction of iodobenzene

The development in the Ullmann cross coupling reaction is not limited to homo-coupling (C-C bond

formation) of aryl iodide. Many protocols have been developed for Ullmann type *O*- and *N*-arylation reactions. Wang and Co-worker reported the use of Nano copper oxide catalyst for the C–O cross-coupling of phenols with aryl halides under ligand-free conditions (Figure 2). The catalyst can be reused for five times under DMSO as solvent and Cs_2CO_3 and KOH as a suitable bases for the cross coupling reactions with phenyl iodides and bromides, respectively.[20]

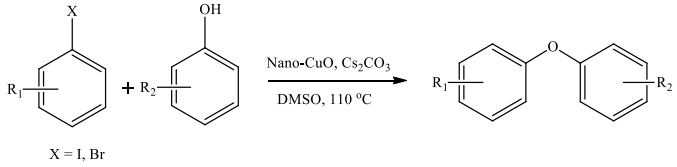

Figure 2. Ullmann C–O cross-coupling of phenols with aryl halides

Y. Kim et al. reported the Ullmann cross-coupling reaction of aryl halides and phenols with a catalytic amount of Cu_2O nanocubes as recyclable catalyst and Cs_2CO_3 as the base in THF at 150 °C.[21] They have examined a wide variety of substrates with C–I, C–Br, and C–Cl bonds, with various phenol to obtain their respective aryl ethers.

Ullmann-type *N*-arylation was recently explored by Pai and Chattopadhyay for arylation of *N*-heterocycles using Cu nanoparticles in the presence of K_3PO_4 as a base (Figure 3).[22] The arylation occurs under mild condition using Cu-NPs and can be used for synthesis of *N*-arylindole, *N*-arylimidazoles, *N*-arylpyrazole, *N*-arylindazole with aryl iodides in good to excellent yields.

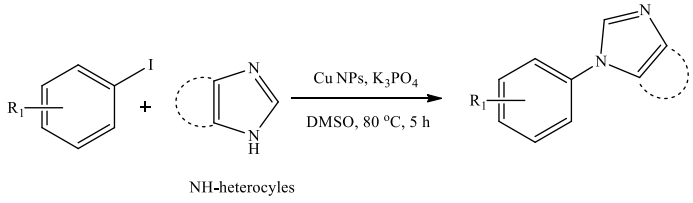

Figure 3. Ullmann-type *N*-arylation of NH-heterocycles with aryl halides

V. GAS PHASE REACTIONS

The best solvent from Green Chemistry point of view is no solvent i.e Solvent free reactions.[23] Consequently, reactions in the gas phase can be conducted in the complete absence of solvents. In this regards catalysts possessing nanostructured frameworks have major role in such gas-phase reactions by enabling the formation of high interfacial areas between the catalyst and reactants. Thus nanostructured support materials such as zeolites and mesoporous metal oxides extensively used as nanocatalytic species.[24] Mechanism wise the nanoporous materials allow reactants trapped in the pores and hence increased contact time with reacting molecules giving product without use of any solvent. In this context, the Cu-Nano and Cu-O Nano particles are widely used in gas phase reactions like NOx Reduction, CO Oxidation and Water gas Shift reaction.

a. NOx Reduction

NOx is one of the air pollutant generated from burning fuel. Thus its reduction (NOx to N_2) has gain considerable attention in recent past (Figure 4). Cu/zeolite nano structured materials prepared by inserting Cu ions into the zeolite structure using a simple ion-exchange reaction with conventional zeolites can serve as highly efficient catalysts for the selective catalytic reduction of NOx.[25]

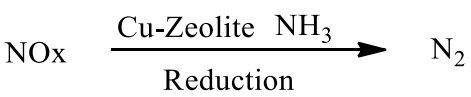

Figure 4. NOx reduction reaction.

The porous structure of zeolite associated with its high surface area allows the absorption of NOx and the Cu ions activate NOx molecules through a redox cycle.

b. CO Oxidation

Carbon monoxide (CO) is also one of the very dangerous air pollutant. The Cu-based nanomaterials have been employed in the catalytic oxidation of CO to CO_2 (Figure 5).

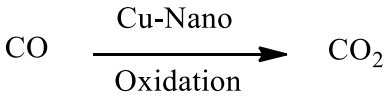

Figure 5. CO oxidation reaction.

Zhou and Coworker have synthesized CuO nanocrystals with different shapes, including CuO NPs, nanobelts, and nanoplatelets, prepared by precipitation methods.[26] All forms of these CuO nanocrystals were tested as catalysts for the conversion of CO to CO_2, revealing a direct relationship between the catalytic reactivity of the CuO nanostructures and the exposed crystal planes, which vary with the crystal shape. The mesoporous CuO nanowalnut-shaped particles are also explored for the same reaction. Chung and group have reported CuO/CeO2 materials, prepared by co-precipitation of nitrates.[27]

c. Water-Gas Shift Reaction

H_2 is an important gas in the chemical industry and also used as fuel. The water-gas shift (WGS) reaction is an attractive approach for H_2 production.[28] This transformation could be performed using oxide-supported Cu nanomaterials, in which intense synergistic effects between Cu and the oxide support have been observed (Figure 6).

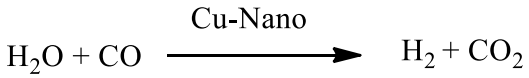

Figure 6. General representation of Water gas shift reaction catalysed by Cu-Nano particles.

Tang et al. explored the WGS reaction over a binary model Cu/ZrO_2. Successively $Cu/ZnO/Al_2O_3$ and $Cu/ZnO/ZrO_2/Al_2O_3$ catalysts were test for this attractive H_2 gas production reaction. The Cu NPs deposited on TiO_2 have been excellent catalysts for the WGS reaction.[29]

VI.CONCLUSION

This article has emphasized the use of Cu and Cu-oxide NPs in catalysis. The Cu-NPs are efficient and multipurpose catalysts that can be used to promote a wide range of organic transformation that go well beyond their traditional roles as metal catalysts. Various diaryl ethers and N-substituted heterocyclic compounds can be effectively prepared by Ullmann-type N-arylation and O-arylation respectively. We further discussed the role of Cu-NPs in gas phase reactions like NOx Reduction, CO Oxidation and Water gas Shift reaction. We believe that this review will serve to stimulate research in the field of Cu nanocatalysis and material science.

VII. REFERENCES

[1]. E. Roduner, Chem. Soc. Rev. 2006, 35, 583.

[2]. G. Evano, N. Blanchard, M. Toumi, Chem. Rev. 2008, 108, 3054–3131.

[3]. N. M. Zain; A. G. F. Stapley; G. Shama, Carbohydrate Polymers, 112, 2014, 195-202.

[4]. M. B. Gawande, A. Goswami, F. Felpin, T. Asefa, X. Huang, R. Silva, X. Zou, R. Zboril, R. S. Varma, Chem. Rev. 2016, 116, 3722–3811.

[5]. M. Yin, C. Wu, Y. Lou, C. Burda, J. T. Koberstein, Y. Zhu, S. O'Brien, J. Am. Chem. Soc. 2005, 127, 9506-9511.

[6]. R. Rupanwal, A. Kulshrestha, N. Singh, N. Sahni, M. Shujauddin, R. Khare, J. Pandey, International Journal of Scientific & Engineering Research, 2017, 8, 1479-1496.

[7]. A. Umer, S. Naveed, N. Ramzan, M. S. Rafique, Selection of A Suitable Method for The Synthesis of Copper nanoparticles. Nano 2012, 07, 1230005.

[8]. D. Mijatovic, J. C. T. Eijkel, A. V. D. Berg, Technologies for Nanofluidic Systems: Top-Down vs Bottom-Up-A Review. Lab Chip 2005, 5, 492–500.

[9]. S. Pal, U. Jana, P. K. Manna, G. P. Mohanta, R. Manavalan, Journal of Applied Pharmaceutical Science, 2011, 01 (06), 228-234.

[10]. S. Yallappa, , J. Manjanna, M. A. Sindhe, N. D. Satyanarayan, S. N. Pramod, K. Nagaraja. Spectrochimica Acta Part A: Molecular and Biomolecular Spectroscopy, 2013, 110, 108–15.

[11]. K. N. Thakkar, S. S. Mhatre, R. Y. Parikh. Nanomedicine: Nanotechnology, Biology and Medicine, 2010, 6 (2), 257–262.

[12]. N. Ojha, G. V. Zyryanov, A. Majee, V. N. Charushin, O. N. Chupakhin, S. Santra, Coordination Chemistry Reviews, 2017, 353, 1–57.

[13]. N. Nagar, V. Devra, Materials Chemistry and Physics, 2018, 213, 44-51.

[14]. K. Saranyaadevi, V. Subha, R.S.E. Ravindran, S. Renganathan, Int. J. Chem. Tech. Res. 2014, 6 (10) 4533-4541.

[15]. J.K.V.M. Angrasan, R. Subbaiya, Int. J. Curr. Microbiol. App. Sci. 2014, 3 (9) 768-774.

[16]. M. I. Din, R. Rehan, Analytical Letters, 2017, 50:1, 50-62.

[17]. M. Samim, N. K. Kaushik, A. Maitra, Bull. Mater. Sci., 2007, 30, 535–540.

[18]. C. Sambiagio, S. P. Marsden, A. J. Blackera, P. C. McGowan, Chem. Soc. Rev., 2014, 43, 3525-3550.

[19]. N. A. Dhas, C. P. Raj, A. Gedanken, Chem. Mater. 1998, 10, 1446-1452.

[20]. J. Zhang, Z. Zhang, Y. Wang, X. Zheng, Z. Wang, Eur. J. Org. Chem. 2008, 5112–5116.

[21]. J. Y. Kim, J. C. Park, A. Kim, A. Y. Kim, H. J. Lee, H. Song, K. H. Park, Eur. J. Inorg. Chem. 2009, 4219–4223.

[22]. G. Paia, A. P.Chattopadhyay, Tetrahedron Letters, 2016, 57, 140-3145.

[23]. G. G. Jernigan, G. A. Somorjai, J. Catal. 1994, 147, 567–577.

[24]. R. Silva, A. V. Biradar, L. Fabris, T. Asefa, J. Phys. Chem. C 2011, 115, 22810–22817.

[25]. S. Brandenberger, O. Krocher, A. Tissler, R. Althoff, Catal. Rev.: Sci. Eng. 2008, 50, 492–531.

[26]. K. B. Zhou, R. P. Wang, B. Q. Xu, Y. D. Li, Nanotechnology 2006, 17, 3939–3943.

[27]. L. C. Chung, C.T. Yeh, Catal. Commun. 2008, 9, 670–674.

[28]. C. Ratnasamy, J. P. Wagner, Catal. Rev.: Sci. Eng. 2009, 51, 325–440.

[29]. Q. L Tang, Z.P. Liu, J. Phys. Chem. C 2010, 114, 8423–8430.

National Conference on "Recent Trends in Mathematical Modeling, Simulation Methods, Computations, and Physical Sciences"
(MMSCP-2019), Organised by Hislop College, Nagpur, Maharashtra, India
International Journal of Scientific Research in Computer Science, Engineering and Information Technology
© 2019 IJSRCSEIT | Volume 4 | Issue 4 | ISSN : 2456-3307

Mathematical Modelling of Water Quality and Engineering of Pili River Stream in Nagpur District of Maharashtra

Ashish Kumar Jha*, Jagruti Roy
Department of Zoology, Hislop College, Nagpur, Maharashtra, India

ABSTRACT

The working plan deals with the preliminary proposal for mathematical modelling of water quality and engineering of Pili River stream located in Nagpur District of Maharashtra (India). The total length of Pili River within the city is about 16.7 Kilometres. Its width varies from 20-40 meters and depth ranges from 2 to 4.5 meters. There has been growing concern for maintenance of water quality and ecosystem along Pili River at both Legislative and Judiciary levels. Therefore it is need of the day to rejuvenate its water quality and habitat. Urbanization had created ecological threat due to immense dumping of domestic wastewater. General background information about natural characteristics of the selected stations along the Pili River and main source of pollution was made for a better understanding of this problem. The calculation was divided into three stages, and the problem was solved using the so-called "combined catch-up / feedback method". Computer memory space is saved as well as calculations speeds up using this method. The complicated hydraulic conditions in stream networks make it very difficult to estimate parameters. While the present developed model can be used for varied stream networks, it is necessary to estimate the parameters of the model according to the local measurements.

I. INTRODUCTION

Criteria for Water Pollution Control

There are different kinds of criteria that are currently used for water pollution control in India, waste water criteria, natural water body criteria, and organic waste discharge criteria (Deininger, 1973). If the waste water control criteria were worked out according to the local economic conditions and the technological level, they would be convenient as they are very concise (Rinaldi and Soncini, 1979). But they fail to link the pollution of waste-water sources with the local environmental conditions, *i.e.*, they do not take the environmental impacts of pollution into account.

The criteria for the quality of natural water bodies are based on the requirements of the water users. They represent the behalf of the water users, but fail to take the real situation into account. The third kind of criteria is mainly for organic waste discharge. These criteria should take into account the distribution of pollution sources, the amount of pollution, the available treatment capacity, the self-purification capacity of the natural water bodies, the demands of water users regarding quantity and

quality and other factors of an aquatic ecosystem (James, 1978).

The variables of the water pollution control problem which is a dynamic system control problem, can be divided into three classes (Thomani, 1972):

1. User demands
— Areal distribution of users
— Water quality desired by users
— Water quantity desired by users
— Future new users, their demands regarding water quality and quantity
— Variations of water demands (quality and quantity) in the future
— Basic and maximum demands (quality and quantity) during different periods
2. Pollution sources
— Distribution of main sources of pollution
— Main categories of pollution
— Amounts of pollution from the various sources
— Capacity of pollution control and waste-water treatment
— Probable future status of pollution sources
— Probable amounts and categories of pollution in the future
— Probable control levels and treatment capacity
3. Self-purification capacity
— Structure of the channels in a stream network
— Hydrological and aquatic conditions in streams
— Present water quality
— Probable unfavourable hydrological conditions in the future
— Probable water quality under most unfavourable hydrological and aquatic conditions
— Required treatment of waste influents to meet the desires of the users under different hydrological and aquatic conditions
— Sewage treatment needed to meet the basic requirements of users under most unfavourable hydrological and aquatic conditions

The third class of variables is decisive for defining the criteria. It combines the pollution sources with the desired water quality and the demands of the water users. Once the desired water quality has been determined, the self-purification capacity is the key factor defining the waste discharge criteria. The mathematical model described below is a powerful tool for this purpose.

Mathematical Modelling of Self-purification Processes in Pili River Stream Networks

The basic principle of founding mathematical models on the water quality in tidal stream networks is the principle of matter equilibrium. i.e., the variant rare of flux of materials on the surface of the system equilibrate the variance of the concentration of the materials inside the system.

The factors that cause the variance of matter concentration inside the system are of physical, chemical and biological origin. Physical factors include convection, turbulent diffusion (or dispersion in one-dimensional problems), settlement (or resuspension) of solid particles and dilution by mixing.

Chemical reactions which cause the variance of the concentration of pollutants include solubility equilbria and acidic reaction. Principally, they cause a shift in pH value and alkalinity, which affects the dissociation of carbonates.

Some people refer to adsorption as a physical reaction; others, as a chemical reaction.

The decomposition of organic pollutants by microbe is the main cause for polluted rivers to be deprived of oxygen. It involves two stages. At the first stage, the organic matter is oxidized by the bacteria. The rate of this reaction is assumed to be proportional to the concentration of the remaining organic matter,

measured in terms of oxygen. This reaction may be expressed as Eq. (1).

$$\frac{dL}{dt} = -K_1 L \quad (1)$$

where

L = concentration of organic matter in terms of BOD [mg/l]

t = time

K_1 = coefficient defining the reaction velocity $[day^{-1}]$

The second stage is nitrification, i.e., oxidation by bacteria of ammonium salts. The rate of this reaction can be expressed as Eq. (2)

$$\frac{dL_N}{dt} = -K_N t \quad (2)$$

Where

L_N = concentration of nitric organic pollutants in terms of nitrification biochemical oxygen demand BOD_N [mg/l]

K_N = coefficient defining the velocity of the nitrification reaction.

Decomposition of Sedimental Sludge at the Bottom of Rivers

The organic matter in the sedimental sludge is decomposed by microbes under anaerobic conditions, which results in the generation of reductive gases such as organic acids, methane, carbon dioxide, hydrogen, etc. These gases are released into the water body or into the interface between water and sediment and combine with the oxygen contained in the water.

Reoxygenation

$$K_3 = f(u, d, \varphi) \quad (7)$$

Water may absorb oxygen from the atmosphere when the dissolved oxygen (DO) is below saturation. The rate at which oxygen is absorbed, or the rate of reaeration, is proportional to the degree of under saturation and may be expressed as in Eq. (3)

$$\frac{dD}{dt} = K_2 (D_2 - D) = K_2 D_d \quad (3)$$

where

D = concentration of dissolved oxygen [mg/l]

D_s = saturation concentration of DO at definite temperature.

K_2 = reaeration coefficient $[day^{-1}]$.

t = time

D_d = dissolved oxygen deficit.

The photosynthesis of aquatic plants is another source of DO in water bodies. The rate of oxygen generation can be obtained from Eq. (4) and Eq. (5).

$$P(t) = P_m \sin \frac{(t - t_{sr})}{t_{ss} - t_{sr}} \qquad t_{sr} < t < t_{ss} \quad (4)$$

$$P(t) = 0 \qquad t_{sr} > t > t_{ss} \quad (5)$$

where

P_m = maximum rate of oxygen generation of aquatic plants during photosynthesis.

t_{sr} = time of sunrise.

t_{ss} = time of sunset.

Another factor affecting the material equilibrium is settling / resuspension. JANSA and AKERLINDH have shown that a term for deoxygenation due to BOD of sediment may be added to the model equations :

$$\frac{dL_b}{dt} = K_3 . L_s . e^{-K} 3^t \quad (6)$$

where

L_b = concentration of organic matter in settled sludge in terms of BOD at time t

L_s = total BOD of settling sludge.

K_3 = coefficient of sedimentation.

Factors affecting the sedimentation rate are flow velocity U, depth of water body d and particle diameter φ :

For elaborating a mathematical model of stationary streams, it is sufficient to take these factors into account. But in a Pili River stream network it is

necessary to include the tidal action and the particular flow conditions as these two factors govern the distribution and concentration of pollutants. Most coefficients are not constant. In a Pili River stream network, flows vary in direction and velocity, but not in a periodic manner as is the case for single estuaries or single tidal streams. In contrast to estuaries, there is no stratification and no crosswise circulating currents. Waters running in stream networks move forward, backward and around, but do not follow definite rules. At the nodes of the stream network, water discharge takes place depending on the geometric characteristics of the channels, the structure of the stream beds, as well as the water levels in the upstream and downstream reaches. There is no constant coefficient for the same amount of discharge. Flow velocities vary considerably, from high velocities in one direction to high velocities in the other direction. The uneven distribution of velocities over the cross-sections of the streams plays an important role in the distribution of pollutants.

Therefore, the unsteadiness of the concentration field, the transportation caused by variable flow velocities, dispersion, and the regulative function of the nodes on the assignment of water discharges in stream networks need to be taken into account. Dispersion may be expressed as Eq. (8).

$$I_x = -E_x \frac{d^2L}{dx^2} \quad (8)$$

where

E_x = coefficient of dispersion $[L^{-2}]$
L = length.
x = longitudinal distance.

The negative sign means that dispersion is directed towards the lower concentration.
Advection may be expressed as Eq. (9)

$$I_{o_a} = U \frac{dL}{dx} \quad (9)$$

Based on the above assumptions, the mathematical model of the water quality in tidal stream networks may be expressed as the following equations :

When $i \neq i,1$

$$\frac{aH}{at} + \frac{1}{B} \frac{aQ}{ax} = 0 \quad (10)$$

$$\frac{aU}{at} + U\frac{aU}{ax} + g\frac{aH}{ax} + g \frac{U|U|}{c^2 d} = 0 \quad (11)$$

$$\frac{a(AL)}{at} + \frac{a(AUL)}{ax} = \frac{a}{ax} \left(A.E_x \frac{AL}{ax}\right) - \sum_{io=1}^{P_0} K_{io}.A.L. + S \quad (12)$$

When $i = i,1$

$$\sum_{i=1}^{P_1} Q_{j_1,i_1} = 0 \quad (13)$$

$$H_{j_1,1} = H_{j_1,2} = \cdots = H_{j_1,i_1} = \cdots = H_{j_1,P_1} \quad (14)$$

$$\frac{aL}{at}.V_{j_1} = \Delta F_{j_1} \quad (15)$$

Initial conditions, j = 0

$$\begin{cases} H\ (i,0) = h\ (i) & (16) \\ U\ (i,0) = u\ (i) & (17) \\ L\ (i,0) = l\ (i) & (18) \end{cases}$$

Marginal conditions, i = f

$$\begin{cases} H\ (i,j) = h\int (f,j) & (19) \\ L\ (i,j) = l\int (f,j) & (20) \end{cases}$$

The equations (10) to (20) constitute the mathematical model of the water quality in tidal stream networks. For water quality simulation using the concentration of dissolved oxygen as indicator, the modeling equations should be hydraulic coupled equations and BOD-DO coupled equations.

$$\frac{aH}{at} + \frac{1}{B}\ \frac{aQ}{ax} = 0 \quad (21)$$

$$\frac{aU}{at} + U\frac{aU}{ax} + g\frac{aH}{ax} + g\ \frac{U\ |U|}{e^2\ d} = 0 \quad (22)$$

$$\frac{a(A.L)}{at} + \frac{a(AUL)}{ax} = \frac{a}{ax}\ \left(A.E_x\ .\frac{aL}{ax}\right) - \sum_{io=1}^{P_0}\ K_{io}\ .A.L. + S \quad (23)$$

$$\frac{a(A.D)}{at} + \frac{a(AUD)}{ax} = \frac{a}{ax}\ \left(A.E_x\ .\frac{aD}{ax}\right) + K_2\ .A.(D_s - D) \qquad i \neq i,1$$

$$- \sum_{io=1}^{P_0}\ K_{io}\ .A.L. + S_1 \quad (24)$$

$$\sum_{i1=1}^{P_1} Q_{j_1},i1 = 0 \quad (25)$$

$$H_{j_{1,1}} = H_{j_{1,2}} = \cdots = H_{j_1,i_1} = \cdots = H_{j_1,P_1} \qquad i = i,1 \quad (26)$$

$$\frac{aL}{at}\ .V_{j_1} = \Delta\ F_{j_1} \quad (27)$$

$$\frac{a0}{at}\ .V_{j_1} = \Delta\ D_{j_1} \quad (28)$$

Marginal conditions, i = f

$$H\ (i,j) = h\ 1\ (f\ ,j) \quad (29)$$
$$L\ (i,j) = l\ \ 1\ (f\ ,j) \quad (30)$$
$$D\ (i,j) = d\ \ 1\ (f\ ,j) \quad (31)$$

Initial conditions, j = 0

$$H\ (i,0) = h\ (i) \quad (32)$$
$$U\ (i,0) = u\ (i) \quad (33)$$
$$L\ (i,0) = l\ (i) \quad (34)$$
$$D\ (i,0) = d0\ (i) \quad (35)$$

where

Eq. (21)	=	so-called continuity equation
Eq. (22)	=	momentum equation
Eq. (23)	=	equation of pollution conservation
Eq. (24)	=	equation of DO conservation
B	=	average width of cross sections, for narrow and wide channels it approximately equals the width of the water surface [m]
A	=	area of the cross section through which waters flow [m^2]
Q	=	water discharge [m^3/e]
c	=	coefficient expressing the roughness of the stream bed. Chezy coefficient
d	=	hydraulic radius; for wide and narrow rivers it usually approximates the average depth of the water in the channels
K_{i0}	=	coefficients defining the decay velocities of pollutants. For organic pollutants, these coefficients define the oxidation velocity (K_1), settling/resuspension velocity (K_3), etc.
s	=	other sources or sinks, including branch influents, etc.
p_p	=	amount of coefficients
io	=	ordinal number
i1	=	ordinal numbers of cross sections located in the areas of stream network nodes
j1	=	ordinal numbers of the nodes of a stream network
V_{j1}	=	water volume at node j1 of the stream network
ΔF_{j1}	=	net flux of pollutants at node j1
h 1(f,j)	=	water levels at marginal sections
l 1(f,j)	=	concentration of pollutants in marginal sections
h(i)	=	original water level of a section
u(i)	=	original flow velocity in a section
l(i)	=	original concentration of pollutants in a section
f	=	ordinal numbers of marginal sections
i	=	ordinal numbers of segments of the stream network
j	=	ordinal numbers of time steps
m	=	total number of time steps
n	=	total number of segments of the stream network
d1 (f,j)	=	concentration of dissolved oxygen in marginal sections
d0 (i)	=	original concentration of a section
D_{j1}	=	net flux of dissolved oxygen at node j1
S_1	=	other source or sink of dissolved oxygen
K_2	=	coefficient defining the rate of reaeration of waters in the stream network

For the above model, it is assumed that the carbonaceous oxygen demand resulting from organic matter degradation is the main factor influencing the dissolved-oxygen balance.

If other factors exert a secondary oxygen demand, such as nitrifying bacteria by the oxidation of ammonia, appropriate equation, which have the same form as Eq. (23) need to be added and appropriate terms need to be added to the equation defining the equilibrium of dissolved oxygen.

Numerical Solution of the Mathematical Model

It we have all coefficients we need and we know the initial and marginal conditions, the equations of the mathematical model can be solved. But it is difficult to find an analytical solution. We need a proper numerical method.

Normally, in natural waters, the flow field is independent of the concentration field unless the concentration of pollutants is so high that it causes marked variations of water density and water viscosity.

The concentration field, however, is not independent of the flow field. Therefore, it is possible to solve the flow first and then the concentration field.

In the same way, the concentration field of organic pollution is independent of that of dissolved oxygen as long as there is dissolved oxygen in the water.

Therefore, we can use the recurrence relations of equations to simplify the calculation. That means we can calculate the flow field first, then, using the results of the flow field as a known condition, we can solve the concentration field of organic pollution and then the concentration field of dissolved oxygen.

In order to speed up the calculation and to save computer storage capacity, the following disposals are adopted: For each time sequence, the equations are solved in combination, while for each time span, the equations are solved by a recurrence method. The processes of the calculation are provided in detail below.

The first step is the calculation of the flow field. The relative equations are the following :

$$\frac{aH}{at} + \frac{1}{B}\frac{aQ}{ax} = 0 \qquad (36)$$

$$i \neq i,1$$

$$\frac{aU}{at} + U\frac{aU}{ax} + g\frac{aH}{ax} + g\frac{U\,|U|}{c^2\ d} = 0 \qquad (37)$$

$$P_1$$

$$Q_{j1,i1} = 0 \qquad (38)$$

$$i1=1 \qquad i = i,1$$

$$H_{j_{1,1}} = H_{j_{1,2}} = \cdots = H_{j_1,i_1} = \cdots = H_{j_1,P_1} \qquad (39)$$

Marginal conditions,

$$H\ (i,j) = h1\ (i,j) \quad i = f \qquad (40)$$

Initial conditions,

$$H\ (i,0) = h\ (i) \quad j = 0 \qquad (41)$$

$$U\ (i,0) = u\ (i) \quad j = 0 \qquad (42)$$

Using finite differences of a four-point implicit pattern, we can transform the differential equations into finite difference equations if the time spans are all of the same magnitude and the space spans are different. The pattern of differences is shown in Fig. 1.

For the variable θ , we have the following formulas :

$$\bar{\theta} = \frac{1}{4}\left(\theta_{i-1}^{j-1} + \theta_{i}^{j-1} + \theta_{i-1}^{j} + \theta_{i}^{j}\right) \qquad (43)$$

$$\frac{a\theta}{at} = \frac{1}{2t}\left(\theta_{i-1}^{j} + \theta_{i}^{j} - \theta_{i-1}^{j-1} - \theta_{i}^{j-1}\right) \qquad (44)$$

$$\frac{a\theta}{ax} = \frac{1}{2\Delta x_1}\left(-\theta_{i-1}^{j} + \theta_{i}^{j} - \theta_{i-1}^{j-1} + \theta_{i}^{j-1}\right) \quad (45)$$

where

θ = average value of the values of four nodes of a network.

Substituting finite difference formulas for the differential terms, we obtain, for stream segment no. i , the following difference equations.

$$\begin{cases} \emptyset 1_{i-1}\, H_{j-1}^{j} + \emptyset 2_{i-1}\, U_{i-1}^{j} + \emptyset 3_{i-1}\, H_{i}^{j} + \emptyset 4_{i-1}\, U_{i}^{j} = \emptyset 5_{i-1} & (46) \\ \Psi 1_{i}\, H_{i-1}^{j} + \Psi 2_{i}\, U_{i-1}^{j} + \Psi 3_{i}\, H_{i}^{j} + \Psi 4_{i}\, U_{i}^{j} = \Psi 5_{i} & (47) \end{cases}$$

Making identical alterations to these two equations, we can obtain equations of the following type.

$$\begin{cases} H_{i-1}^{j} + a_{i-1}\, U_{i-1}^{j} + b_{i-1}\, H_{i}^{j} = R_{i-1} & (48) \\ U_{i-1}^{j} + a_{i}\, H_{i}^{j} + b_{i}\, U_{i}^{j} = R_{i} & (49) \end{cases}$$

For each stream segment not located in the node regions, we have coupled equations similarly to the above, where a, b, $\emptyset$, Ψ are factors.

For the segments located in the node area, we have equations like Eq. (38) and Eq. (39). Adding the equations of the marginal and initial conditions, we obtain closed and solvable equations.

For the total stream network, the equations are of the following type :

$$A \,.\, \underline{\bar{X}} = R \quad (50)$$

Take a stream network of the following type as an example.

We can see that the coefficient matrix is of the tridiagonal type with some coefficients being discrete. Equations of this type can be solved with the “combined catch-up/feedback method”. This method includes two steps. The first step is the “catch-up process”. Using the boundary conditions, and beginning with the first equation, one equation after the other is transformed together with the last equation by means of identical alternation to eliminate a variable. The second step is the “feedback process”, conducted in opposite direction. Feeding the latest boundary condition into the last equation, we obtain the value of the last equation but one, we obtain the value of the last variables but one. In this way, one by one, we obtain the values of all variables. When making a catch-up step with the equations related to the nodes of the stream network, we must make an identical alternation with the equation having a discrete coefficient in order to bring the discrete co-efficient a step closer to the tridiagonal.

The second step of solving the equations of the model is the calculation of the concentration field of the organic pollutants.

The relevant equations are :

$$\begin{cases} \frac{a(AL)}{at} + \frac{a(AUL)}{ax} = \frac{a}{ax}\left(A.E_x.\frac{aL}{ax}\right) - \sum_{io=1}^{P_0} K_{1o}\,.\,A.L. + S \qquad i \neq i1 & (51) \\ \frac{aL}{at}\,.\,V_{j1} = \Delta F_{j1} \qquad i = i1 & (52) \end{cases}$$

Marginal conditions,

$$L\ (i,j) = 1\ (f, j) \qquad i = f \quad (53)$$

Initial conditions,

$$L\ (i,0)\ =\ l\ (i) \qquad j = 0 \qquad (54)$$

The requisite hydraulic conditions and the relevant data on the structure of the channels are provided by the computation above.

Using finite differences of the four-point implicit pattern, the differential equation can be transformed into a finite difference equation. Fig. 4 shows the difference pattern. The time and space spans are the same as used for the calculation of the flow field.

For variable θ , we have the following formulae :

$$\frac{a\theta}{at} = \left(\theta_i^j - \theta_i^j\right)/\Delta t \qquad (55)$$

$$\frac{a\theta}{ax} = \Delta x_{1+1}\ \frac{\Delta x_i}{(\Delta x_1 + \Delta x_{i+1})}\theta_{i+1}^j + \frac{\Delta x_{i+1} - \Delta x_i}{\Delta x_1 \bullet \Delta x_{i+1}}\ \theta_i^j - \frac{\Delta x_{i+1}}{\Delta x_i\,(\Delta x_i + \Delta x_{i+1})}\theta_{i-1}^j \qquad (56)$$

$$\frac{a^2\theta}{ax^2} = \frac{4\left(\theta_{i+1}^j - 2\,\theta_i^j + \theta_{i-1}^j\right)}{(\Delta x_1 + \Delta x_{i+1})^2} \qquad (57)$$

Using these formulas to replace the partial derivative terms of the differential equation and to put it in order, we obtain difference equations of the following type :

$$L_{i-1} + a_i' L_i + b_i' L_{i+1} = R_i' \qquad (58)$$

where a_i' , b_i' and R_i' are coefficients.

For each two segments, we have an equation of this type. The segments between two cross sections that are related to the nodes of the stream network are the so-called false segments. For these segments we use the equilibrium equation to connect the flows in the relevant channels. With the marginal conditions added, the equations are closed and can be solved. The coefficient matrix of the equations is of the tridiagonal type, the coefficients of the equations for the false segments being discrete. These equations can be solved with the combined catch-up/feedback method mentioned above.

Here, the letter L could be the concentration of BOD, of NH_3-N, NO_3 –N, NO_2-N or any other oxygen consuming material. Taking into account several kinds of factors of the biochemical oxygen demand, we obtain several groups of equations of the same type as discussed above.

The third step deals with the calculation of the concentration of dissolved oxygen. The relevant equations are :

$$\frac{a(A.D)}{at} + \frac{a(A.U.D)}{ax} = \frac{a}{ax}\left(A.E_x.\frac{aD}{ax}\right) + K_2\,.A.(D_s - D) - \sum_{io=1}^{P_0} K_{io}\,.A.L. + S_1 \qquad i \neq i,1 \qquad (59)$$

$$\frac{aD}{at}\,.V_{j1} = \Delta\, D_{j1} \qquad i = i,1 \qquad (60)$$

Marginal conditions,

$$D\ (i,j)\ = d1\ (f,j) \qquad i = f \qquad (61)$$

Initial conditions,

$$D\ (i,0)\ =\ d0\ (i) \qquad j = 0 \qquad (62)$$

These equations have the same structure as those for organic pollutants and can be solved in the same way.

Having completed all the three steps, we can turn to the calculation of the next time stage and repeat the three steps of calculation. In this way, steps by step,

we obtain the results of all variables at different times and places.

II. DISCUSSION AND CONCLUSION

Mathematical models of water quality are powerful tools to study pollution processes in rivers, especially in tidal stream networks (Fu, 1982). It is impossible to assess the present and future conditions of the water quality in a tidal stream network without mathematical models. By using the models, we can provide planers, managers and decision-makers with sufficient and concrete information, especially information for hypothetical cases. However, models cannot do the work of planners, managers and decision-makers.

The mathematical model of water quality in tidal stream networks has universal significance and can be used for various tidal stream networks (Rich, 1981). When applying the model to a given stream network, it is necessary to incorporate the cross sections of this system, to evaluate the coefficients and to calibrate the model using the information available on the system under study.

The information obtained by measurements and monitoring is most important in developing a mathematical model of water quality (Zhang, 1982). Since there are many channels in a stream network, a sufficient number of measuring points is needed to obtain reliable information. Measurements should be made, and samples taken, continuously and simultaneously at all points. It is not easy to obtain sufficient information. But if the model is well founded, it is considerably easier to study and manage the water resources in stream networks. Measurements should always be taken over two full tides in order to avoid being hoodwinked by false mathematical phenomena in the early period of calculation (Zhan, 1981).

III. REFERENCES

[1]. DEININGER, R. A. (1973). Models for Environmental pollution control, Ann Arbor.
[2]. FU, G. (1982). Planning of Water Pollution Control System, Qin Hua.
[3]. JAMES, A. (1979). Mathematical Models in water pollution control, John Wiley & Sons.
[4]. RICH, L. G. (1981). Environment System Engineering, Beijing.
[5]. RINALDI, S. & SONCINI, R. (1979). Modeling and Control of River Quality, New York.
[6]. THOMANN, R. V. (1972). System Analysis and Water Quality Management, New York.
[7]. ZHAN E. (1982). Environmental Hydraulice, He Hai.
[8]. ZHANG S. (1982). Water Quality Management and Planning. He Hai.

National Conference on "Recent Trends in Mathematical Modeling, Simulation Methods, Computations, and Physical Sciences"
(MMSCP-2019), Organised by Hislop College, Nagpur, Maharashtra, India
International Journal of Scientific Research in Computer Science, Engineering and Information Technology
© 2019 IJSRCSEIT | Volume 4 | Issue 4 | ISSN : 2456-3307

Comparative Study of Symmetric Key Cryptographic Algorithms CAST, IDEA, RC, Camellia and SAFER

Dr. Harshala B. Pethe[1], Dr. Manish T. Wanjari[2]
[1]Dr. Ambedkar College, Deekshabhoomi Nagpur, Maharashtra, India
[2]SSESA's, Science College, Congress Nagar, Nagpur , Maharashtra, India

ABSTRACT

Information security plays very important role in storing and transmitting the data through unsecured channel. In the network security, cryptography plays vital role to maintain the CIA triad that is Confidentiality, Integrity, Authentication and non-repudiation of information. Therefore the security of information is much important in data storage and transmission process. Cryptography also ensures that the message should be sent without any change and only the intended authorized person can be able to read the message. There are various cryptographic techniques developed for achieving secure communication. Using cryptography, the data is encoded before sending it and decoded after receiving, Cryptographic algorithms are broadly divided into two types, symmetric key and asymmetric key cryptographic algorithms. This paper deals with the comparative study of various symmetric key cryptographic algorithms CAST, IDEA, RC, Camellia and SAFER.

Keywords : Symmetric key cryptography, CAST, IDEA, RC, Camellia and SAFER

I. INTRODUCTION

Cryptography deals with the securing of digital data. It refers to the design of mechanisms based on mathematical algorithms that provide fundamental information security services. It is an establishment of a large toolkit containing different techniques in security applications.

Depending on the key used, cryptographic algorithms are divided into major two types:

1) Symmetric key or private key cryptography.
2) Asymmetric key or public key cryptography.

The private cryptography is an encryption process where key used to encrypt the message is the same as the key decrypting the message [1]. Private key cryptography is fast and efficient, making it ideal for large data transmissions. Private key cryptography is more effective when used with public key cryptography because it is much faster.

II. SYMMETRIC KEY OR PRIVATE KEY CRYPTOGRAPHY

Some symmetric key cryptographic algorithms are explained below:

2.1 Carlisle Adams and Stafford Tavares (CAST)

CAST was designed in Canada by Carlisle Adams and Stafford Tavares. They claim that the name refers to their design procedure and should conjure up images

of randomness, but note the authors' initials. The example CAST algorithm uses a 64-bit block size and a 64- bit key.

The algorithm uses six S-boxes with an 8-bit input and a 32-bit output. Construction of these S-boxes is implementation-dependent and complicated CAST-128 is a DES–like substitution-permutation crypto algorithm, employing a 128-bit key operating on a 64-bit block. CAST-256 is an extension of CAST-128, using a 128-bit block size and a variable length (128, 160, 192, 224, or 256 bit) key. CAST is named for its developers, Carlisle Adams and Stafford Tavares and is available internationally. CAST-256 was one of the Round 1 algorithms in the AES process [2, 3].

2.2 International Data Encryption Algorithm (IDEA)

IDEA algorithm takes input text of size 64 bits at a time and divide it in evenly; i.e., 64 bit plain text is divided into 4 sub-blocks, each of 16 bits in size. Following are the basic operations needed in the entire process.

Operations needed in the first 8 rounds

1. Multiplication modulo $2^{16}+1$.
2. Addition modulo 2^{16}.
3. Bitwise XOR.

Operations needed in the OUTPUT TRANSFORMATION phase

1. Multiplication module $2^{16}+1$.
2. Addition modulo 2^{16}.

The above mentioned operations are performed on 16 bit sub-blocks. For simplicity of expressing the operations, we denote, Multiplication modulo $2^{16}+1$ by * symbol, and Addition modulo 2^{16} by, + symbol. And bitwise XOR will be represented by its usual symbol. Using 25-bit circular left shift operation on the original key, other subsequent sub-keys are produced, used in different rounds. For instance, among the total no. of 52 keys- Sub-key K1 is having first 16bits of the original key, sub-key K2 is having the next 16 bits, and so on till sub-key K6. For ROUND1, sub-keys K1 to K6 use first (16x6=) 96 bits of the original cipher key. In ROUND2, sub-key K7 & K8 take the rest of the bits (bits 97 to 128) of the original cipher key. Then we perform circular left shift (by 25bits) operation on the original key. As a result the 26th bit of the original key shifted to the first position and becomes the first bit (of the new shifted key) and the 25th bit of the original key, moves to the last position and becomes the 128th bit (after first shift). This process continues till ROUND8, and also in the OUTPUTPUT TRANSFORMATION phase; i.e., after the ROUND8, the key is again shifted left by 25 bits and the first 64 bits of the shifted key is taken for use, and used as sub-keys K49 to K52 in the OUTPUT TRANSFORMATIONMATION phase[4-6].

2.3 Rivest Cipher (RC)

RC algorithms were first invented by Ron Rivest. "RC" stands for Rivest Cipher. The RC algorithms are widely deployed in many networking applications because of their favorable speed and variable key-length capabilities [7].

RC1

RC1 was never published. It was the first step which Rivest took in order to proceed with designing a series of symmetric key algorithms popularly known as the Rivest Cipher Algorithms. Later, different variants were designed and continuous research has been carried out by the researchers. The main idea of research was to design a Symmetric Key encryption algorithm that could be used by the users to protect their data as it passes through the network.

RC2

It is a block encryption algorithm, developed in 1987. It was considered as a proposal for the DES replacement. It is a secret key block encryption algorithm which uses a variable size key from 1 byte to 128 bytes. It consists of input and output block size

of 64-bit each. This algorithm was designed to be easily implemented on 16-bit microprocessors. If the key encryption has been performed, then this algorithm runs twice as fast as DES. The algorithm itself involves 3 further sub algorithms viz. Key Expansion, Encryption, and Decryption. This was designed as a proposal to replace the existing DES Algorithm [8].

RC3

RC3 was broken before ever being used. When the RC3 algorithm was being developed at RSA security, It was broken at the same time. Hence, it was not used.

RC4

RC4 is a stream cipher, symmetric key encryption algorithm. The same algorithm is used for both encryption and decryption. The data stream is simply XORed with the series of generated keys. The key stream does not depend on plaintext used at all. A variable length key from 1 to 256 bit is used to initialize a 256-bit state table. Vernam stream cipher is the most widely used stream cipher based on a variable key-size. It is popular due to its simplicity. It is often used in file encryption products and secure communications, such as within SSL. The WEP (Wireless Equivalent Privacy) protocol also used the RC4 algorithm for confidentiality[9, 10].

A stream cipher using variable-sized keys; it is widely used in commercial cryptography products, although it can only be exported using keys that are 40 bits or less in length. RC4 is a stream cipher, symmetric key algorithm. The same algorithm is used for both encryption and decryption as the data stream is simply XORed with the generated key sequence. The key stream is completely independent of the plaintext used. It uses a variable length key from 1 to 256 bit to initialize a 256-bit state table. The state table is used for subsequent generation of pseudo-random bits and then to generate a pseudo-random stream which is XORed with the plaintext to give the ciphertext. The algorithm can be broken into two stages: initialization, and operation. In the initialization stage the 256-bit state table, S is populated, using the key, K as a seed. Once the state table is setup, it continues to be modified in a regular pattern as data is encrypted.

The steps for RC4 encryption algorithm is as follows:

1- Get the data to be encrypted and the selected key.

2- Create two string arrays.

3- Initiate one array with numbers from 0 to 255.

4- Fill the other array with the selected key.

5- Randomize the first array depending on the array of the key.

6- Randomize the first array within itself to generate the final key stream.

7- XOR the final key stream with the data to be encrypted to give cipher text.

It was also used by many other email encryption products. The cipher can be expected to run very quickly in software. It was considered secure until it was vulnerable to the BEAST attack.

RC5

RC5 is a 32/64/128-bit block cipher developed in 1994. It was designed by Ronald Rivest for RSA Data Security (now RSA Security) in December of 1994. It is a symmetric block cipher having a variable number of rounds, word size and a secret key. It uses data-dependent operations heavily. It is a simple algorithm which has a low memory requirement. It is suitable for hardware or software. It is fast and also provides security if suitable parameters are chosen. This algorithm makes use of magic numbers. Due to the data-dependent rotations, differential cryptanalysis and linear cryptanalysis is not possible. The key used is strong if it is long. However, if the key size is short, then the algorithm is weak [11].

RC6

It was an AES finalist developed in 1997. It is a block cipher which uses 128 bit block size and supports key sizes of 128, 192 and 256 bits. It was designed in order to meet the requirements of the AES. It is an

improvement of the RC5 Algorithm. It provides even better security against attacks which may be possible in the RC5 Algorithm. It makes use of 4 registers (Each one of 32 bit) and is more secure than the RC5. It is also protected from various other possible security attacks. It uses fewer rounds and offers a higher throughput [12].

RC7

To improve the encryption efficiency of the already existing RC6 algorithm [13], RC7 has been proposed which takes relatively less time to encrypt data and is comparatively more flexible. Instead of four working registers, RC7 makes use of six such registers which makes it a better alternative to RC6 [14].

2.4 Camellia

A secret-key, block-cipher crypto algorithm developed jointly by Nippon Telegraph and Telephone (NTT) Corp. and Mitsubishi Electric Corporation (MEC) in 2000. Camellia has some characteristics in common with AES: a 128-bit block size, support for 128, 192, and 256 bit key lengths, and suitability for both software and hardware implementations on common 32-bit processors as well as 8-bit processors (e.g., smart cards, cryptographic hardware, and embedded systems). Camellia was jointly developed by Nippon Telegraph and Telephone Corporation and Mitsubishi Electric Corporation in 2000. Camellia specifies the 128-bit block size and 128-, 192-, and 256-bit key sizes, the same interface as the Advanced Encryption Standard (AES). Camellia is characterized by its suitability for both software and hardware implementations as well as its high level of security. From a practical viewpoint, it is designed to enable flexibility in software and hardware implementations on 32-bit processors widely used over the Internet and many applications, 8-bit processors used in smart cards, cryptographic hardware, embedded systems, and so on. Moreover, its key setup time is excellent, and its key agility is superior to that of AES. Camellia has been scrutinized by the wide cryptographic community during several projects for evaluating crypto algorithms. In particular, Camellia was selected as a recommended cryptographic primitive by the EU NESSIE (New European Schemes for Signatures, Integrity and Encryption) and also included in the list of cryptographic techniques for Japanese e-Government systems which were selected by the Japan CRYPTREC (Cryptography Research and Evaluation Committees).

2.5 Secure and Fast Encryption Routine (SAFER)

Secret-key crypto scheme designed for implementation in software. Versions have been defined for 40, 64, and 128 bit keys. SAFER K-64 stands for Secure and Fast Encryption Routine with a Key of 64 bits. There are no patent, copyright or other restrictions on its use. The algorithm has a block and key size of 64 bits. It is not a Feistel network like DES, but an iterated block cipher: The same function is applied for some number of rounds. Each round uses two 64-bit sub keys, and the algorithm only uses operations on bytes.

SAFER K-64 is an integrated cipher in the sense that encryption is performed by applying the same transformation repeatedly for r rounds, then applying an output Transformation; r = 6 is recommended but larger values of r can be used if desired for even greater security. Each round uses two 8-byte (64-bit) subkeys determined by a key schedule from the secret 8-byte user-selected key. The output transformation uses another 8-byte subkey determined by the key schedule. One unusual feature of SAFER K-64 is that, in contrast to most recently proposed iterated block ciphers, encryption and decryption are slightly different (i.e., they differ by more than just the reversal of the key schedule).
This algorithm uses only byte operations in the processes of encryption and decryption, which makes

it particularly useful in applications such as smart cards where very limited processing power is available. Some bit-level rotations of bytes are used in the key schedule, but this is done "once and for all", i.e., until the user-selected key is changed. To achieve security with such simple processing, SAFER K-64 exploits following two new cryptographic concepts:
(1) an unorthodox linear transform, which we call the Pseudo-Hadamard Transform (PHT), that allows the cipher rapidly to achieve the desired "diffusion" of small changes in the plaintext or the key over the resulting ciphertext [It is usually the case in block cipher design that one struggles to obtain such diffusion by carefully selecting permutations to imbed within the cipher and then doing massive statistical testing to see which ones give acceptable diffusion. As will be seen, the PHT provides a systematic way to ensure that the cipher provides the necessary diffisuion--in fact, the diffusion provided by the PHT appears to be better than that in any other cipher that we know and
(2) the use of additive key biases that eliminate the "weak keys" that plague most block ciphers. SAFER K-64 includes a recursive procedure for generating these key biases that is easy to implement and that provides the very "random" biases desired [15].

III. COMPARISON OF SYMMETRIC KEY ALGORITHMS

	CAST -256	**IDEA**	**RC-6**	**Camellia**	**SAFER**
Key Length	128,160, 192, 224 or 256	128	128,192 or 256	128, 192, 256	64
Block Size	128	64	128	128	64
Rounds	48	8.5	20	18 or 24	8

IV.CONCLUSION

Internet applications are growing very fast, so there is a need to protect such applications. Cryptographic algorithms play a main role in information security systems. In this paper a comparative study between CAST, IDEA, RC, Camellia and SAFER were presented into three factors, which are key length, block size, and number of rounds. From the study it is clear that, CAST-256 is found to be more secured as it requires more rounds the other compared algorithms.

V. REFERENCES

[1]. William Stalling “Cryptography and network security” Pearson education, 2nd Edition.
[2]. H B. Pethe, Dr. S. R. Pande “Implementation of Advanced Encryption Standard Algorithm” International Journal of Computer Science and Information Technologies, Vol. 7 (4) , 2016, 1868-1871.
[3]. Rishabh Jain, Rahul Jejurkar, Shrikrishna Chopade, Someshwar Vaidya, Mahesh Sanap “AES Algorithm Using 512 Bit Key Implementation for Secure Communication” International Journal of Innovative Research in Computer and Communication Engineering Vol. 2, Issue 3, March 2014 ISSN(Online): 2320-9801 ISSN (Print): 2320-9798
[4]. Sandipan Basu, "INTERNATIONAL DATA ENCRYPTION ALGORITHM (IDEA) – A TYPICAL ILLUSTRATION" Journal of Global Research in Computer Science Volume 2, No. 7, July 2011 ISSN: 2229-371X.
[5]. Harivans Pratap Singh et al, "Secure-International Data Encryption Algorithm" International Journal of Advanced Research in Electrical, Electronics and Instrumentation Engineering Vol. 2, Issue 2, February 2013 ISSN (Print) : 2320 – 3765 ISSN (Online) : 2278 – 8875.

[6]. Snehal Patil et al, "An Enhancement In International Data Encryption Algorithm For Increasing Security" International Journal of Application or Innovation in Engineering & Management (IJAIEM) Volume 3, Issue 8, August 2014 ISSN 2319 - 4847.

[7]. Sheetal Charbathia and Sandeep Sharma, "A Comparative Study of Rivest Cipher Algorithms" International Journal of Information & Computation Technology.ISSN 0974-2239 Volume 4, Number 17 (2014), pp. 1831-1838.

[8]. MILIND MATHUR, AYUSH KESARWANI, "COMPARISON BETWEEN DES , 3DES , RC2 , RC6 , BLOWFISH AND AES" Proceedings of National Conference on New Horizons in IT - NCNHIT 2013.

[9]. Allam Mousa et al, "Evaluation of the RC4 Algorithm for Data Encryption" International journal of Computer Science and Applications, Volume 3, No 2, June 2006.

[10]. P. Prasithsangaree, P. Krishnamurthy, "Analysis of Energy Consumption of RC4 and AES Algorithms in Wireless LANs" GLOBECOM 2003.

[11]. Vikas Tyagi, Shrinivas Singh, "ENHANCEMENT OF RC6 (RC6_EN) BLOCK CIPHER ALGORITHM AND COMPARISON WITH RC5 & RC6" Journal of Global Research in Computer Science Volume 3, No. 4, April 2012 ISSN:2229-371X.

[12]. P.Sritha1, R.Ashokkumar et al, "A new modified RC6 algorithm for cryptographic applications" International Journal of Advanced Research in Computer and Communication Engineering Vol. 3, Issue 12, December 2014 ISSN (Online) : 2278-1021 ISSN (Print) : 2319-5940.

[13]. T. Shimoyama, K. Takeuchi and J. Hayakawa, “Correlation Attack to the Block Cipher RC5 and the Simplified Variants of RC6”, 3rd AES Conference, (2004).

[14]. Rashmi, Vicky Chawla et al, "The RC7 Encryption Algorithm" International Journal of Security and Its Applications Vol. 9, No. 5 (2015), pp. 55-60.

[15]. James L. Massey , "SAFER K-64: A Byte-Oriented Block-Ciphering Algorithm" Reprinted from Fast Software Encryption (Ed. R. Anderson), Lecture Notes in Computer Science No. 809. New York: Springer, 1994, pp. 1-17.

National Conference on "Recent Trends in Mathematical Modeling, Simulation Methods, Computations, and Physical Sciences"
(MMSCP-2019), Organised by Hislop College, Nagpur, Maharashtra, India
International Journal of Scientific Research in Computer Science, Engineering and Information Technology
© 2019 IJSRCSEIT | Volume 4 | Issue 4 | ISSN : 2456-3307

Electrochemical Properties of CNF/$CoFe_2O_4$ Composite for Supercapacitor Application

Nutan V. Mangate#, Rounak R. Atram, Subhash B. Kondawar*
Department of Physics, Rashtrasant Tukadoji Maharaj Nagpur University, Nagpur, Maharashtra, India
#Corresponding Author Email: sbkondawar@yahoo.co.in
*Presenter Author Email: kanchanutanmangate@gmail.com

ABSTRACT

This paper presents the facile technique of decoration of $CoFe_2O_4$ nanoparticles on electrospun carbon nanofibers (CNF) by two step approach via electrospinning and hydrothermal for supercapacitor. Fabrication of CNF by electrospinning process is followed by decoration of $CoFe_2O_4$ on CNF using one pot hydrothermal method. CNF/$CoFe_2O_4$ nanocomposite hybrid was characterized by x-ray diffraction, scanning electron microscopy and energy dispersive x-ray spectroscopy for their structural, surface morphological and elemental properties. The charge transfer mechanism and mass diffusion process was studied using electrochemical impedance technique using frequency range 0.01Hz to 1MHz. Electrochemical behavior was studied using cyclic voltammetry and galvanostatic charge-discharge that showed the maximum specific capacitance 188.36 Fg^{-1} at current density 0.5 Ag^{-1} with potential window -0.2 to 1.0 V. Results showed that CNF/$CoFe_2O_4$ nanocomposite is potential candidate as electrode for supercapacitor.

Keywords : Electrospun Carbon Nanofibers, Scanning Electron Microscopy, Polyacrylonitrile, Dimethylformamide, EIS, EDLC

I. INTRODUCTION

Over the past decade, the rapid development of industrialization has resulted in increased demand for energy [1]. Supercapacitors can be considered as a great alternative to conventional energy sources in the application where we need to store or release the huge amount of energy in very short time [2]. Supercapacitor can be divided into two basic types according to their charge storage mechanism. First one is electric double layer capacitor which stores the charge non-faradically and the second one is pseudocapacitor which stores the charge faradically [3]. The porous carbon materials such as carbon aerogel, graphene, carbon nanotubes, activated carbon and carbon nanofibers with high surface areas have been mostly used electrode materials in EDLCs. Typical active pseudocapacitive materials includes metal oxides/ hydroxides such as RuO_2, MnO_2, $NiO/NI(OH)_2$, $Co_3O_4/Co(OH)_2$, etc and conducting polymers [4,5]. Among them RuO_2 was once the most studied metal oxide for supercapacitors because of its ultrahigh theoretical capacitance [4]. EDLC suffers from low specific capacitance and energy density whereas pseudocapacitive material suffers from limited stability during long term cycling. So, the use of single material as an electrode is definitely limits some practical applications. So, in order to go beyond the limitations of using single component electrode materials, multi-component electrode materials have

been explored to enhance the energy storage performances by taking advantage of each component's unique functionality and their synergistic effects [4].

Spinel ferrites (MFe_2O_4, M = Mn, Co or Ni) are of great interest for their remarkable magnetic, catalytic, optical and electrical properties, especially they exhibit attributes such as different redox states, electrochemical stability [6]. Among these materials, $CoFe_2O_4$ exhibits a good theoretical capacity (916 mAh g^{-1}) [7], excellent chemical stability, naturally abundance and environmental benignity [8]. Electrospun carbon nanofibers (CNF) have been considered as the promising conductive support for metal oxides due to their high surface area, excellent mechanical property, high electrical conductivity, chemical stability and low cost of synthesis [9]. Therefore, the combination of CNF and $CoFe_2O_4$ are expected to enhance the conductivity, specific capacitance and cycling stability of composite electrode. Herein, we focus on the decoration of $CoFe_2O_4$ on CNF by simple one-pot hydrothermal method whereas the CNF are fabricated using electrospinning.

II. EXPERIMENTAL

2.1 Fabrication of CNF by electrospinning

The electrospinning solution was prepared by adding 10 wt % of polyacrylonitrile (PAN) in 10 ml of N-N dimethylformamide (DMF) with continuous magnetic stirring at 70 °C for 2 hrs. The prepared solution was then transferred to syringe for electrospinning. Processing parameters like flow rate 1 ml/hr, voltage 20 kV and distance between the needle tip and collector 15 cm were fixed during electrospinning. The electrospun PAN fibers were collected and dried overnight at 70 °C. These PAN nanofibers were first stabilized in muffle furnace at 200 °C for 1 hr, carbonized at 600 °C for 1 hr in nitrogen atmosphere and finally activated at 400 °C for 1 hr in presence of air. The nitrogen supply was maintained till the temperature reduced to 400 °C.

2.2 Decoration of $CoFe_2O_4$ on CNF by hydrothermal

The uniform dispersion of CNF was done by sonicating it in distilled water for 3 hr. Fe and Co precursors were taken in 1:2 stoichiometry ratio with 24 mmol urea dissolved in distilled water and magnetically stirred for 1 hr. The two solutions were then mixed well together by 1 hr magnetic stirring. The prepared solution was transferred to the 100 ml stainless steel Teflon autoclave for hydrothermal process at 120 °C for 10 hr. The as-synthesized material was centrifuge and washed several times with distilled water and finally dried.

III. RESULTS AND DISCUSSION

3.1 Scanning electron microscopy (SEM)

SEM images of CNF and CNF/$CoFe_2O_4$ are shown in Fig. 1(a) and (b) respectively. SEM images display the fabrication of CNF by electrospinning and hydrothermally decorated $CoFe_2O_4$ nanoparticles on carbon nanofibers. The heavy decoration of $CoFe_2O_4$ nanoparticles on CNF is helpful for electrolyte transport, thereby creating surface area for redox reaction and high specific capacitance.

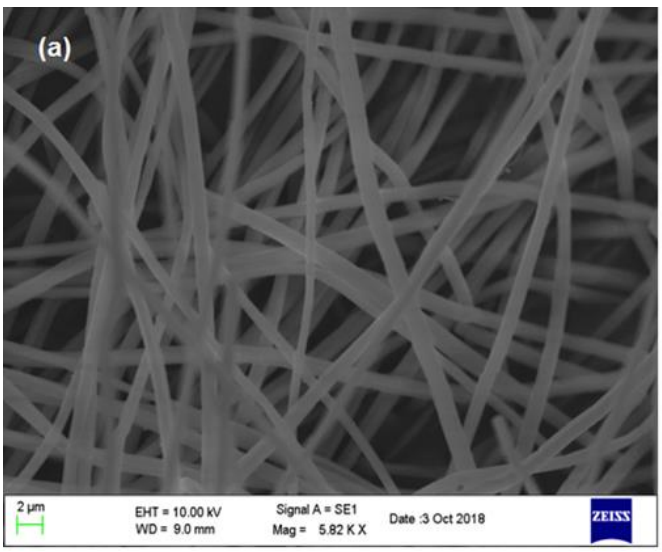

(a)

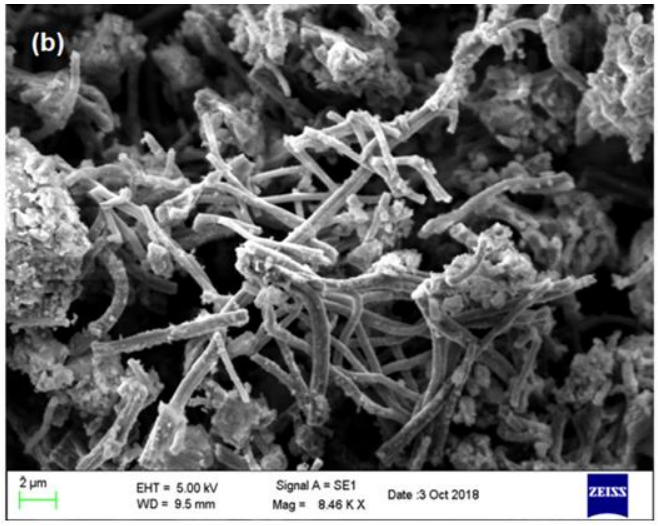

(b)

Fig. 1: SEM images of (a) CNF and (b) CNF/$CoFe_2O_4$ composite

3.2 Electrochemical properties

CV curves of CNF/$CoFe_2O_4$ before and after cycling at different scan rate are shown in Fig. 2(a) and (b) respectively. In the CV curve of CNF/$CoFe_2O_4$, a pair of redox peaks indicates the pseudocapacitive behavior of CNF/$CoFe_2O_4$. Reduction peaks are correspond to the conversion reaction of Fe^{3+} and Co^{2+} to their metallic states and oxidation peak are observed which attributed to the oxidation of the Fe and Co to Fe^{3+} and Co^{2+} respectively. As the scan rate is increased from 5 mV/s to 75 mV/s, the total peak current increases demonstrating the good rate property and excellent capacitance behavior [6]. It was clearly found that the shape of CV curves maintained similar with the increment of scan rate from 5 to 75 mV/s, indicating electrode possesses an excellent rate capability. Additionally, the oxidation and reduction peaks were slightly shifted to a higher and a lower potential with increase of scan rate respectively. This should be due to polarization effect of electrode material at high scanning speeds [8]. The frequency response of an electrode material is studied using an electrochemical impedance spectroscopy. EIS measurement was performed in the frequency range from 0.01Hz – 1MHz under open-circuit potential conditions. Nyquist plot of CNF/$CoFe_2O_4$ composite electrode is represented in Fig 2(c). The semicircle in the high frequency region represents the charge- transfer resistance found to be 10.1 Ω arises due to charge transfer process at the electrode-electrolyte interface, whereas the straight line in the low frequency region represents the ion-diffusion, associated with the mass transfer [7]. An intercept at high frequency region with real part (Z') is attributable to solution resistance found to be 0.337 Ω which includes ionic resistance of electrolyte, intrinsic resistance of active material and contact resistance of active material and current collector [10].

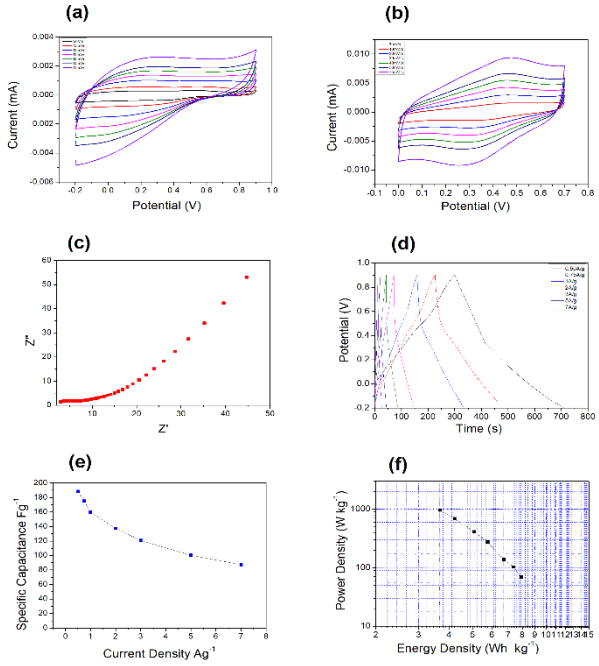

Fig. 2: (a) CV curve before cycling (b) CV curve after cycling at different scan rate (c) Nyquist plot (d) GCD curve at different current density (e) Specific capacitance at different current density (f) Ragone plot.

To further calculate the specific capacitance of CNF/$CoFe_2O_4$ composite hybrid electrode, the GCD measurements were performed with potential range -0.2 to 1.0V at different current density of 0.5-7 Ag^{-1}. GCD curve of CNF/$CoFe_2O_4$ is shown in Fig 2(d).

Based on the discharge time of electrode, the specific capacitance of electrode was calculated by using equation (1);

$$C = \frac{I \times \Delta t}{\Delta V} \quad (1)$$

Where, C is specific discharge capacitance in Fg^{-1}, I is current density in Ag^{-1}, Δt is the discharge time and ΔV is potential drop during discharge. The nonlinear variation of potential versus time indicates that the capacitive performance due to both electric double layer and pseudocapacitance. This might be due to electrochemical adsorption-desorption reaction at the interface between electrode and electrolyte [10]. Fig. 2(e) shows the specific capacitance at different current density. The specific capacitance could reach to 188.36 Fg^{-1} at lowest current density of $0.5Ag^{-1}$. Ragone plot of CNF/$CoFe_2O_4$ is shown in Fig. 2(f) which shows the maximum energy density 7.91 $Whkg^{-1}$ at power density 963.67 Wkg^{-1} could be achieved.

IV. CONCLUSION

CNF/$CoFe_2O_4$ composite was successfully fabricated by simple electrospinning and hydrothermal method. $CoFe_2O_4$ nanoparticles were heavily decorated on the surface of CNF. The specific capacitance of CNF/$CoFe_2O_4$ was found to be 188.36 Fg^{-1} at lowest current density of 0.5 Ag^{-1}. The maximum energy density 7.91 $Whkg^{-1}$ at power density 963.67 Wkg^{-1} was achieved. The results showed that CNF/$CoFe_2O_4$ composite material is a potential candidate for supercapacitor application.

V. REFERENCES

[1] X. Guo, C. Yang, G. Huang, Q. Mou, H. Zhang, B. He, Design and synthesis of CoFe2O4 quantum dots for high performance supercapacitors, Journal of Alloys and Compounds 764 (2018) 128-135.

[2] J. Libich, J. Maca, J. Vondrak, O. Cech, M. Sedlarikova, Supercapacitors: Properties and applications, Journal of Energy Storage 17 (2018) 224-227.

[3] L. Jinlong, Y. Meng, L.Tongxiang, H. Miura, Facile synthesis of Co3O4@MnO2 core-shell nanocomposites for high-performance supercapacitor, Materials Letters (2017).

[4] P. Xiong, J. Zhu, X. Wang, Recent advances on multi-component hybrid nanostructures for electrochemical capacitors, Journal of Power Sources 294 (2015) 31-50.

[5] Z. S. Iro, C. Subramani, S. S. Dash, A Brief Review on Electrode Materials for Supercapacitor, Int. J. Electrochem. Sci, 11 (2016) 10628-10643.

[6] P. Xiong, H. Huang, X. Wang, Design and synthesis of ternary cobalt ferrite/graphene/polyaniline hierarchical nanocomposites for high- performance supercapacitors, Journal of Power Sources 245 (2014) 937-946.

[7] J. Choi, K. Seong, J. Kang, M. Hwang, J. M. Kim, X. Jin, Y. Piao, Fluoride ion-mediated morphology control of fluorine-doped $CoFe_2O_4$/graphene sheet composites for hybrid supercapacitors with enhanced performance, Electrochemical Acta 279 (2018) 241-249.

[8] L. Yue, S.Zhang, H. Zhao, Y. Feng, M. Wang, L. An, X. Zhang, J. Mi, One-pot synthesis $CoFe_2O_4$/CNTs composite for asymmetric supercapacitor electrode, Solid State Ionics 329 (2019) 15-24.

[9] M. Zhi, A. Manivannan, F. Meng, N. Wu, Highly conductive electrospun carbon nanofiber/MnO_2 coaxial nano-cables for high energy and power density supercapacitors, Journal of Power Sources 208 (2012) 345-353.

[10] V. S. Kumbhar, A. D. Jagadale, N. M. Shinde, C. D. Lokhande, Chemical synthesis of spinel cobalt ferrite ($CoFe_2O_4$) nano-flakes for supercapacitor application, Applied Surface Science 259 (2012) 39-43.

IJSRCSEIT

www.ijsrcseit.com

International Journal of Scientific Research in
Computer Science, Engineering and Information Technology
(International Journal Bimonthly Publication)
www.ijsrcseit.com

Published by :
TechnoScience Academy

www.technoscienceacademy.com

National Conference on "Recent Trends in Mathematical Modeling, Simulation Methods, Computations, and Physical Sciences"

Organised by

Department of Mathematics, Department of Computer Science, & Department of Physics and Electronics, HISLOP College, Nagpur, Maharastra, India

Email: editor@ijsrcseit.com, ijsrcseit@gmail.com